NOTE TO USERS

Copyrighted materials in this document have not been scanned at the request of the author. They are available for consultation in the author's university library.

149-153

This reproduction is the best copy available.

UMI®

University of Alberta

Characterization of Porous Pharmaceutical Powders

by

Michael Patrick McKay

A thesis submitted to the Faculty of Graduate Studies and Research in partial fulfillment of the

requirements for the degree of Master of Science

in

Chemical Engineering

Department of Chemical and Materials Engineering

Edmonton, Alberta

Fall, 2005

Library and Archives Canada

Published Heritage Branch

395 Wellington Street
Ottawa ON K1A 0N4
Canada

Bibliothèque et Archives Canada

Direction du Patrimoine de l'édition

395, rue Wellington
Ottawa ON K1A 0N4
Canada

Your file Votre référence
ISBN: 0-494-09241-6
Our file Notre référence
ISBN: 0-494-09241-6

NOTICE:
The author has granted a non-exclusive license allowing Library and Archives Canada to reproduce, publish, archive, preserve, conserve, communicate to the public by telecommunication or on the Internet, loan, distribute and sell theses worldwide, for commercial or non-commercial purposes, in microform, paper, electronic and/or any other formats.

The author retains copyright ownership and moral rights in this thesis. Neither the thesis nor substantial extracts from it may be printed or otherwise reproduced without the author's permission.

AVIS:
L'auteur a accordé une licence non exclusive permettant à la Bibliothèque et Archives Canada de reproduire, publier, archiver, sauvegarder, conserver, transmettre au public par télécommunication ou par l'Internet, prêter, distribuer et vendre des thèses partout dans le monde, à des fins commerciales ou autres, sur support microforme, papier, électronique et/ou autres formats.

L'auteur conserve la propriété du droit d'auteur et des droits moraux qui protège cette thèse. Ni la thèse ni des extraits substantiels de celle-ci ne doivent être imprimés ou autrement reproduits sans son autorisation.

In compliance with the Canadian Privacy Act some supporting forms may have been removed from this thesis.

While these forms may be included in the document page count, their removal does not represent any loss of content from the thesis.

Conformément à la loi canadienne sur la protection de la vie privée, quelques formulaires secondaires ont été enlevés de cette thèse.

Bien que ces formulaires aient inclus dans la pagination, il n'y aura aucun contenu manquant.

Canada

Abstract

The motivation of this thesis was the desire to characterize the effective density of inhaled pharmaceutical powders consisting of porous, micron-sized particles where other experimental methods may not apply. A system of collecting pressure drop and velocity data for packed beds of particles analogous to that utilized by Ergun was created, employed, and the data was analyzed using the Ergun and Richardson-Zaki equations. Using materials with known properties, the Ergun equation was found to be acceptable with most solid particles studied save non-spherical particles with very large size distributions, but does not properly model flow through highly-porous, micron-sized particles. The Richardson-Zaki equation provides appropriate results for the effective density and geometric and aerodynamic diameters for highly porous, micron-sized particles. This process could provide dry pharmaceutical manufacturers with a valid new method of determining the effective density. Further work is required to verify, refine, and qualify the accuracy of the method.

Acknowledgements

Many people helped give me the opportunity to pursue this degree. However, the following persons deserve note as their contributions deserve my sincerest thanks and gratitude:

- Drs. Forbes and McCaffrey for their guidance, patience, and funding;
- The support staff of the Department of Chemical Engineering;
- Drs. Craig Dunbar and Rick Batycky of Alkermes;
- My family and friends for their constant encouragement.

Table of Contents

1.0 Introduction **1**
2.0 Theory **9**
2.1 Bulk Density 10
2.2 Particle Density 11
2.3 Methods of Particle Density Determination 12
2.4 Pressure Drop in Packed Beds 14
2.5 Ergun's Method 15
2.7 Analytical Solutions and other Recent Studies 20
3.0 Experimental Setup **22**
3.1 Experimental Procedure 25
3.2 Materials 27
3.2.1 175 μm Glass Spheres 27
3.2.2 135 μm Glass Spheres 27
3.2.3 175 μm and 135 μm Glass Spheres 27
3.2.4 Pharmatose 27
3.2.5 Respitose 28
3.2.6 Sigma-Aldrich Lactose 28
3.2.7 Alkermes Representative Porous Pharmaceutical Powder 28
4.0 Results and Discussion **30**
4.1 Validation of Apparatus 30
4.1.1 Validation using Glass Spheres 30
4.1.1 Bimodal Distribution of Spherical Particles 40
4.1.2 Non-Spherical Plate-Like Particles 43
4.2 Effect of Shape and Size Distribution 47
4.2.1 Influence of Moderate Size Distribution and Slight Porosity 47
4.2.2 Influence of Moderate Distribution and Non-Spherical Shape 53
4.2.3 Discussion of the Effect of Shape on the Experimental Method 56
4.2.4 The Application of the Richardson-Zaki Equation to Solid Materials 56
4.2.5 High Flow Rate Regime 58
4.3 Characterization of Porous Pharmaceutical Powders 60
4.3.1 Characterization of Size & Distribution 60
4.3.2 Pressure Drop Experiments for Density Determination 67
4.3.3 Diameter of Particles from Pressure Drop Results 76
4.3.4 Aerodynamic Diameter 78
4.3.5 Aerodynamic Diameter of Deagglomerated Particles 79
5.0 Conclusions **85**
6.0 Future Work **88**
7.0 References **91**

List of Tables

Table 1:	Plexiglass™ Column Specifications	22
Table 2:	Summary of the density predictions of applying the Ergun and Richardson-Zaki equations to the solid materials	57
Table 3:	Summary of the Geometric Size Distributions of Deagglomerated AIR® Representative Porous Pharmaceutical Powder.	66
Table 4:	Comparison of the Effective Density Results from the Ergun and Richardson-Zaki Equations	75
Table 5:	Aerodynamic Diameters of the Representative Porous Pharmaceutical Particles	79
Table 6:	Aerodynamic Size Distributions of the AIR® Representative Porous Pharmaceutical Powder	80

List of Figures

Figure 1:	Schematic Diagram of Experimental Setup	22
Figure 2:	Volumetric Flow Rate versus Controller Percent of Range Reading for the Matheson 8272-0432 Mass Flow Transducer.	23
Figure 3:	Volumetric Flow Rate versus Controller Percent of Range Reading for the Matheson 8272-0421 Mass Flow Transducer.	24
Figure 4:	Scanning Electron Micrograph of 175 μm glass spheres. Scale bar is 600 μm.	31
Figure 5:	Scanning Electron Micrograph of 135 μm glass spheres. Scale bar is 600 μm.	32
Figure 6:	Typical data for pressure gradient versus velocity (for downward flow) for the 135 μm glass spheres. Bulk density given in g/cm^3. Lines are trends in the data.	33
Figure 7:	Typical data for pressure gradient versus velocity (for downward flow) for the 175 μm glass spheres. Bulk density given in g/cm^3. Lines are trends in the data.	34

Figure 8: Pressure drop method for characterizing 135 μm glass spheres. The line is a linear regression of the data. 35

Figure 9: Pressure drop method for characterizing 175 μm glass spheres. The line is a linear regression of the data. 36

Figure 10: Pressure drop method for characterizing 135 μm glass spheres including data points outside of the error of the linear regression. The line is a linear regression of the data. 38

Figure 11: Ergun Method for 175 μm & 135 μm glass sphere mixture. Line is a linear regression of the data. 42

Figure 12: Scanning Electron Micrograph of Sigma-Alrdich Lactose particles. Scale bar is 60 μm. 44

Figure 13: Ergun's Method for Sigma Lactose. The line is a linear regression of the data. 45

Figure 14: Pressure Gradient versus Superficial Velocity for Sigma Lactose. Lines are fits of the data. 46

Figure 15: Scanning Electron Micrograph of Pharmatose. Scale bar is 600μm. 49

Figure 16: Plot of ρ_{Bulk} and $(\rho_{Bulk}^2/a)^{1/3}$ as per Ergun's Method for Pharmatose with the data segregated into compacted and un-compacted beds. The line is a linear regression of the un-compacted data points. 51

Figure 17: Ergun Method for Pharmatose. The line is linear regression of data. 52

Figure 18: Scanning Electron Micrograph of Respitose. Scale bar is 200 μm. 54

Figure 19: Ergun Method for Respitose. The line is a linear regression of data. 55

Figure 20: Scanning Electron Micrograph of Representative porous pharmaceutical particles. Scale bar is 600μm. 61

Figure 21: Close-up Scanning Electron Micrograph of a Representative porous pharmaceutical particle. Scale bar is 30μm. 62

Figure 22: Example of the Scanning Electron Micrograph of Representative porous pharmaceutical particles used to estimate the equivalent diameter. Scale bar is 150 μm. 64

Figure 23: Histogram of equivalent diameters of Representative porous pharmaceutical particles using the method of Davies, 1979. 65

Figure 24: Geometric Diameter of Representative porous pharmaceutical versus Primary Pressure 67

Figure 25: Ergun Method for Representative Porous Pharmaceutical Powder Samples A, B, and C 70

Figure 26: Plot of the Residual Errors for Sample C 71

Figure 27: Ergun Equation for Samples A, B, and C for data without visual voids 73

Figure 28: Richardson-Zaki Equation and Packed Bed method for Samples A, B, and C for data without visual voids. 74

Figure 29: Aerodynamic Diameter of Representative Porous Pharmaceutical Particles versus Primary Pressure 82

Nomenclature

a, a', a"	Coefficient relating velocity and pressure gradient
A, B	Ergun Equation Constants
CFC	Chlorofluorocarbon
d_p	Diameter, μm
d_{Aero}	Aerodynamic Diameter, μm
d_{Geo}	Geometric Diameter, μm
DPI	Dry Powder Inhaler
g	Gravitational Constant, m/s^2
K, B, L	Davies Equation Parameters
l	Packing Height, mm
ΔP	Pressure difference, Pa
SEM	Scanning Electron Micrograph
v	Velocity, mm/s
ε	Porosity or Void Fraction of the Bed
$\varepsilon_{Intraparticle}$	Porosity of the Particle
μ	Viscosity, kg/m/s or Pa·s
ρ	Density, g/cm^3
$\rho_{Aerated}$	Aerated Density, g/cm^3
$\rho_{Apparent}$	Apparent Density, g/cm^3

ρ_{Bulk}	Bulk Density, g/cm^3
ρ_{Eff}	Effective Density, g/cm^3
$\rho_{Envelope}$	Envelope Density, g/cm^3
ρ_f	Fluid Density, g/cm^3
ρ_{Solid}	Solid Density of Material, g/cm^3
ρ_{Tap}	Tapped Density, g/cm^3
τ	Shear Stress, N/m^2
χ	Shape Factor

1.0 Introduction

In 2001, the pharmaceuticals industry was valued at over $364 billion US worldwide (Class, 2002). The drug delivery portion of the pharmaceuticals industry, which includes inhaled pharmaceuticals, is valued at over $43 billion US and is expected to post a growth rate of 11.3% over the next four years (D'Aquino, 2004). This tremendous growth will fuel investment in required areas in research and development in inhaled pharmaceuticals.

The main goal of inhaled pharmaceutical aerosols is to deposit the particles deep within the lungs (Finlay, 2001). The challenge of drug delivery is that the respiratory tract is constructed with defenses against particles found in nature. Particle size, inhalation flow rate and other variables are important factors that determine where and whether an inhaled particle will deposit in the respiratory tract. Larger particles can settle by gravity onto the lining of the conducting airways of the lungs while sedimentation may occur in the alveolated ducts in the lungs. Another mechanism by which particles get trapped in the lungs is by inertial impaction as the air flows through the curved passages and bifurcations. A large portion of the particles do not normally reach the lungsdue to the filtering action of the nose and mouth. The filtering action is largely due to impaction. For smaller particles, typically less than 3 μm, diffusion can be responsible for the deposition in the respiratory tract. In general, diffusion is only important in the alveolar region and at low flow rates. Particles must generally be from 1 to 5 μm to be deposited deep within the lungs.

The human lungs offer potential as a non-invasive point of delivery for peptides and proteins to the body for either a local or a systemic effect (Smith and Bernstein, 1996, Patton and Platz, 1992). The lungs offer a tremendous surface area immediately accessible to an inhaled drug with a low local level of metabolic activity and elevated blood flow can distribute the drug throughout the body providing for either a systemic or local effect (Bosquillon *et al.*, 2001).

Mechanisms within the human lung can efficiently remove inhaled particles in time periods ranging from minutes to hours (Edwards *et al.*, 1997). For example, the upper airway has cilia that function as elevators to remove particles from the body (Pavia, 1984). However, particles must meet certain criteria in order to bypass these defenses. Particles larger than 5 μm are typically not inhaled because they cannot be aerosolized or are hindered by the body's defenses (Heyder *et al.*, 1986), such as the cilia noted above. Particles smaller than 1μm are inhaled, but are not retained in the lungs and are removed from the lungs upon exhalation (Edwards, 2002). Particles possessing an aerodynamic diameter in the range of 1 to 5 μm can bypass these defenses and enter the lungs while remaining long enough to deliver a therapeutic effect (Goodman *et al.*, 1994).

This has been a particular concern in the history of the treatment of asthmatics (Dellamary *et al.*, 2000). The history of inhaled pharmaceuticals has been well covered elsewhere (Sciarra and Cutie, 1990), and only a brief discussion will be offered here. Interest in inhaled pharmaceuticals culminated in the first propellant-driven metered dose inhalers in the 1950s (Sciarra and Cutie, 1990). In the 1950s, asthmatics had to ingest

large doses of asthma drugs in order for the drugs to reach the lungs, which were typically greater than a hundred times the required dose to induce a therapeutic response (Edwards, 2002).

In the 1960s, industrial experts developed the propellant-driven metered dose inhaler (Edwards, 2002). In conjunction with inhalation, the particles are aerosolized by volatile chlorofluorocarbons (CFC) (Williams *et al.,* 1998, Edwards, 2002). These hand-held devices reduce the dosage required by releasing the drug particles through a perfume valve. A portion of the particles would then fall into the optimum particle size capable of delivering a therapeutic effect (Edwards, 2002).

Commercial inhalation therapy did not see much change during the 1970s and 1980s since the asthma refinements of the 1960s. CFCs are declining in use due to their association with ozone depletion (Molina and Rowland, 1974) and subsequent international agreements to limit their impact. As a result, new methods of introducing asthma drugs into the lungs have been developed, including new propellant mixtures (Williams *et al.,* 1998), aqueous droplets delivered by nebulizers (Dunbar *et al.,* 1998), and dry powder inhalers (DPI) (Williams *et al.,* 1998; Dunbar *et al.,* 1998; Bosquillion *et al.,* 2001).

The development of new non-CFC volatile chemicals, in particular hydrofluorocarbons (HFA), has been difficult due to the low solubility of their approved surfactants. As of 2000, only two (HFA-134a and HFA-227) have been approved for use (Dellamary *et al.*

2000). One limitation of HFA mixtures is their requirement for optimization for particles of different density (Williams *et al.*, 1998).

In recent years, trials have culminated in delivering to the market inhaled pharmaceuticals through dry powder inhalers (Batycky *et al.*, 1999). A dry powder inhaler induces a small amount of drug powder into the air stream as the patient inspires (Voss and Finlay, 2002). Dry powder inhaler technology avoids the use of any propellant and is more portable, less expensive, and easier to use than nebulizer technology (Bosquillion *et al.*, 2001). Research has revealed that the efficiency of dry powder inhalers depends on three properties of the particles: the size, shape, and density (Dunbar *et al.*, 1998).

The optimum aerodynamic diameter of inhaled particles is 1 to 5 μm (Dunbar *et al.*, 1998). The aerodynamic diameter is defined as the diameter of a sphere of unit density having the same falling velocity as the particle (Davies, 1979) or as follows:

$$d_{Aero} = \left(\frac{\rho_{Envelope}}{\chi} \right)^{0.5} d_{Geo} \qquad (1)$$

where $\rho_{Envelope}$ is the envelope density, or the mass inside the hydrodynamic volume (including both the particle and entrained fluid), also referred to hereafter as the effective density, ρ_{eff}; χ is a shape factor; and d_{Geo} is the geometric diameter of the particle (Edwards *et al.*, 1997; Edwards, 2002).

Most inhaled pharmaceutical particles manufactured for DPIs are approximately spherical and have geometrical and aerodynamic diameters of roughly of 1 to 5 μm (Edwards, 2002). The particles tend to be small enough that the inter-particle forces are greater than the gravitational or aerodynamic forces (Dunbar *et al.*, 1998; Voss and Finlay, 2000), causing aggregation (Edwards *et al.*, 1997). The inhaler must therefore generate enough force to entrain the particles in the flow field (to fluidize them) and establish deagglomeration (Voss and Finlay, 2000) or else the respirable portion of the dose will be low and inefficient (Edwards *et al.*, 1997). Agglomerated particles that have a d_{Aero} larger than 5 μm will not provide any appreciable therapeutic benefit (Edwards *et al.*, 1997). As a result, inhalation devices larger than previous propellant-driven metered dose inhalers have been developed (Finlay *et al.*, 1997). The particles are often paired with larger (100μm) carrier particles (termed excipients) which induce initial fluidization and aid in deagglomeration (Dunbar *et al.*, 1998). However, this limits the potential efficiency of engineered inhaled pharmaceutical powders. Larger particles that maintain an optimum aerodynamic diameter will suffer less aggregation and thereby increase the efficiency.

Particles such as asbestos are long rod-like particles that, due to their shape, have an aerodynamic diameter that is smaller than the equivalent diameter of the plan area of the particle (Davies, 1979). Inhaled pharmaceuticals manufactured along these lines could eliminate the aggregation that plagues smaller particles. However, the potentially toxic effects of altering the shape of the particle has resulted in most manufacturers' producing

spherical particles with both geometrical and aerodynamic diameters in the range of 1 to 5 μm (Edwards, 2002).

The other variable in equation (1) (Sciarra and Cutie, 1990) is the envelope density. A particle may have a lower envelope density than the bulk density of the solid material due to either aggregation (chained or globular aggregates) or voids (pores) within the particle that are filled with fluid (Davies, 1979). Manufacturing methods such as spray-drying and the use of supercritical fluids offer advantages over classical milling in that they allow for better control of particle shape, size, and composition (Edwards, 2002). Such control allows for more precise distributions of excipients (sugars, amino acids, lipids, and polymers) in the particles rather than having separate excipient particles. This type of production may customize the shelf-life, particle size, morphology (Edwards, 2002), and the drug dissolution rate in the lung (D'Aquino, 2004). These abilities can be used to alter the density of the particle to fulfill the promises of dry powder inhaler technology by altering the envelope density.

Several companies are taking advantage of these recent manufacturing advances to develop novel particle types for DPIs (Dellamary *et al.*, 2000, Batycky *et al.*, 1999). Developments in inhaled particle whose envelope density differs from unity have been ongoing for many years and show great promise (Edwards *et al.*, 1997, Dellamary *et al.*, 2000). For example, Alkermes have spearheaded large porous particle technology, including AIR® technology. AIR® technology produces geometrically larger (5-20μm),

highly porous particles which minimize the effect of agglomeration while maintaining an optimum aerodynamic size for inhalation therapy.

Large, highly porous particles offer several benefits. Unlike smaller particles that must be manufactured and then mixed with excipient particles (normally lactose), the AIR® particles are typically manufactured in a one-step spray drying process (Batycky *et al.*, 1999). These particles avoid the macrophages that perform phagocytosis of particles in the deep lung (Warheit and Hartsky, 1993). The hope is to allow for larger doses through controlled or sustained release. This would provide an extended therapeutic duration for the inhaled drug. The resulting avoidance of injections would lead to improved patient compliance (D'Aquino, 2004). In summary, large porous particles propose to achieve greater efficiencies than other dry powder inhaler particles (Batycky *et al.*, 1999).

AIR® is very interested in completely characterizing the particles they manufacture in order to meet and exceed FDA requirements. For example, AIR® uses cascade impactors and terminal velocity experiments to determine the aerodynamic size of the particles upon inhalation. Inertial impaction methods (such as cascade impactors) are among the only methods currently available for determining the mass median aerodynamic size distribution of dry powder aerosols (Finlay and Gehmlich, 2000). Cascade impactors are cheap, relatively easy to use and offer a direct and reproducible method of determining the aerodynamic mass distribution of a stable aerosol (Stapleton and Finlay, 1998).

One characteristic of particular interest with respect to inhaled drug delivery is particle porosity. The porosity of the particles is critical as it directly affects the aerodynamic size, and thus the effectiveness of the drug. The porosity and the effective density are related by:

$$\rho_{Eff} = \rho_{Solid}(1-\varepsilon_{Intraparticle}) \quad (2)$$

Therefore, if a method could be developed to determine the effective density, the porosity of the particles, $\varepsilon_{Intraparticle}$, could be determined.

A method based on Ergun's 1951 study uses flow and pressure drop data obtained from packed beds to predict the effective density of particles. This method offers a potential analytical technique for determining both the porosity and the effective density for inhaled particles.

This study focuses on employing Ergun's method to characterize aerosolized pharmaceutical powders. First, an experimental method was developed analogous to that Ergun describes. The method was tested against a variety of materials and verified the validity of the experimental setup. Second, the experimental setup was employed with large, porous particles supplied by Alkermes. The data collected was used to determine the suitability of employing Ergun's method to determine effective density.

2.0 Theory

The purpose of this work is to develop and test a method of determining the effective density of micron-sized, porous, and permeable particles designed for pharmaceutical inhalation therapy. The density of a particle may be defined in several ways. The first two sections of the Theory section clarify the different densities used in this work. The third section covers the capabilities and shortcomings of various methods of particle density determination.

The experimental method is based upon a method of particle density determination developed by Ergun. A condensed review of the work in the area of packed beds prior to Ergun is given in the fourth section. The basis of the Ergun equation and the development of the density determination method are described in the fifth section.

The Richardson-Zaki equation describes the flow through a packed bed of permeable particles. The application of this equation to the permeable pharmaceutical particles was considered and the derivation of a method of effective density determination is developed in the sixth section.

Considering the vast interest in flow in packed beds, there is no surprise at discovering a plethora of literature on the subject. The seventh section of the Theory section explores more recent developments and their potential application to the method under consideration.

2.1 Bulk Density

The bulk density is a commonly measured property of powders. The bulk density of a powder is defined as the mass divided by the volume that powder encompasses, including the void volume (i.e. spaces between the particles) within that volume (Svarovsky, 1987). The definition of the volume of a powder may vary. When a powder occupies the greatest possible volume, the bulk density is taken as the aerated bulk density. The aerated bulk density is defined as that of a powder that has a thin film of fluid between the particles (Svarovsky, 1987).

Poured bulk density, the most widely used bulk powder property (Svarovsky, 1987), is aptly named. The powder is poured into a standard volume (usually 50 to 1000 ml). The powder may be allowed to settle for up to 10 minutes before scraping off the top (Svarovsky, 1987). The powder and container are then weighed to determine the poured bulk density.

The tapped density is another form of bulk density (Svarovsky, 1987). The procedure for determining tapped density involves loading a specified mass or volume of powder into a container. The filled container is then dropped from a standard height a precise number of times (Svarovsky, 1987). The methods available vary from manual to mechanical devices, in the number of taps, the frequency of the taps, and whether a constant volume is achieved (Svarovsky, 1987). The Federal Drug Administration in the United States has a standard method for inhaled pharmaceuticals. Alkermes has had to slightly modify the device to limit the amount of powder that would aerosolize with each tap.

The various measurable bulk densities may be correlated to other properties (i.e. porosity). Bulk density may then be used as an indirect measurement of those associated properties. The difference between the aerated and tapped density may be expressed in terms of the Hausner Ratio ($\rho_{Tap}/\rho_{Aerated}$) (Hausner, 1967; Svarovsky, 1987; Abdullah and Gelhart, 1999) or Compressibility ($100\% \times (\rho_{Tap} - \rho_{Aerated})/ \rho_{Tap}$) (Svarovsky, 1987). The Hausner Ratio has been correlated against other properties of the powders, such as sphericity and inter-particle cohesion (Abdullah and Gelhart, 1999).

2.2 Particle Density

The mass of a particle divided by the volume the particle occupies would suffice as a definition for the density of a particle; however, one can define the particle volume (and mass within) in numerous ways (Svarovsky, 1987). Svarovsky provides the following definitions that will be used henceforth:

Solid Density: This is the density of the solid material of which the particle is made. The volume used to determine the true particle density excludes both closed and open pores.

Apparent Particle Density: The volume used to determine the apparent particle density includes the closed pores as well as the solid material. The apparent density is measured by gas or liquid pycnometry.

Effective (or Aerodynamic) Particle Density: The volume used includes both the closed and open pores. This volume is within an aerodynamic envelope as "seen" by the fluid flowing past the particle. It is of primary interest in fluidization, sedimentation, and flow through packed beds. The effective density is denoted as ρ_{Eff}.

2.3 Methods of Particle Density Determination

Pycnometers provide: solid density, if the particle has no closed pores; apparent density, if the particle has closed pores and the open pores remain open; and, effective density, if the open pores are filled, either with wax or fluid impregnation (Svarovsky, 1987). This method would reveal the effective density if there was a method of impregnating the open pores of the AIR® particles without altering the particles themselves, but this may not be possible with all formulations. This method would reveal either the solid or apparent density, depending on whether or not the particles have closed pores. Water pycnometry is not feasible, as the AIR® particles used in this study were made of water-soluble peptides, sugars, and other organic material.

Tapped and aerated bulk densities provide insight into the effective density (Abdullah and Gelhart, 1999), but without assuming a void fraction for either, the effective density cannot be determined solely through these tests (Svarovsky, 1987). Some authors have assumed a void fraction of 0.21 for the tapped density measurement (Bosquillon *et al.*, 2001). However, the void fraction for tapped powders is known to vary with size and shape of the particles (Svarovsky, 1987).

Bulk density measurements may be used to approximate the effective density, if the void volume is assumed (Svarovsky, 1987). This method determines the maximum bulk density of two powders of similar size and shape, one with known effective density and the other unknown (Svarovsky, 1987). Assuming the void fraction at maximum bulk density to be identical for both powders, the ratio of effective densities should be identical to the ratio of the bulk densities (Svarovsky, 1987). If the particles of known effective density differ in shape from those with the unknown density, an experimental factor (from 0.82 to 1.22) must be introduced to compensate for the difference in shape (Svarovsky, 1987). The method may give an approximation of the effective density, provided a particle with a known effective density of similar size and shape to the AIR® particles could be established.

Performing time of flight tests does not produce the desired results. Results indicate the particles have a d_{Aero} of 1-5μm particles, thus confirming the intended design of AIR® particles, but without revealing the effective density or the porosity of the particles.

The methods listed above provide consistent results and insight into the porosity of the particles, but do not supply a direct approach to determining either the porosity of the particles or the effective density. A method based on Ergun's 1951 paper uses flow and pressure drop data obtained from packed beds of powders to predict the effective density of porous particles (ρ_{eff}) (Svarovsky, 1987; Ergun, 1951). This method could provide Alkermes with a desired approach to characterization and is worthy of examination.

2.4 Pressure Drop in Packed Beds

Packed beds of materials have been well studied. The study of fluid flows in beds of packed particles is of interest in many fields. Geologists study the permeability of consolidated material such as sandstones in the interest of gas and oil exploration (Sahimi, 1995). Various industries are interested in the flow behavior of permeable or porous particles relative to the liquid in which the particles are immersed in flocculating beds or settling ponds (Masliyah *et al.*, 1987).

Darcy's Law is a macroscopic description applicable for low Reynold's number systems (Darcy, 1856). Darcy's Law is the basis of most packed bed correlations. Limits to Darcy's Law include the study of particles that deviate strongly from spherical shape, particles that possess a broad particle-size distribution, or consolidated material (such as cement) (Nield and Bejan, 1992). Darcy's Law is not applicable to systems where the mean free path of gas particles approaches the pore size (Sahimi, 1995; Pruess and Persoff, 1998). However, this is not a concern as the mean free path of air at ambient temperature and pressure is approximately 70 nm, while the particles to be studied possess diameters greater than 1 μm, or 1000 nm.

Refinements to Darcy's law by Dupuit, Slichter (Wyllie and Gardner, 1958, Wyllie and Gardner, 1958), Forchheimer (1901), Blake (1922), Kozeny (1927), Burke and Plummer (1928), and Carman (1937) led to Ergun's work that combined both the viscous and kinetic regimes of flow through packed beds in a semi-empirical equation.

2.5 Ergun's Method

Ergun developed a method of determining the effective density in 1951. Ergun's technique exploits the dependence of the bulk density on the void fraction in both viscous and kinetic flow regimes.

Ergun introduced a known mass of powder into a tube, and then aerated the bed by flowing upwards and vibrating the bed to various bulk densities. The height of the bed is directly proportional to the void fraction of the bed of particles. As the bed expands, the space between the particles becomes larger and the void fraction increases. As the bed height is reduced, the particles become more tightly spaced. This results in a reduction in the void fraction. Since the bulk density is a function of the void fraction, the variation in bed height determines the bulk density.

Once the bed height was set, Ergun reversed the flow (now downwards) and measured the pressure drop versus flow-rate. The Ergun method requires acquiring pressure drop versus flow-rate at several different bed heights. As such, this routine was repeated for several different bed heights.

Fitting the pressure drop and velocity data at low flow rates in the viscous regime to the following equation using least squares regression determines the slope (value of a) at each bed height or ρ_{Bulk}:

$$\frac{\Delta P}{l} = aU \tag{3}$$

Where ΔP/l is the pressure gradient and U is the superficial velocity. The following derivation allows us to find ρ_{Eff} from the bulk density and corresponding slope (a). Since the slope, a, is a function of porosity, ε, as follows (Ergun, 1951):

$$\frac{\Delta P}{l} = a' \frac{(1-\varepsilon)^2}{\varepsilon^3} U \tag{4}$$

The relationship between effective density and bulk density can be written as follows:

$$\varepsilon = 1 - \frac{\rho_{Bulk}}{\rho_{Eff}} \tag{5}$$

Rearranging equation (3) yields:

$$\frac{\Delta P}{lU} = a \tag{6}$$

Substituting equation (5) and (6) into equation (4) yields:

$$a = \frac{a'(\rho_{Bulk} / \rho_{Eff})^2}{(1-\rho_{Bulk} / \rho_{Eff})^3} \tag{7}$$

Rearranging equation (7) gives:

$$\rho_{Eff} - \rho_{Bulk} = \rho_{Eff} \left(\frac{a'}{\rho_{Eff}^2} \right)^{1/3} \left(\frac{\rho_{Bulk}^2}{a} \right)^{1/3} \tag{8}$$

Since ρ_{Eff} is constant, equation (8) reduces to:

$$\rho_{Bulk} = \rho_{Eff} - a'' \left(\frac{\rho_{Bulk}^2}{a} \right)^{1/3} \tag{9}$$

Plotting ρ_{Bulk} versus $(\rho_{Bulk}^2/a)^{1/3}$ as in equation (9) reveals ρ_{Eff} as the y-intercept. This method assumes that the constant a' is identical for all void fractions. This assumption is not entirely true as the tortuosity factor may vary with the void fraction. However, the error induced is considered to be less than 10% (Svavorsky, 1987).

An analogous treatment in the kinetic regime will also expose an equation that relates effective density to the bulk density with ρ_{Eff} as the y-intercept (Ergun, 1951). However, this thesis will deal only with the low flow regime. The study of only one flow regime provides a straight-forward experimental setup. The low flow regime was chosen as the simpler of the two regimes to study.

In 1952, Ergun proposed a semi-empirical equation that unites data from a plethora of studies in both the viscous and kinetic regimes with the theoretical developments of Blake, Kozeny, and Carman as follows:

$$\frac{\Delta P}{l} = 150\frac{(1-\varepsilon)^2}{\varepsilon^3}\frac{\mu U}{d_P^2} + 1.75\frac{(1-\varepsilon)}{\varepsilon^3}\frac{\rho_f U^2}{d_P} \tag{10}$$

where ρ_f is the fluid density (Ergun, 1952). Macdonald *et al.* (1979) revisited Ergun's equation using data from several contributors. Macdonald *et al.* (1979) propose that the coefficients determined by Ergun should be revised so that the Ergun equation appears as:

$$\frac{\Delta P}{l} = 180\frac{(1-\varepsilon)^2}{\varepsilon^3}\frac{\mu U}{d_P^2} + 1.8\frac{(1-\varepsilon)}{\varepsilon^3}\frac{\rho_f U^2}{d_P} \tag{11}$$

Among the conclusions of their study suggest that the Ergun equation is the most suitable overall equation for porosities ranging from 0.36 to 0.92. Although other equations are more accurate within narrow porosity ranges, the Ergun equation should predict the pressure drop for a wide variety of unconsolidated material to within 50% (Macdonald *et*

al., 1979). No mention of the suitability of Ergun's equation for permeable particles is given.

Some authors have extrapolated these findings to determine either the specific area or diameter of the particles using the viscous portion of equations (10) or (11) (Casal *et al.*, 1985; Oh *et al.*, 2001; Margiatto and Siegell, 1983), also known as the Carman-Kozeny, Blake-Kozeny, or Carman-Blake-Kozeny equation. Since the void fraction may be calculated using equation (5), the viscous portion of the Ergun equation (10) or (11) may be rearranged to yield the diameter as follows:

$$d_P = \sqrt{\frac{A(1-\varepsilon)^2 \mu}{\varepsilon^3 a}} \tag{12}$$

where A is the viscous regime constant from the Ergun equation. Ergun determined A to be 150 (Ergun, 1952). Macdonald *et al.* (1979) discovered A to be 180. The diameter determined with the value determined by Macdonald *et al.* is less than 10% higher than that determined with the value Ergun found. A will be taken as 180 forthwith.

2.6 Richardson and Zaki

Richardson and Zaki (1954) undertook a theoretical treatment of the viscous drag force exerted by a swarm of highly permeable particles relative to a fluid at low velocities. Richardson and Zaki developed a semi-empirical equation that takes the form:

$$\frac{\Delta P}{l} = \frac{18}{d_p^2} \mu U \frac{(1-\varepsilon)}{\varepsilon^{4.65}} \tag{13}$$

It has been proposed that a system of permeable particles is analogous to a swarm of particles (Neale *et al.*, 1973, Liu and Masliyah, 1996, Masliyah *et al.*, 1987). The swarm

proposal differs from the basis of the Ergun equation (that the flow through packed beds is equivalent to flow through channels formed by the particles). The Richardson-Zaki equation may provide a better estimate of the effective density than the Ergun equation as it takes into account flow within a permeable particle.

The following derivation is analogous to that performed by Ergun (1951) and allows us to determine the effective density (ρ_{Eff}) from the data collected using pressure drop in packed beds and the Richardson-Zaki equation. Again, the pressure drop and velocity data at low flow rates in the viscous regime should be fit to the following equation using least squares regression determines values of a at each ρ_{Bulk}:

$$\frac{\Delta P}{l} = aU \tag{14}$$

Assuming a constant fluid viscosity and constant particle diameter, the Richardson-Zaki equation (13) may take the following form:

$$\frac{\Delta P}{l} = a' \frac{(1-\varepsilon)}{\varepsilon^{4.65}} U \tag{15}$$

The relationship between effective density and bulk density is as follows:

$$\varepsilon = 1 - \frac{\rho_{Bulk}}{\rho_{Eff}} \tag{16}$$

Rearranging equation (14) yields:

$$\frac{\Delta P}{lU} = a \tag{17}$$

Substitution of equations (16) and (17) into equation (15) and rearranging yields:

$$a = \frac{a'(\rho_{Bulk} / \rho_{Eff})}{(1 - \rho_{Bulk} / \rho_{Eff})^{4.65}} \tag{18}$$

Rearranging equation (18) gives:

$$\rho_{Eff} - \rho_{Bulk} = \rho_{Eff}\left(\frac{a'}{\rho_{Eff}}\right)^{1/4.65}\left(\frac{\rho_{Bulk}}{a}\right)^{1/4.65} \tag{19}$$

Since ρ_{Eff} is constant, equation (19) reduces to:

$$\rho_{Bulk} = \rho_{Eff} - a''\left(\frac{\rho_{Bulk}}{a}\right)^{1/4.65} \tag{20}$$

Plotting ρ_{Bulk} versus $(\rho_{Bulk}/a)^{1/4.65}$ as in equation (20) reveals ρ_{Eff} as the *y*-intercept.

The diameter of the particle can be determined using equations (16) and (20). The Richardson-Zaki equation (13) may be rearranged to give:

$$d_P = \sqrt{\frac{18(1-\varepsilon)\ \mu}{\varepsilon^{4.65} a}} \tag{21}$$

2.7 Analytical Solutions and other Recent Studies

Casal *et al.* (1985) proposed a new method to determine the effective density of a powder using only two bulk densities; however, Svavorsky (1987) states that this method was developed by Gelhart (1986). In either case, should the Ergun method prove effective, these may provide for efficient analysis of the data collected.

Ergun dismisses the potential use of a completely analytical solution for the pressure drop in packed beds (Ergun, 1952). Ergun indicated that the factors affecting the pressure drop were too great in number and are not disposed to strict analysis.

Progress in mathematics (such as Brinkman's famous work in 1949) and computing power have contributed to our understanding of flow in packed beds. However, a review of the required data for implementation negates this approach.

A number of studies have delivered equations for describing flow through packed beds of either solid or permeable particles (Neale *et al.*, 1973, Matsumoto and Suganuma, 1973, Masliyah and Polikar, 1980, Davis and Stone 1993, Du Plessis, 1994, Liu and Masliyah, 1996, Margiatoo and Siegel, 1993). The conclusions may indicate that the permeability of a particle may contribute greatly to the overall permeability of a packed bed, especially for either small or highly permeable particles (Neale *et al.*, 1973, Davis and Stone, 1993). In most cases, the equations mentioned above require the diameter and/or the permeability of the particles. Some authors claim that the knowledge of the particle diameter is simply acquired (Margiatoo and Siegel, 1993), while others require the internal porosity of the particle to scale the permeability (Martys *et al.*, 1994). This may be true of some methods (such as pycnometry and geometric diameter determination by sieve sizing) available to other fields of research, but those methods are incompatible with the AIR® particles. This limits the potential for determining the effective density through packed beds to semi-empirical equations such as the Ergun and Richardson-Zaki equations.

3.0 Experimental Setup

The schematic diagram of the experimental setup is shown in Figure 1. Detailed specifications for the column are shown in Table 1.

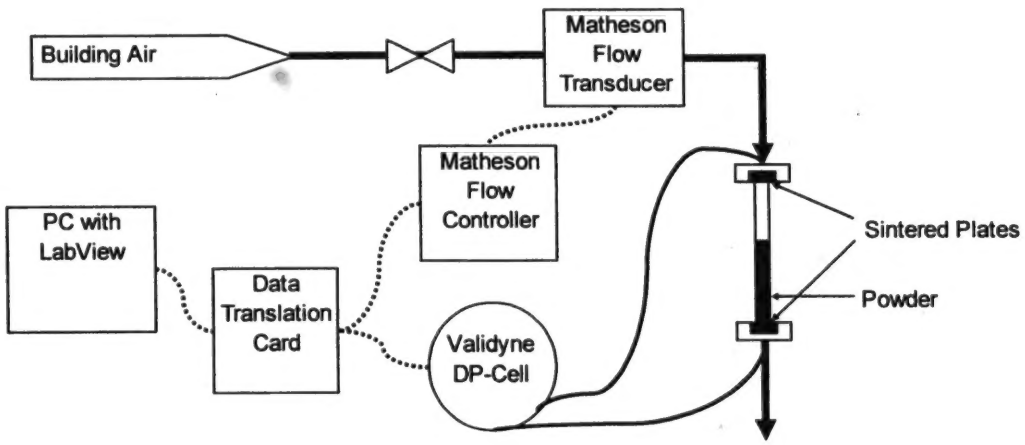

Figure 1. Schematic Diagram of Experimental Setup

Table 1. Plexiglass™ Column Specifications.

Column Internal Diameter	19 mm
Column External Diameter	25 mm
Flange Diameter	89 mm
Sintered Plate Diameter	28 mm
Column Height, Flange to Flange	300 mm

The column, with an inner diameter of 19mm, was constructed of Plexiglass™. The column was originally fitted with pressure taps along the side, but these were removed as the taps filled with powder on several occasions.

The air was dry and is processed through a molecular sieve unit at the University of Alberta Physical Plant. No moisture collected in the piping when the air was flowed through an ice bath for several hours.

The air flow rate was controlled and measured using one of two Matheson Mass Flow Transducers and the Matheson Multiple Flow Controller (Model 8274). The mass flow transducers were calibrated with a bubble column and stopwatch. Figures 2 and 3 show the calibration equations for both Matheson flow transducers.

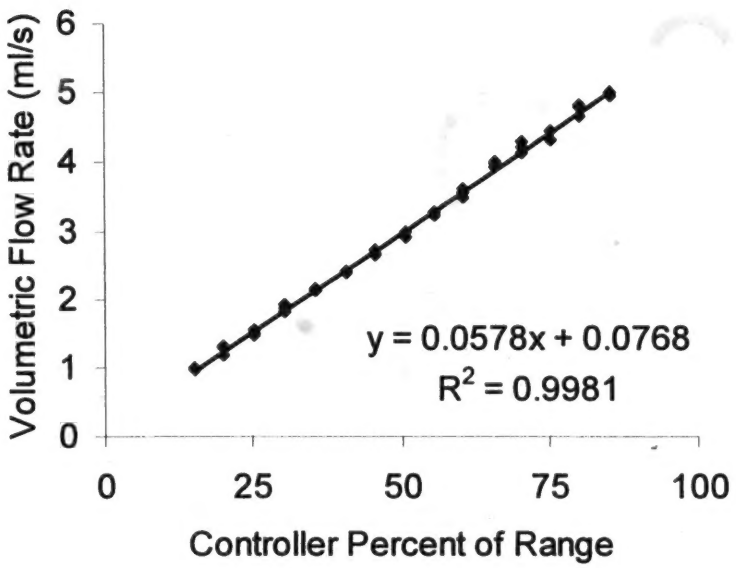

Figure 2. Volumetric Flow Rate versus Controller Percent of Range Reading for the Matheson 8272-0432 Mass Flow Transducer.

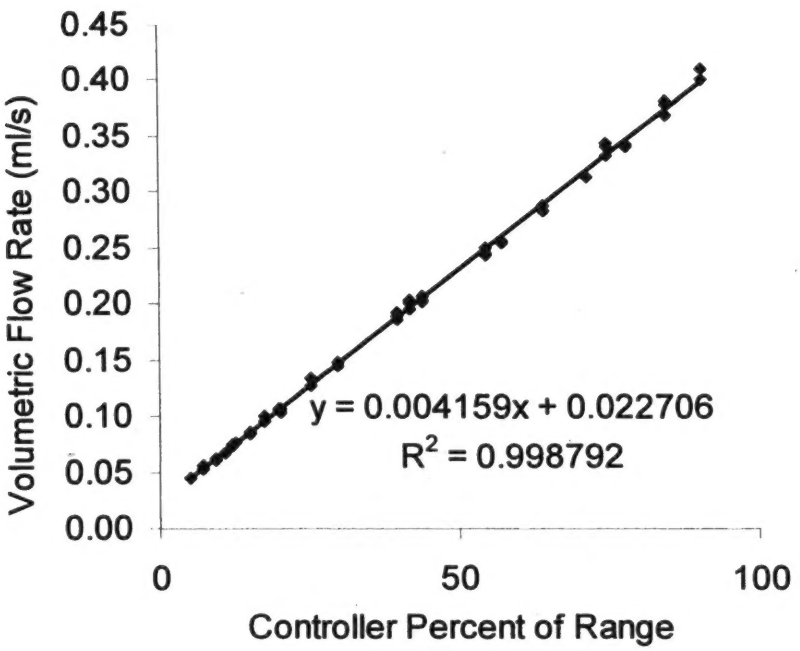

Figure 3. Volumetric Flow Rate versus Controller Percent of Range Reading for the Matheson 8272-0421 Mass Flow Transducer.

A Validyne Ultra Low Range Wet-Wet Differential Pressure Transducer (0-3.5 inH2O) with an accuracy of ±0.25% of full scale is used to measure the pressure drop across the packed bed.

The analog signals from the mass flow controller and DP-Cell were connected to a Data Translation card. The Data Translation card converted the analog signals into digital signals. These were transmitted to the PC via a USB port. The PC supports both the USB connection from the Data translation Card and the National Instruments LabVIEW 6i. National Instruments LabVIEW 6i records and displays the data.

3.1 Experimental Procedure

The description of a typical run to collect data for the 135 μm glass spheres is detailed below:

1. The first step is to charge the column with a known mass of powder. This is done by weighing the column before and after filling or by weighing the powder on tray prior to loading into the column.
2. The column was secured to a support and leveled. The data acquisition system was started to record the flow and pressure drop as a function of time.
3. First, the flow of air was set to flow upwards through the column to fluidize the powder while using a personal vibrating massager to set the packing height (and, hence, the bulk density). Superficial velocities required to partially fluidize the 135 μm glass spheres were 5 to 10 mm/s.
4. The air flow and the vibration were stopped. The height was measured with a laser level. The mass and height information were used along with the column internal diameter to determine the bulk density.
5. The air flow was reversed to flow downwards through the column to measure the pressure drop. Record the volumetric flow-rate and pressure drop. Alter the flow. Collect 6 to 12 flow rate and pressure drop data points for every packing height. Data should be collected over as large a range as possible. The flow rate should not alter the packing height to avoid altering the bulk density and it should not be such that the range of the DP-Cell is exceeded to ensure an accurate reading. Allow some time (10 to 300 seconds) for the pressure reading to stabilize. In

Ergun's study, the data was collected data at the highest flow-rate first to prevent changes in the packing (1951). In the present study, the pressure drop measurements were begun at the highest flow-rate. The maximum flow rates were determined based on two criteria.

6. The air flow direction was then reversed to set a new packing height. Reset the packing to a new height and repeat the experiment. Collect data at 2 to 5 different packing heights.

Alternative methods of setting the packing height involve tapping or vibrating the column without flowing upwards to set the bulk density. The packing may be also compressed by downwards air flow. Data collected using these different methods of setting the packing height may be seen in the results section. Other researchers have vibrated the packing without upwards flow to set the packing height (Casal *et al.*, 1985).

The error in the effective density was calculated using the method described by Holman (1978). An average of the error for every point was used to determine the error in the ratio of pressure gradient divided by the superficial velocity, $\Delta P/l/U$, or slope, a. Average values of ρ_{Bulk} and a were used to calculate the error in the case of ρ_{Eff}. The error in the pressure measurements was stated as 0.25% of the full range, or 0.00875 inches of H_2O, the error in the flow meters was taken as 0.1 ml/s for the Matheson 8272-0432 and 0.0095 ml/s for the Matheson 8272-0421, the error in the height measurement was taken as 0.5 mm, and the error in the diameter was taken as 0.1 mm.

3.2 Materials

3.2.1 175 μm Glass Spheres

Glass spheres were obtained from B. Braun Melsungen (Catalogue # 854150). The quoted size range of the particles is 0.17 to 0.18 mm. These particles were used to verify the experimental setup. The density of glass is given as between 2.18 and 2.60 g/cm^3 by Perry and Green (1984). Kirk-Othmer (1991) lists the density of glass as between 2.13 and 5.42 g/cm^3 with an average of 2.60 g/cm^3. Only a few, use-specific glasses have densities listed above 2.9 g/cm^3. Other references list the density of glass as between 2.225 and 2.500 g/cm^3 (Incropera and DeWitt, 1996).

3.2.2 135 μm Glass Spheres

The 135 μm glass spheres were sieved the particles to obtain the required size. The stated diameter of the particles is 135 μm and the stated density is 2.65 g/cm^3. The particles were mono-distributed.

3.2.3 175 μm and 135 μm Glass Spheres

In order to resolve the influence of size distribution on the Ergun equation, 100g of 175 μm glass spheres was mixed with 100g of 135 μm glass spheres. The spheres were agitated together in a beaker by hand to induce mixing in attempt to achieve a bimodal blend of the two sets of glass spheres.

3.2.4 Pharmatose

A sample of Pharmatose DCL 11 was obtained from DMV International (lot number 10094615). Pharmatose DCL 11 is a free-flowing, spray-dried, α-lactose monohydrate

(>99.0%) intended for direct compression into tablets. The certificate of analysis states the median size of the particles as 110 ± 25μm. SEMs were used to observe the size, size distribution, and shape of the Pharmatose DCL 11 particles. Literature values for the solid density of lactose are between 1.525 and 1.540 g/cm^3 (Ash and Ash, 2003; Rowe *et al.*, 2002).

3.2.5 Respitose

A sample of Respitose SV003 was obtained from DMV International (lot number 10105473). Respitose SV003 is a α-lactose monohydrate (>99.0%) intended for dry powder inhalation. The certificate of analysis states the portion of particles below a size of 32μm as 9.0%, below 63μm as 92.0% and below 100μm as 100.0%. SEMs were used to observe the size, size distribution, and shape of the Respitose SV003 particles. Literature values for the solid density of lactose are between 1.525 and 1.540 g/cm^3 (Ash and Ash, 2003; Rowe *et al.*, 2002).

3.2.6 Sigma-Aldrich Lactose

α-lactose (milk sugar) monohydrate was obtained from Sigma (catalog number L-8783, lot number 30K0189). No size was specified for the particles. SEMs of the α-lactose were used to determine the approximate size of the particles.

3.2.7 Alkermes Representative Porous Pharmaceutical Powder

Alkermes provided 3 AIR® technology samples (A, B, and C) of a powder consisting of representative porous pharmaceutical powder (Lot # 403080). Sources cite the effective

density of the large, porous particles as less than approximately 0.1 to 0.4 g/cm^3 (Edwards *et al.*, 1997, Batycky *et al.*, 1999).

Some powders are hydroscopic and may adsorb water from the air. This may swell the particles or even fill the internal pores of the particles. To maintain consistency, these powders were desiccated in a desiccator for at least 24 hours prior to packing the column.

4.0 Results and Discussion

4.1 Validation of Apparatus

Dry pharmaceutical powders are an important new improvement to the method of aerosolized drug delivery and could be applied to the treatment of a variety of diseases. Crucial design attributes for the dry powder inhalation of therapeutics are the reproducibility of the dose and particle size distribution. For deep lung delivery of the therapeutic agent, the powders have to be very small. Characterization of these micron-sized powders poses a significant technical challenge. The purpose of this study was to determine if dry pharmaceutical powders (therapeutic agents and excipients) could be characterized by a classic equation developed by Ergun in which the pressure drop across a packed bed is measured at different gas velocities. If successful, this method could be used to determine both effective particle density and mean particle diameter.

4.1.1 Validation using Glass Spheres

To apply the pressure drop method to the characterization of dry pharmaceutical powders, a device was constructed similar to those used for the characterization of sand, coke and catalyst particles (Sahimi, 1995). Validation of the experimental apparatus was done using pressure drop experiments that were conducted using well characterized spherical, essentially mono-distributed glass spheres. Using spherical particles with a narrow size distribution to verify the experimental approach was important as several researchers have identified non-spherical shapes (Ergun & Orning, 1949, Casal *et al.*, 1985) and broad size distributions (MacDonald *et al.*, 1979) as factors resulting in

disagreement between collected data and the results of Ergun's method. Two separate sets of 135 μm and 175 μm glass spheres were studied. These particles were ideal for testing and verifying the experimental method as Ergun used data from similarly sized sand particles and sieved coke (Ergun, 1951). An SEM of the 175 μm glass spheres is shown in Figure 4. The particles are spherical and approximately 175 μm in diameter. An SEM of the 135 μm glass spheres is shown in Figure 5. The particles are mostly spherical and approximately 135 μm in diameter. From the SEMs, it appears that the 135 μm glass spheres possess a larger size distribution and more shape variation than the 175 μm glass spheres. However, both sets of glass spheres appear to be mono-distributed in size.

Figure 4. Scanning Electron Micrograph of 175 μm glass spheres. Scale bar is 600 μm.

Figure 5. Scanning Electron Micrograph of 135 μm glass spheres. Scale bar is 600 μm.

Pressure drop across the packed bed and velocity data were collected according to the method described in the Experimental Setup section 3.0. A mass of approximately 15 to 20 grams of glass spheres was used. The velocities varied from 2 to 20 mm/s. The height, and hence the density, of the packing was varied by flowing air upwards through the column at different rates to obtain a stable packing density. Pressure drop was measured by flowing down through the column. Figure 6 and 7 show the pressure gradient versus superficial velocity for various bulk densities for the 135 μm and 175 μm glass spheres, respectively.

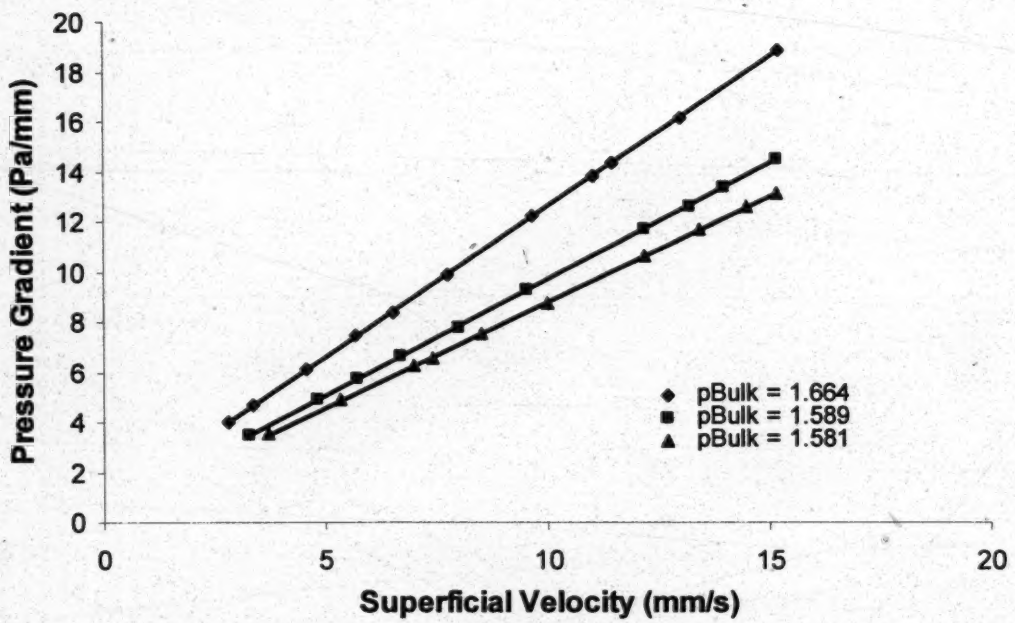

Figure 6. Typical data for pressure gradient versus velocity (for downward flow) for the 135 μm glass spheres. Bulk density given in g/cm^3. Lines are trends in the data.

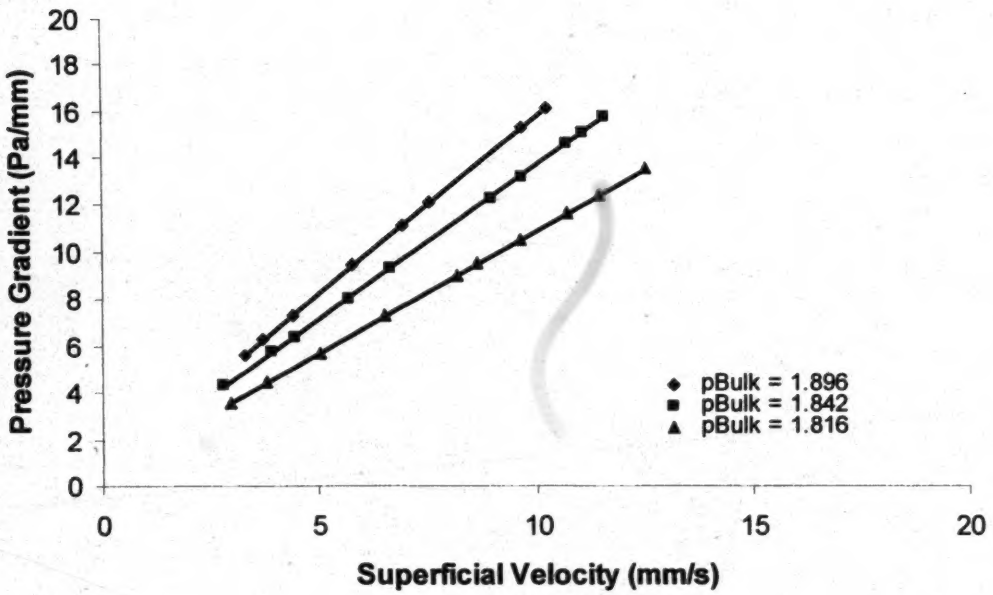

Figure 7. Typical data for pressure gradient versus velocity (for downward flow) for the 175 μm glass spheres. Bulk density given in g/cm^3. Lines are trends in the data.

The relationship between the pressure gradient and the velocity for each of the bulk densities tested were linear for both sizes of particles. Importantly, the intercepts of the lines passed through the origin in every case. This is important because, while the pressure drop associated with very low gas superficial velocities cannot be measured reproducibly, for a velocity of zero a pressure gradient of zero was expected from both Darcy's equation (1856) and Ergun's work (1951). As the bulk density increased, the slope (*a*) of the pressure gradient vs. superficial velocity plot increased as expected from equation (3). At a given superficial velocity, as the bulk density increased, the corresponding pressure gradient increased as well. Both of these observations were due to the reduction in void fraction and are in agreement with Ergun's equation (1952).

In order to determine the effective density, which is equal to the solid density for solid, non-porous particles, the bulk density is plotted versus $(\rho_{Bulk}{}^2/a)^{1/3}$. The *y*-intercept of this line is taken as the effective density. For the 135 and 175 μm glass spheres, this relationship is presented in Figures 8 and 9, respectively. Using linear regression, the density of the 135 μm glass spheres was determined to be 2.73 ± 0.06 g/cm^3. This result is within the range of the stated density for the glass spheres, from 2.18 g/cm^3 to 2.90 g/cm^3 (Kirk-Othmer, 1991) and is within 3% of the stated density of 2.65 g/cm^3. For the 175μm glass spheres, the density was determined to be 2.93 ± 0.04 g/cm^3. This result was also within the range of the density for the glass spheres.

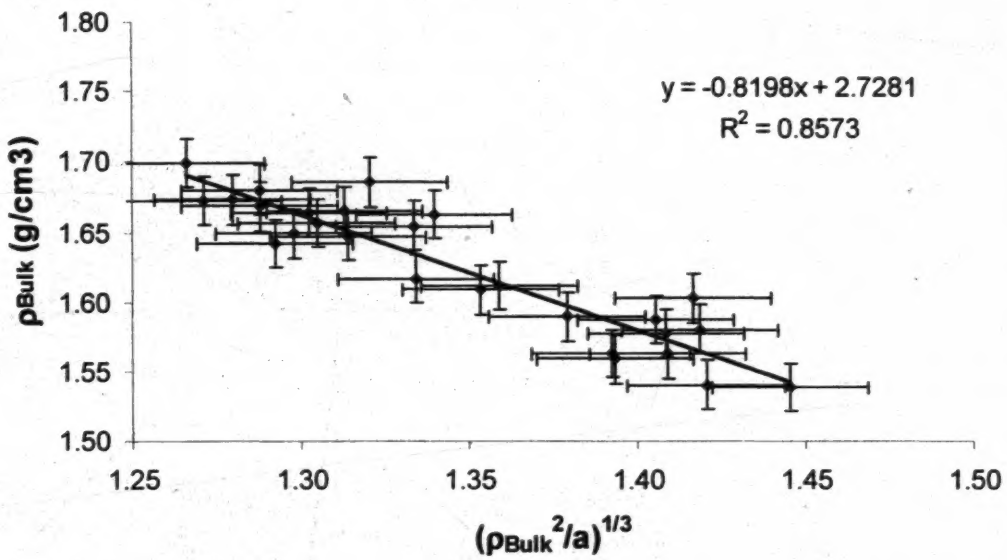

Figure 8. Pressure drop method for characterizing 135 μm glass spheres. The line is a linear regression of the data.

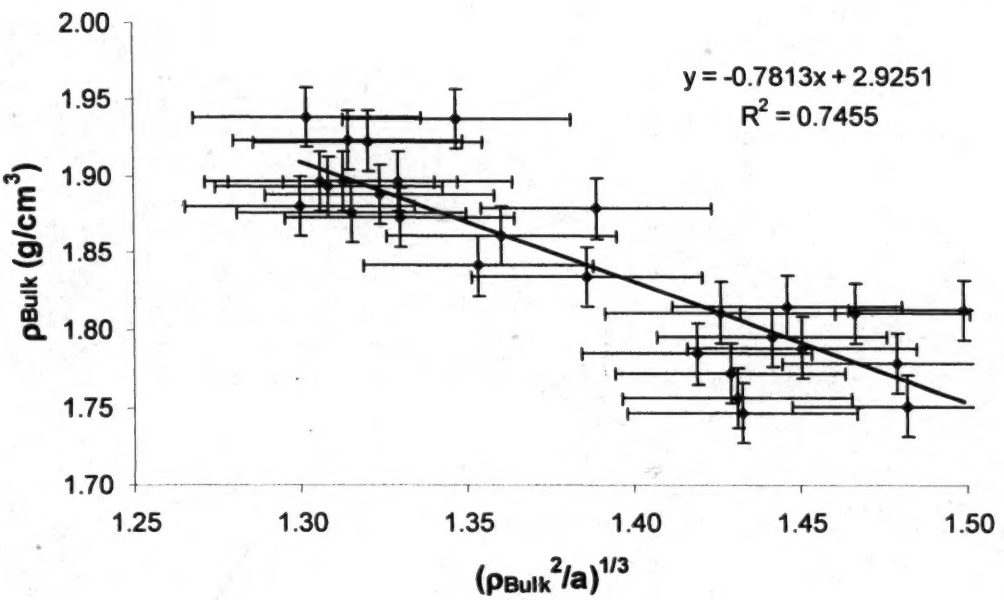

Figure 9. Pressure drop method for characterizing 175 μm glass spheres. The line is a linear regression of the data.

The mean particle diameter was also calculated using the experimental data presented in Figures 8 and 9. First, the effective particle density that was determined from the pressure drop data was used to calculate the void fraction of the column at various bulk densities using equation (16). The particle diameter was then determined using the Blake-Kozeny portion of the Ergun equation with the Macdonald *et al.* modification, equation (12). Using an effective particle density of 2.73 g/cm^3 for the 135 μm particles, the calculated mean particle diameter was 130 μm. This result was within 4% of the stated value of the diameter and is close to that observed in the SEM in Figure 5. For the 175 μm glass spheres, the diameter as determined by the Blake-Kozeny equation was 141 μm. This result was within 20% of the stated value of the diameter. A scanning electron

micrograph (Figure 4) reaffirms the particles are spherical and approximately 175 μm in diameter. The larger error associated with the diameter prediction of the 175 μm particles may be a result of the propagation of the error in the measurement of the effective particle density.

Sources of error in the prediction of both the effective particle density and the mean diameter were attributed mainly to four sources: bed packing uniformity and the measurement of bulk density, flow rate and pressure drop. The error in the effective density was calculated using the uncertainty analysis method first described by Kline and McClintock (1953) as detailed by Holman (1978). In this method, the uncertainty propagation depends on the squares of the uncertainties in each of the independent variables. An average of the error for every point was used to determine the error in the ratio of pressure gradient divided by the superficial velocity, $\Delta P/l/U$, or slope, a.

Uniformly packing the bed of particles is critical for the pressure drop measurements. When the air flowed upward through the packed bed, occasionally "bubbles" were observed on a portion of the surface. Svarovsky (1987) referred to this phenomenon as volcanoes. These volcanoes were attributed to high porosity channels created by the localized high flow rates within the bed. Beds containing high porosity channels would offer lower resistance than a uniform bed of randomly packed particles. It was therefore important to avoid collecting data from packed beds influenced by volcanoes. If "volcanoes" were to occur, the values of ρ_{Bulk} and a would be distorted. Generally, the value of a would be lower than expected and this would result in a higher than expected

value of $(\rho_{Bulk}{}^{2}/a)^{1/3}$. All of the points affected by volcanoes should lie above the regression line. Other data points that are outside of the error of the linear regression are most likely caused by systematic errors such as glass spheres penetrating the pressure taps, which leads to a lower than expected bed height, or poor execution of the method. Figure 10 shows the pressure drop data for the 135 μm glass spheres with eleven additional measurements outside of the error of the linear regression. The R^2 of the fit decreased from 0.86 to 0.52 and the predicted effective density decreased slightly from 2.73 to 2.68 g/cm^3, but the change is within error (± 0.06 g/cm^3).

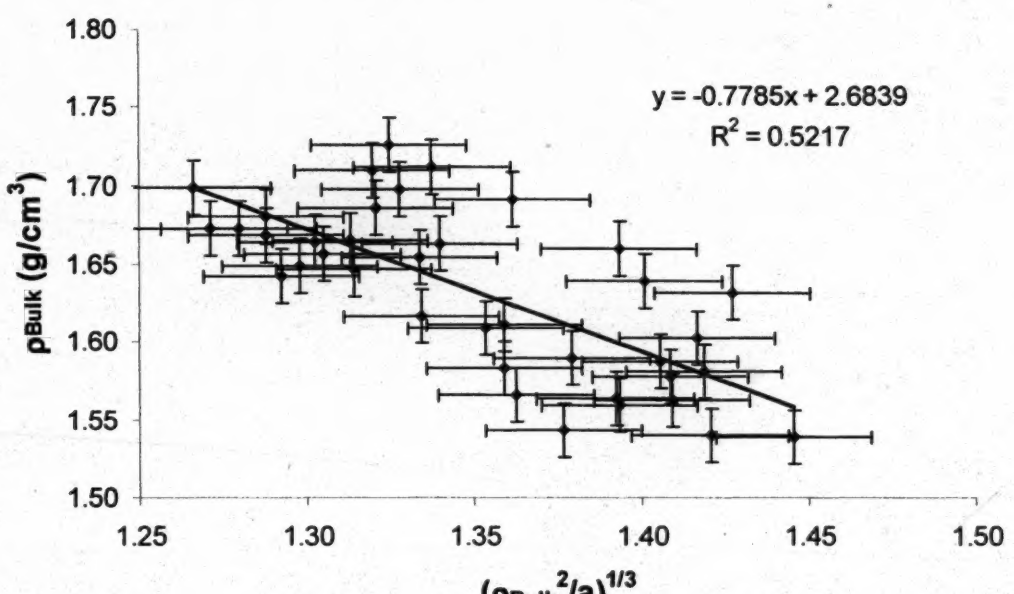

Figure 10. Pressure drop method for characterizing 135 μm glass spheres including data points outside of the error of the linear regression. The line is a linear regression of the data.

Another source of error is in the measurement of the bulk density of the bed. After the bed was expanded by flowing air upwards through the bed and vibrating the column, the air was stopped and the height of the bed was measured. In this phase of the study, the bed height was measured by eye using a ruler. The error in the height measurement was estimated to be ± 2 mm. Once this measurement was identified as a major source of error, a laser level was used to measure the height of the column to within approximately ± 0.5 mm. This improved method was used to determine bulk densities of all subsequent packings reported in this thesis.

Further sources of error were associated with the measurement of the gas flow rate and the pressure drop across the packed bed. The same flow controller was used to control the entire range of gas velocities. Thus, there was a larger relative impact of the error when controlling the lower air flow rates. In Figures 8 and 9, it can be seen that the horizontal error bars for the 175 μm glass spheres were slightly larger than those shown in the corresponding data for the 135 μm glass spheres. In part, the difference in calculated errors was attributed to the lower gas velocities used to characterize the larger glass spheres; this can be seen by comparing Figures 6 and 7. In this phase of the study, a manometer was used to measure the pressure drop across the packed bed. The relative error of the measurement increased with lower pressures. For the characterization of the subsequent particles, this manometer was replaced with a high quality pressure transducer.

Based on the agreement between the results of the analysis of the data and the literature and stated values for the 135 μm and 175 μm glass spheres, it is concluded that the approach taken herein adequately describes systems of mono-dispersed, spherical particles in the general size range of some pharmaceutical powders. The good agreement between the predicted and literature values for both the solid density and diameter indicates that the experimental method may be used effectively to characterize dry pharmaceutical powders. These preliminary results coupled with improvements in the experimental technique appear to reproduce the experimental method employed by Ergun and warrants the extension of the study to the application of the method to actual pharmaceutical particles.

4.1.1 Bimodal Distribution of Spherical Particles

Pharmaceutical powders used in inhalation therapy may not consist of a mono-dispersed particle sizes. Accordingly, the distribution may not be as narrow as that of the mono-dispersed glass spheres above. It was therefore important to discover the limitations of the Ergun method with regards to the particle size distribution. In this section, the influence of a bimodal particle size distribution on the results of the experimental method is explored. No literature was uncovered regarding the subject of packed bed experiments with particles possessing a bi-modal distribution. This does not allow comparison to prior studies and definite conclusions, but provides the basis for exploratory work of the effect of bimodal distributions upon the Ergun method.

The bimodal distribution was prepared by mixing equal masses of 175 μm and 135 μm glass spheres used in the previous section. Equal masses of the 175 μm and 135 μm glass

spheres were weighed and then poured into a beaker. The glass spheres were combined by re-pouring the blend of glass particles and then shaking the container by hand. This process was repeated at least a dozen times to ensure adequate mixing.

Figure 11 displays the experimental data for the relationship between ρ_{Bulk} and $(\rho_{Bulk}{}^{2}/a)^{1/3}$ for the mixture of 175 μm and 135 μm glass spheres. The relationship reveals a density of 2.78 ± 0.03 g/cm^3. This is within the range of density for glass (Kirk-Othmer, 1991). The predicted diameter of 134 μm is within 16% of the average diameter of the bimodal distribution. The result in diameter of 134 μm may be representative of the increased influence of the smaller, 135 μm glass sphere particles. For wide particle size distributions, even a small fraction of smaller particles will cause the calculated diameter to be smaller (MacDonald *et al.*, 1979).

The 135 μm glass spheres could fill the spaces between the 175 μm glass spheres. The channels formed between the two different glass spheres would more closely resemble those of the 135 μm glass spheres in size and shape. The air would then flow through channels resembling those of the 135 μm glass spheres. No further analysis or data was collected to explore this theory.

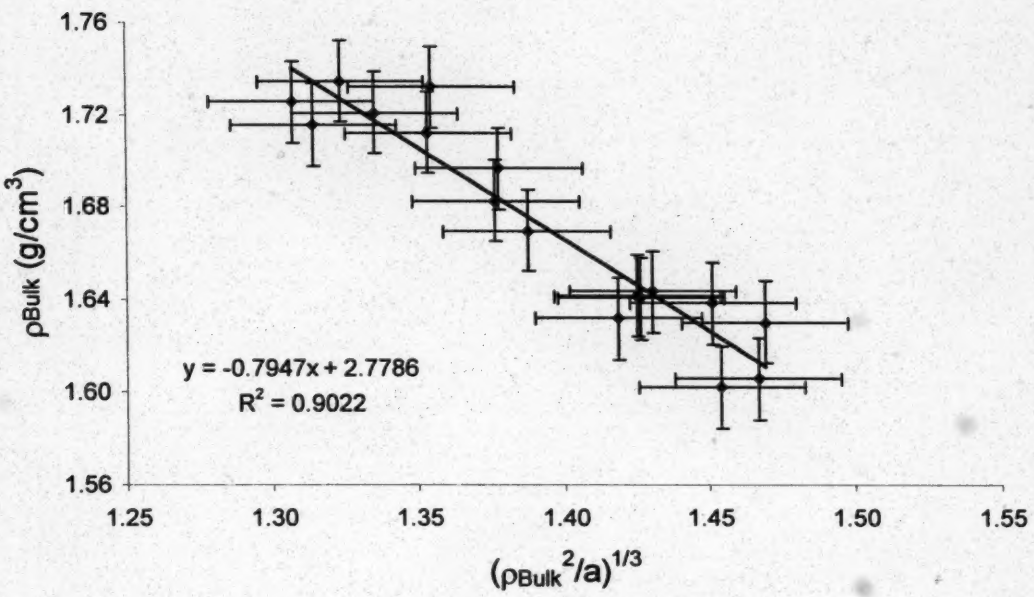

Figure 11. Ergun Method for 175 μm & 135 μm glass sphere mixture. Line is a linear regression of the data.

The improvement in the accuracy and precision from the data collected, due to the addition of the pressure transducer and laser level, for the 135 μm glass spheres (Figure 10) to the 175 μm and 135 μm glass sphere mixture (Figure 11) is readily apparent. The impact of the laser level and pressure transducer may be seen in two areas. The accuracy has improved as the error bars for the 175 μm and 135 μm glass sphere mixture were smaller than those for the 135 μm glass spheres. The precision of the data appears to have improved as all of the data points were within error of the linear regression. This improvement in the quality of the data improves the reliability of the analysis and confidence in the subsequent conclusions.

In this case, a bimodal distribution of spheres where the diameters do not vary by more than 30% appear to be adequately modeled by the Ergun equation. The experimental procedure appears to be rigorous enough to study bimodal distributions of particles where two sizes differ by less than 30%. The influence of the smaller particles upon the results may not be representative, as substantiated by the calculated diameter of 134 μm (MacDonald *et al.*, 1979). This qualifies the method to study powders consisting of particles of significant size variations.

4.1.2 Non-Spherical Plate-Like Particles

The extension of the Ergun method to samples with broad size distributions of particles of non-spherical particles could verify the application of the method to a variety of particles. To evaluate non-spherical plate-like particles, the Ergun method was tested with lactose particles manufactured using a cake drying method, as opposed to the spray-drying method used to manufacture the Pharmatose and the Respitose particles.

An SEM of the lactose is shown in Figure 12. From the SEM, the particles appear solid, but non-spherical and widely distributed in size (1 to 150 μm), more so than any other powder studied herein. The smaller particles will tend to lower the porosity assumed for fluid passage, causing higher than expected pressure drops (Pagano *et al.*, 1998, Narayan *et. al.*, 1997). This would yield similar results to those observed with the mixture of 135 and 175 μm glass spheres presented in section 4.1.1. The non-spherical shapes include plates, which could induce horizontal flow that deviated from the assumed flow within channels. Some authors stated that even Darcy's Law may not be suitable for broad particle distributions (Nield & Bejan, 1992).

Figure 12. Scanning Electron Micrograph of Sigma-Aldrich Lactose particles. Scale bar is 60 μm.

The lactose was desiccated for at least 24 hours prior to use. Data was collected as described in the Experimental section. A mass of approximately 15 to 20 grams of lactose was used. The velocities observed were on the order of 1.5 to 4.5 mm/s. Figure 13 illustrates the least-squares fit between the bulk density ρ_{Bulk} and $(\rho_{Bulk}{}^{2}/a)^{1/3}$. The determined effective density is 0.52 g/cm^3. This is approximately a third of the solid density of approximately 1.53 g/cm^3 given by the literature (Ash and Ash, 2003, Rowe *et al.*, 2002). However, there is no evident relationship displayed in Figure 13 between ρ_{Bulk} and $(\rho_{Bulk}{}^{2}/a)^{1/3}$. It appears that the data do not comply with the application of the Ergun equation.

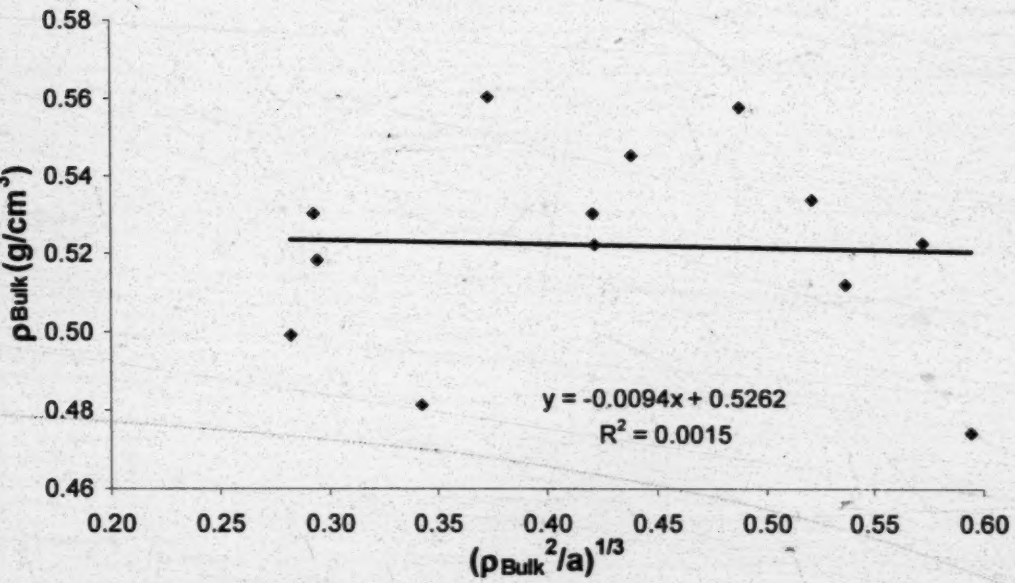

Figure 13. Ergun's Method for Sigma Lactose. The line is a linear regression of the data.

Further problems of applying the Ergun method to the Sigma-Aldrich lactose sample are displayed in Figure 14, which shows the relationship between the pressure gradient and the superficial velocity for four separate bulk densities. As expected, the relationships are linear and appear to pass through the origin. Ergun's equation (1952), however, predicts an increase in pressure drop with increasing bulk density at a given velocity. The increase in bulk density corresponds to a decrease in void fraction. A lower void fraction corresponds to a further restriction of the flow resulting in an increased pressure gradient. Figure 14 does not follow the expected pattern. The increase in bulk density does not correspond to an increase in pressure gradient at a given velocity. Furthermore, the measured pressure gradient was equivalent at two separate bulk densities.

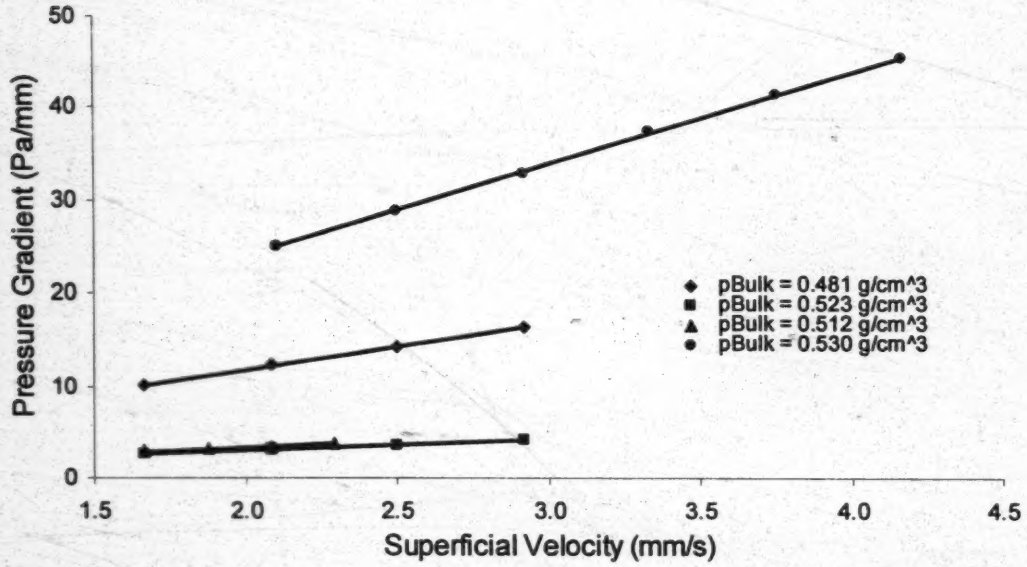

Figure 14. Pressure Gradient versus Superficial Velocity for Sigma Lactose. Lines are fits of the data.

The Ergun method was tested with cake dried, solid lactose particles consisting of highly non-spherical shapes. The particles also possessed a broad size distribution. There was no apparent agreement between the data and the literature density. The results of the analysis indicate that the particles were not subject to the Ergun equation, and, thus, not subject to the Ergun method. The Ergun method was deemed inappropriate to study the Sigma-Aldrich lactose as the particles had a large size distribution and were highly-non-spherical. This points to limitations cited by others (Nield & Bejan, 1992, MacDonald *et al.*, 1979) to the study of irregular, widely size dispersed particles using the Ergun method. It can be concluded that consideration should be given to both the size distribution and shape of the particles prior to employing the experimental method. However, the knowledge of the limitations of the method is useful as it provides a basis

with which to reject particles incompatible with Ergun's equation. This limitation should not be critical to the application of the Ergun method to the analysis of dry pharmaceutical powders, because cake drying is not generally used by the industry to formulate their inhaled powders.

4.2 Effect of Shape and Size Distribution

Pharmaceutical powders used in inhalation therapy may not consist of a mono-dispersed or strictly spherical particle sizes. The Sigma-Aldrich lactose is a prime example of the potential variation in size dsitributions that may be present. It is therefore important to discover the limitations of the Ergun method with regards to the particle size distribution before extending the study to micron-sized porous particles. In this section, the application of the Ergun method is explored for inhaled pharmaceutical excipients that are spherical or irregularly shaped.

4.2.1 Influence of Moderate Size Distribution and Slight Porosity

The dry pharmaceutical particles of primary interest to this thesis may not consist of perfectly spherical particles such as the glass spheres. The study of particles that are characterized as non-spherical or slightly porous would greatly aid in justifying the application of the Ergun method to characterize inhaled pharmaceuticals. The study of relatively large, excipient particles used by some pharmaceutical companies as carrier particles for inhaled drug therapy will prove ideal in this function and will further validate the Ergun method for use with micron-sized, porous particles. An example of one such type of sample is Pharmatose, a spray-dried α-lactose powder that is manufactured for use as an inhaled pharmaceutical excipient.

Pharmatose differs from the AIR® particles as the Pharmatose particles range in size from 10 to 200 μm in size. A SEM of Pharmatose is shown in Figure 15. It can be seen that the particles are spherical with a mean diameter of approximately 100 μm. The manufacturer states that the particles mean diameter is 110 ± 25 μm. The particles appear to have rough surfaces. From the SEM images, the particles do not appear to have large pores. Although the Pharmatose particles are essentially spherical and have a diameter on the same order of magnitude as the glass spheres, they differ from the glass spheres in two areas: the Pharmatose particles have rough surfaces and possess a wider particle size distribution than the two samples of solid, mono-dispersed glass spheres.

Figure 15. Scanning Electron Micrograph of Pharmatose. Scale bar is 600μm.

The pressure drop experiments for the Pharmatose packing were conducted as previously described for the glass spheres in section 4.1. The column was filled with 7 to 10 grams of powder. To avoid interference with atmospheric humidity (water can cause swelling) the powder was desiccated for at least 24 hours prior to use. Data was collected as described in the Experimental section.

To obtain pressure drop data, the sample was subjected to a downward flow of air. Unlike the glass spheres, Pharmatose was observed to compact due to downwards flow. The compaction is a reduction in the bed height (and an increase in the bulk density) due to

downwards flow. Ergun (1951) also noted this compaction and suggested the highest flow-rate or velocity should be measured first.

To determine the effect of compaction on the Ergun method, separate data were collected for un-compacted (aerated and vibrated) and compacted beds to observe whether the data were in agreement. Data was first collected by aerating and vibrating the bed. These data represented the un-compacted data. The rate of downward flowing air was then increased until compaction was observed. Pressure drop data was collected using these compacted beds. Both the un-compacted (or aerated) and compacted data are shown in Figure 16.

The compacted data points appear to be representative of the powder as the data points are within error of the least-squares regression line of the un-compacted data, indicating that compaction did not add any non-uniform structure to the bed. The effective density prediction did not change whether the compacted data were included in the Ergun analysis. This is in agreement with the alterations performed by other researchers who have tapped or vibrated the filled column without flowing upwards to set the packing height (Casal *et al.*, 1985, Svarovsky, 1987). This finding is important, because it allowed for the data to be collected over a larger range of velocities.

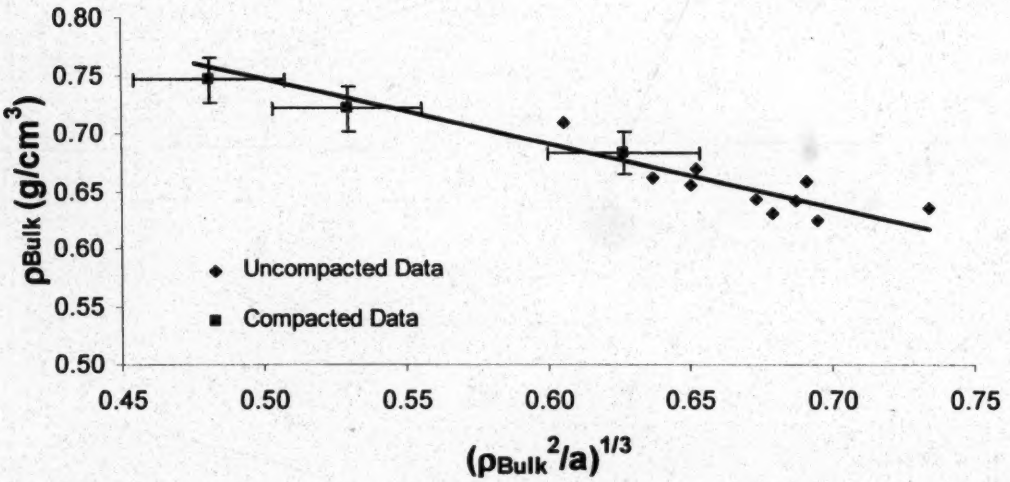

Figure 16. Plot of ρ_{Bulk} and $(\rho_{Bulk}^2/a)^{1/3}$ as per Ergun's Method for Pharmatose with the data segregated into compacted and un-compacted beds. The line is a linear regression of the un-compacted data points.

Pharmatose may be compacted without affecting the density determination by the Ergun method. It does not necessarily follow, however, that other powders tested in this study would behave similarly. Therefore, data collected for other powders were segregated to ensure there was good agreement between the un-compacted and compacted data prior to merging the data to determine the effective density.

Figure 17 displays the experimental data for the relationship between ρ_{Bulk} and $(\rho_{Bulk}^2/a)^{1/3}$ for the Pharmatose particles. The relationship reveals a density of 1.25 ± 0.03 g/cm^3, which is within 19% of the literature value of the solid density of approximately 1.53 g/cm^3 (Ash and Ash 2003, Rowe *et al.*, 2002). The linear regression fit was adequate with a R^2 value of 0.84 and all 18 data points within error of the least-squares line. The

error bars for $(\rho_{Bulk}^2/a)^{1/3}$ are larger than those seen in Figures 8, 9, and 10 for the glass spheres as the range of observable velocities was limited by the pressure drop measurement. The smaller Pharmatose particles created a larger pressure drop at a given velocity, hence, the limit of the DP-cell was reached at a lower velocity than for the glass spheres. Despite the larger error bars, the analysis delivers, as previously stated, a R^2 value of 0.84 and all 18 data points within error of the least-squares line.

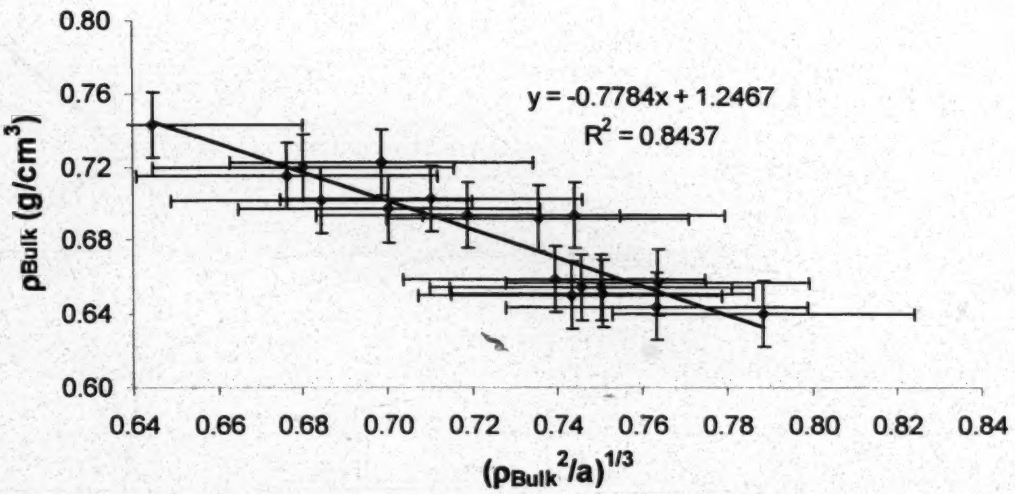

Figure 17. Ergun Method for Pharmatose. The line is a linear regression of data.

The average diameter as determined by equation (12) for Pharmatose, 92 μm, is within the stated average diameter of 110 ± 20 μm and that seen in the SEMs. This further supports the application of the Ergun method to porous particles.

Based on the agreement between the results of the analysis of the data and the literature and stated values for Pharmatose, it is concluded that the approach taken herein

satisfactorily describes the particles tested. This warrants the extension of the study to the application of the method to other pharmaceutical particles with a unimodal size distribution, including those possessing non-spherical shapes or broad size distributions.

4.2.2 Influence of Moderate Distribution and Non-Spherical Shape

The shape of inhaled pharmaceutical particles may not be entirely spherical, depending upon the source of the particles. The extension of this study to the application of the Ergun method to non-spherical particles of a relatively narrow size distribution will further justify the Ergun method's suitability to study micron-sized inhaled pharmaceuticals. Respitose was used to test the Ergun equation as the particles are highly non-spherical. A SEM of Respitose is shown in Figure 18. The particles include rough cubes, pyramids, and boxes with sides ranging in size from 20 to 180 μm in size. The particles appear to have solid and non-porous structure. The certificate of analysis states the portion of particles below a size of 32 μm as 9.0%, below 63 μm as 92.0% and below 100 μm as 100.0%.

The pressure drop experiments for the Respitose packing were conducted as previously described for the glass spheres in section 4.1. The column was filled with 5 to 7 grams of powder. The Respitose particles were also desiccated for at least 24 hours prior to use. During the pressure drop experiments, Respitose could be compacted by downwards flow; the same phenomena observed with the Pharmatose particles. As with the Pharmatose particles, the compacted and un-compacted data were in agreement.

Figure 18. Scanning Electron Micrograph of Respitose. Scale bar is 200 μm.

Figure 19 displays the relationship between ρ_{Bulk} and $(\rho_{Bulk}{}^{2}/a)^{1/3}$ for the Respitose particles, as well as the calculated errors. The relationship reveals a density of 1.30 ± 0.04 g/cm^3. This is within 15% of the literature value for the solid density of lactose of approximately 1.53 g/cm^3 (Ash and Ash, 2003, Rowe *et al.*, 2002).

However, the relationship is weak (R^2 value of 0.27). 5 of the 27 data points do not agree within error of the regression line. Two of those data points are part of the same experiment, the first performed of the series. It may be that powder volcanoes or a loss of powder to the taps affected the data collection, as appears to have occurred with the 135 μm glass spheres. The first experiment was also used to gauge the appropriate mass of

particles and velocities needed for subsequent experiment. These data points may suffer from additional error as a result.

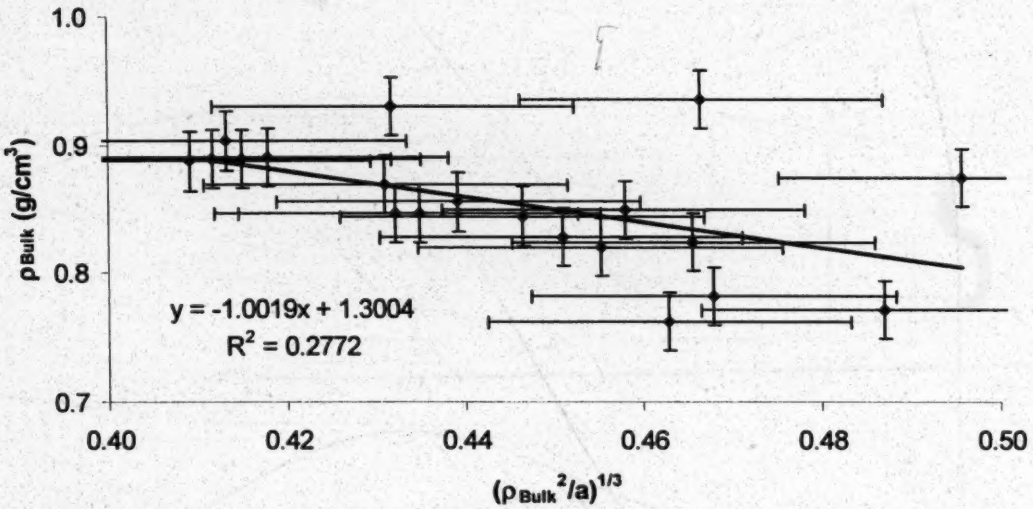

Figure 19. Ergun Method for Respitose. The line is a linear regression of the data.

Eliminating the first set of data (which contains two of the data points that are in disagreement with the linear regression) that appears to have a systematic error delivers a better fit. The new linear regression has a R^2 of 0.74 and 17 of 18 data points within error of the least-squares line. The data yield an effective density of 1.62 ± 0.04 g/cm^3. This is within 6% of the solid density of approximately 1.53 g/cm^3 given by the literature (Ash and Ash, 2003, Rowe *et al.*, 2002).

Using the effective density as 1.62 g/cm^3, the diameter was determined to be 32 μm. The diameter result from this analysis should be the mean diameter, which can be lower than the result of size analysis for particles of irregular shape (McDonald *et al.*, 1979). Considering both this fact and the mean diameter determined via the method, it may be

concluded that results agree with the stated value of the diameter from the manufacturer (which places 81% of the particles between 32 μm and 63 μm). The determined diameter is also within the size range of particles seen in the SEMs. These results support the extension of the study to other pharmaceutical particles, possibly even porous, micron-sized particles.

4.2.3 Discussion of the Effect of Shape on the Experimental Method

The Ergun method was successfully used to characterize lactose particles manufactured for use as excipients in dry powder inhalers. These particles consisted of solid, spherical and highly non-spherical particles that were not mono-dispersed in size. The agreement between the determined density and diameter and the literature density and the supplied size distribution appears to validate the experimental method for use with non-ideal particles. Attention to the sources of potential error may improve the accuracy of the method. These include volcanoes formed during bed expansion, elimination of the pressure taps, and utilization of the first run solely to gauge the amount of powder and flow rates required. The loss of mass to the pressure taps affected the accuracy of the bulk density. At a given height, the apparent bulk density would be higher than the actual bulk density due to the loss of mass in the column. This resulted in lower than expected pressure drops while performing experiments.

4.2.4 The Application of the Richardson-Zaki Equation to Solid Materials

The measurement of the pressure drop in packed beds coupled with the Ergun equation has shown success in predicting the effective density of spherical and non-spherical particles of narrow, wide, and bimodal distributions. However, the Ergun equation is

based upon solid, impermeable particles. The AIR® inhaled pharmaceutical particles have been described as porous and may not be impermeable.

The Richardson-Zaki equation (equation (13)) was developed for highly porous particles in packed beds and may provide an improved analysis of the porous inhaled pharmaceutical particles. To test if this method was generally applicable to porous and solid particles, the data collected for solid particles was analyzed using the Richardson-Zaki equation. Table 2 summarizes the results of applying both the Ergun and the Richardson-Zaki equation to the solid materials employed in this study.

Table 2. Summary of the density predictions of applying the Ergun and Richardson-Zaki equations to the solid materials

Material	Literature value of Density (g/cm^3)	Ergun Effective Density (g/cm^3)	Richardson-Zaki Effective Density (g/cm^3)
135 μm glass spheres	2.6 – 2.9	2.73	3.15
175 μm glass spheres	2.6 – 2.9	2.93	3.31
135 μm & 175 μm mixture	2.6 – 2.9	2.78	3.09
Pharmatose	1.53	1.25	1.39
Respitose	1.53	1.62	1.82

For all of the solid materials, the Richardson-Zaki equation gave higher predictions than the Ergun equation. For Pharmatose, the Richardson-Zaki equation gave better agreement

between the Pharmatose effective density and the literature value, but the diameter (as determined using equation (21)) was determined to be 55 μm, which is half of the stated value for the mean diameter.

One can conclude that the application of the Richardson-Zaki equation to solid particles in packed beds does not yield appropriate density or diameter values. This is logical as the Richardson-Zaki equation was developed for porous and permeable particles.

4.2.5 High Flow Rate Regime

The Ergun equation describes both a low flow rate, or viscous flow, regime and a high flow rate, or kinetic, regime. Either regime may be used to determine the effective density of particles. A comparison of the results of the two regimes can demonstrate the consistency of the measurements. However, many researchers limit experiments to the low flow rate regime (Casal *et al.*, 1985, Margiatoo & Siegel, 1983) when using the Ergun equation. The Richardson-Zaki equation was developed solely for the low flow rate regime.

Some preliminary data was collected with the 175 μm glass spheres at high flow rates (see Appendix A). Although the data appear to follow the patterns described by Ergun and may provide adequate determinations of the effective density, the high flow rate method was abandoned for several reasons. The method proved difficult as the packing would only remain stable in a small range of bulk densities. This limited the variation in the height of the packing, and, thus, the range over which the data could be collected. Given the compaction that was observed with both Pharmatose and Respitose, it was

probable that the representative porous pharmaceutical powder would only compact to one bulk density at high flow rates, negating the use of either the Ergun or Richardson-Zaki equations.

The pressure drops experienced with the 175 μm glass spheres was on the order of 205 kPa with velocities of ~25 m/s. In order to achieve the kinetic regime with the representative porous pharmaceutical particles, which are approximately $1/10^{th}$ the size of the 175 μm glass spheres, velocities of 250 m/s would be required (as calculated based on the Reynold's number). The pressure drops expected would be on the order of 20500 kPa, as the Ergun equation states that the pressure drop is proportional to the square of the velocity in the kinetic regime.

Most instrument and plant air systems operate at 550 kPa or less. This is true of the University of Alberta. It would be possible to use cylinders of compressed helium gas, which are available at pressures up to approximately 15000 kPa. This may be suitable. The use of helium will avoid a portion of the Joule-Thomson effect (as opposed to nitrogen) while maintaining a non-explosive exhaust gas (as opposed to hydrogen). The equipment designed for this program was not designed to handle these extreme conditions. Piping and vessels capable of handling such design pressures are expensive. Lowering the packing height to reduce the pressure drop is not an option unless a better method of measuring the packing height becomes available. Hence, the manufacture of such a system was beyond the scope and budget of this thesis.

4.3 Characterization of Porous Pharmaceutical Powders

The primary focus of this work was to develop a method to determine the effective density of highly porous micron-sized dry pharmaceutical particles. The pressure drop method developed in this thesis was tested against a representative porous pharmaceutical powder supplied and manufactured by Alkermes. The representative porous pharmaceutical powder was supplied as three separated samples, referred to hereafter as samples A, B, and C.

4.3.1 Characterization of Size & Distribution

Scanning electron micrographs of the representative porous pharmaceutical powder prior to use in the experimental setup are presented in Figures 20 and 21. The particles consisted of agglomerates of approximately 10 to 70 μm in size. The agglomerates were made up of smaller, spherical particles, ranging in size from 0.1 to 10 μm. This structure makes the agglomerates highly porous and permeable, and thus ideal for use as inhaled pharmaceuticals as outlined in the Introduction section. All three samples, A, B, and C, provided similar SEMs.

Figure 20. Scanning Electron Micrograph of Representative porous pharmaceutical particles. Scale bar is 600µm.

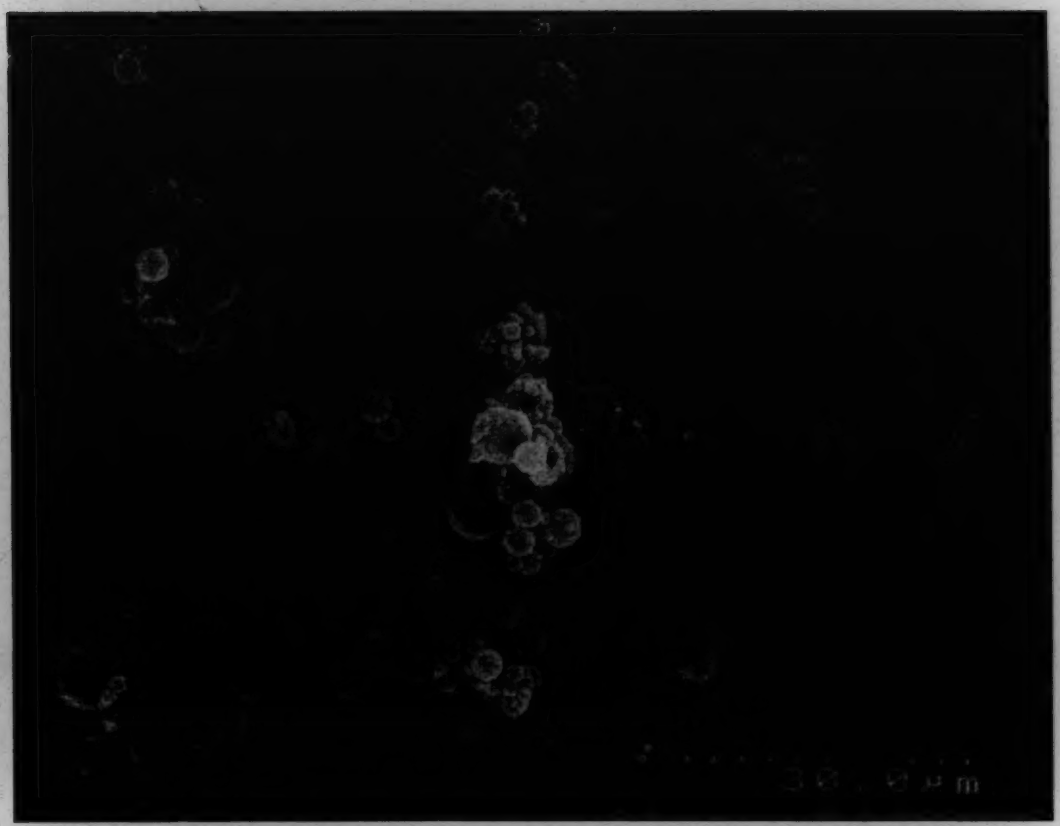

Figure 21. Close-up Scanning Electron Micrograph of a Representative porous pharmaceutical particle. Scale bar is 30μm.

It was important to determine the stability of the particle's structure as the experimental method for pressure drop studies involved expanding the bed using upwards flowing gas and vibration of the column followed by packing the particles very tightly by flowing downwards to set the packing height. If the particles were altered by the experimental method, the data collected would not be representative of the representative porous pharmaceutical powder. To determine if the agglomerates had changed in size, SEMs were taken of the representative porous pharmaceutical powder after use in the

experimental setup (Appendix C). As expected for such small particles, no appreciable or observable changes were observed in the structure of the particles.

An equivalent agglomerate diameter was determined using SEMs to use as an approximation for comparison to the results of the pressure drop experiments. Though using SEMs to provide quantifiable data for the particles is not rigorous, it may provide exploratory qualitative data. The equivalent diameter of the agglomerates was determined by gauging the size (length and width) of 431 particles from SEMs with 150 μm scale bars, such as that seen in Figure 22. This magnification allowed for the measurement of particles size while containing a large number of particles within the SEM. The length and width of each particle was recorded. The equivalent diameter of particles was determined using the following equation (Davies, 1979):

$$d_p = \sqrt{\frac{4}{\pi} KBL} \tag{22}$$

where L is the length, B is the breadth or width taken at a right angle to the length and K is 0.77 for rounded particles and 0.75 for angular particles.

Figure 22. Example of the Scanning Electron Micrograph of Representative porous pharmaceutical particles used to estimate the equivalent diameter. Scale bar is 150 μm.

A histogram of the equivalent diameters may be seen in Figure 23. The distribution appears to be uniform and could be described by the χ^2 distribution. This is an acceptable distribution for the data (Montgomery & Runger, 1994). The average equivalent diameter is found to be 32.8 μm. Most researchers, however, use a mass equivalent diameter. The equivalent diameters were taken to the third exponent to find an equivalent volume. The average volume was calculated and then taken to the 1/3 power to deliver a mass weighted equivalent diameter of 39.4 μm. This method assumes a constant effective density for all the particles, regardless of size, and yields an estimate of the geometric diameter of the particle that includes all the void space or porosity within the particle.

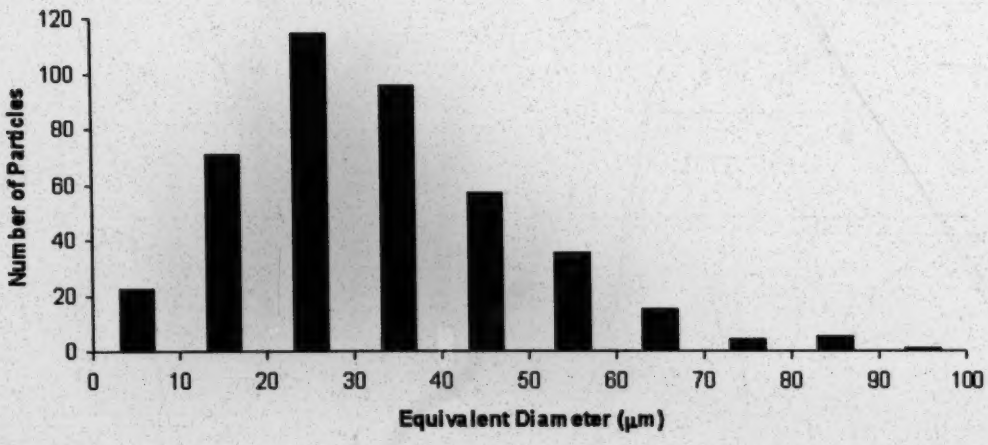

Figure 23. Histogram of equivalent diameters of Representative porous pharmaceutical particles using the method of Davies, 1979.

Alkermes supplied the geometric particle size distributions for representative porous pharmaceutical particles for a dispersed powder (Appendix E). This data provides an additional means of validating the results of the pressure drop method. The method used to determine the geometric particle size distribution aerosolizes the powder under different pressure gradients (and, hence, flows). The powder is then subjected to laser diffraction to determine the size of the particles under flowing conditions. The particles deagglomerate under the applied pressure producing smaller particles. As expected, a larger pressure gradient results in smaller particles, whether the method of small particle generation was by deagglomeration or by fracturing of the particles themselves. The data is summarized in Table 3 below.

Alkermes also provided bulk and tapped density measurements from standard methods. The bulk and tapped densities for the AIR® particles were 0.018 g/cm^3 and 0.031 g/cm^3,

respectively. These measurements from Alkermes provide a means of logically verifying the results of the pressure drop experiments as effective density should be larger than the bulk and tapped densities (Svarovsky, 1987).

Table 3. Geometric Size Distributions of Deagglomerated AIR® Representative Porous Pharmaceutical Particles.

Primary Pressure (bar)	Depression Pressure (mbar)	Diameter (μm)		
		D_{10}	D_{50}	D_{90}
0.5	4	5.1	21.2	48.1
1.0	7	3.8	14.2	32.1
2.0	16	2.7	9.6	22.3
4.0	35	2.3	7.3	15.7

D_{10} is the tenth percentile, D_{50} is the median size, and D_{90} is the ninetieth percentile.

A plot of the median geometric diameters provided by Alkermes versus the primary pressure applied to deagglomerate is shown in Figure 24. The trend in Figure 24 is based on the diameter data supplied by Alkermes. The geometric diameter determined using image analysis from the SEMs and using Davies method is also shown in Figure 24 as a square point at a pressure gradient of zero. Although it is clear that passing the particles through an orifice leads to deaggregation (Dunbar *et al.*, 1998), there is apparently no theoretical equation that relates primary pressure drop to the amount of deagglomeration. In the case of the data presented in Figure 24, the deagglomeration of AIR® particles is

proportional to the inverse of the square root of the pressure drop. The agreement of the Davies geometric diameter with the data supplied by Alkermes appears to validate the Davies geometric diameter.

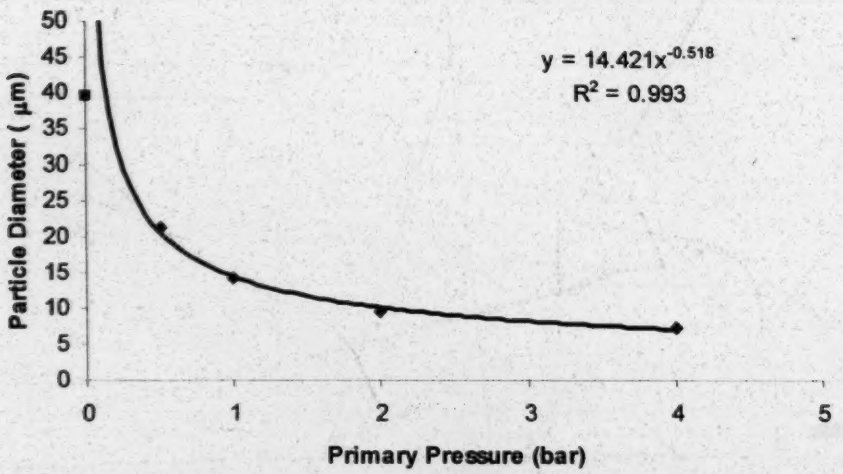

Figure 24. Geometric Diameter of Representative Porous Pharmaceutical Particles versus Primary Pressure. The diamond data points represent the median geometric diameters provided by Alkermes. The square data point represents the geometric diameter determined using Davies method.

4.3.2 Pressure Drop Experiments for Density Determination

The primary aim of this work has been to develop a method to determine the effective density of highly porous micron-sized dry pharmaceutical particles. The pressure drop method originally developed by Ergun and applied to dry pharmaceutical powders in this thesis was tested against the representative porous pharmaceutical powder. The

representative porous pharmaceutical particles were employed as highly porous, micron-sized particles.

Data were collected for the representative porous pharmaceutical particles in a manner similar to that used for the other powders, as described in the Experimental section. In order to avoid interference with atmospheric humidity, the representative porous pharmaceutical powders were desiccated for at least 24 hours prior to use. On the order of 1 gram was weighed and then loaded into the column. The column was secured in a horizontal position prior to setting the bed height.

The high porosity that make the representative porous pharmaceutical particles effective for pulmonary drug delivery, also make achieving a stable packing in the column significantly more challenging than with the solid particles. This was evidenced by the difficulties in inducing an upward flow to set the bed height. If an upward flow was started, particles would bridge across the column or remain suspended in the air after the upwards flow was halted. During the initial stage of experimentation, large voids visible to the naked eye could be seen in the bed. When flowing gas upward through the packed bed, occasionally a portion of the surface "bubbled" with particles at one point on the surface. Svarovsky (1987) refers to this phenomenon as volcanoes. Volcanoes are not to be confused with widespread bubbling, which occurs over the entire surface (Svarovsky 1987). The volcanoes appeared to originate from a semi-permanent channel within the bed. During the process of setting the bed height, the column was vibrated. If the vibration was removed before or at the same time as the upward air flow ceased, an

interesting phenomenon occurred; the bed was far more permeable than expected. The bed was often tapped or vibrated without any upwards flow or compressed with downwards flow to eliminate these macro-voids.

The data were segregated based on the occurrence of macro-voids to determine whether the data were in agreement with data collected without macro-voids. The height of the bed was set by one of or a combination of upward flow, tapping, vibrating, or downward flow. Pressure gradients measurements were then collected versus downwards flow.

Both the Ergun and Richardson-Zaki equations were used to analyze the data. The relationships between ρ_{Bulk} and $(\rho_{Bulk}{}^2/a)^{1/3}$ for samples A, B, and C for the Ergun equation are illustrated in Figure 25. The curves in Figure 25 are representative of the Ergun equation. The effective density, as determined by the Ergun equation, for samples A, B, and C were 0.047, 0.050, and 0.051 g/cm^3, respectively. Problems were encountered, however, with the application of the Ergun equation to the data. After reviewing Figure 25, the relationship between the linear regression and the data becomes suspect. The problem is that the data in Figure 25 displays nonlinear relationships when the untapped, tapped, and compacted data are included together, rather than the linear form that is predicted from the Ergun theory. To further illustrate this problem, the residual errors are plotted versus $(\rho_{Bulk}{}^2/a)^{1/3}$ (as in Figure 26 for sample C), and it is apparent that the residual errors are not randomly distributed with $(\rho_{Bulk}{}^2/a)^{1/3}$.

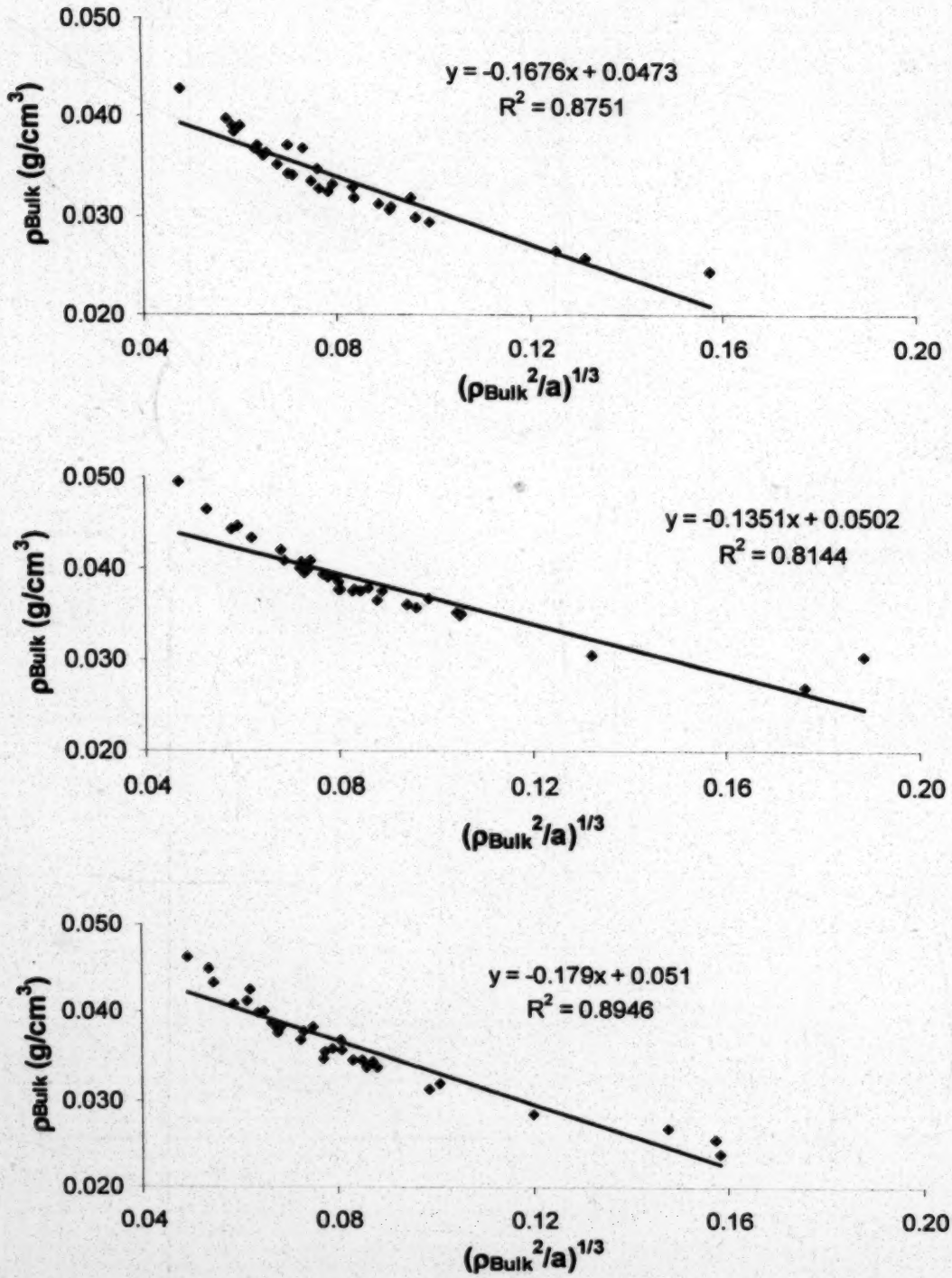

Figure 25. Ergun Method for Representative Porous Pharmaceutical Powder Samples A, B, and C.

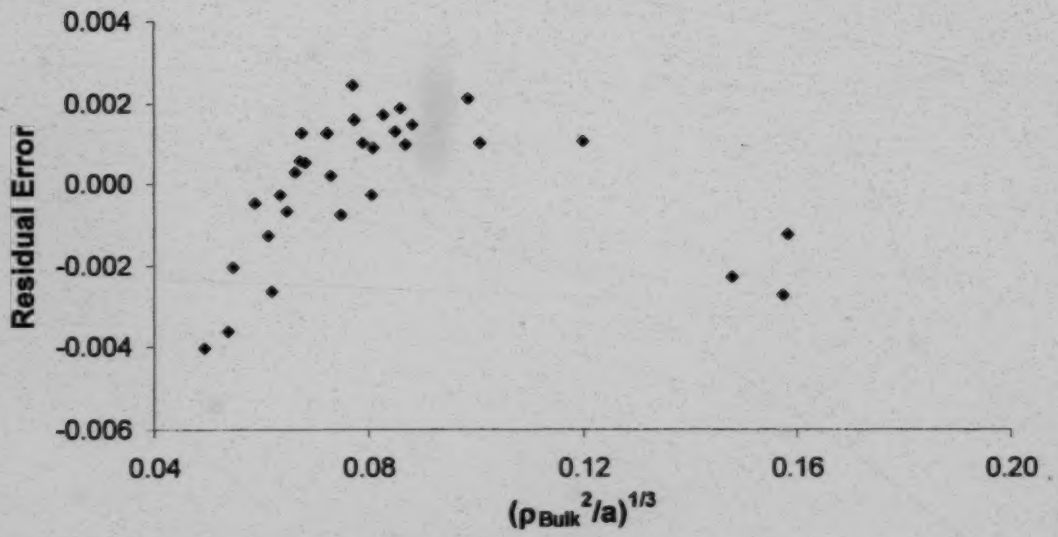

Figure 26. Plot of the Residual Errors for Sample C

The dependence of the residual error to $(\rho_{Bulk}{}^2/a)^{1/3}$ in Figure 26 may be a result of the volcanoes that occurred during packing, where large void spaces created regions of low pressure drop. The observed pressure drops were lower by an order of magnitude than those expected from the Ergun equation, Richardson-Zaki equation, or previous data. The observed pressure gradient was low for column packings that experienced volcanoes during bed expansion or had visible void spaces. When the column was tapped once or twice or the vibrations were maintained longer than the upwards air flow, the measured pressure drop was in good agreement with the rest of the data. Volcanoes may be attributed to high porosity channels created by the localized high flow rates within the bed. These channels persisted after the cessation of the upward flow and appeared to be several millimeters in size, which fits the description given by Svarovsky (1987). Beds containing high porosity channels would offer lower resistance than a randomly packed bed. The effect of the volcanoes on the accuracy and repeatability of the Ergun method

has not been determined in this study. It is possible that volcanoes may have contributed to the error in the data.

One conclusion from these results is column packings containing visible void spaces cannot be described by the Ergun equation. This limitation is because the Ergun theory assumes that the particles are closely packed or in contact with one another to form channels for flow. When the data that contained visual voids are excluded, the effective density predicted by the Ergun equation for samples A, B, and C is 0.057 ± 0.001, 0.062 ± 0.001, and 0.063 ± 0.001 g/cm^3, respectively (Figure 27). The relationships were, as expected, linear between ρ_{Bulk} and $(\rho_{Bulk}^2/a)^{1/3}$.

When the same data was analyzed using the Richardson-Zaki equation, ρ_{Bulk} is plotted against $(\rho_{Bulk}/a)^{1/4.65}$ as seen in Figure 28 for samples A, B, and C. The effective density predicted using the Richardson-Zaki equation for samples A, B, and C are 0.062 ± 0.001, 0.070 ± 0.001, and 0.070 ± 0.001 g/cm^3, respectively. The relationships between ρ_{Bulk} and $(\rho_{Bulk}/a)^{1/4.65}$ are linear, which is consistent with the theory.

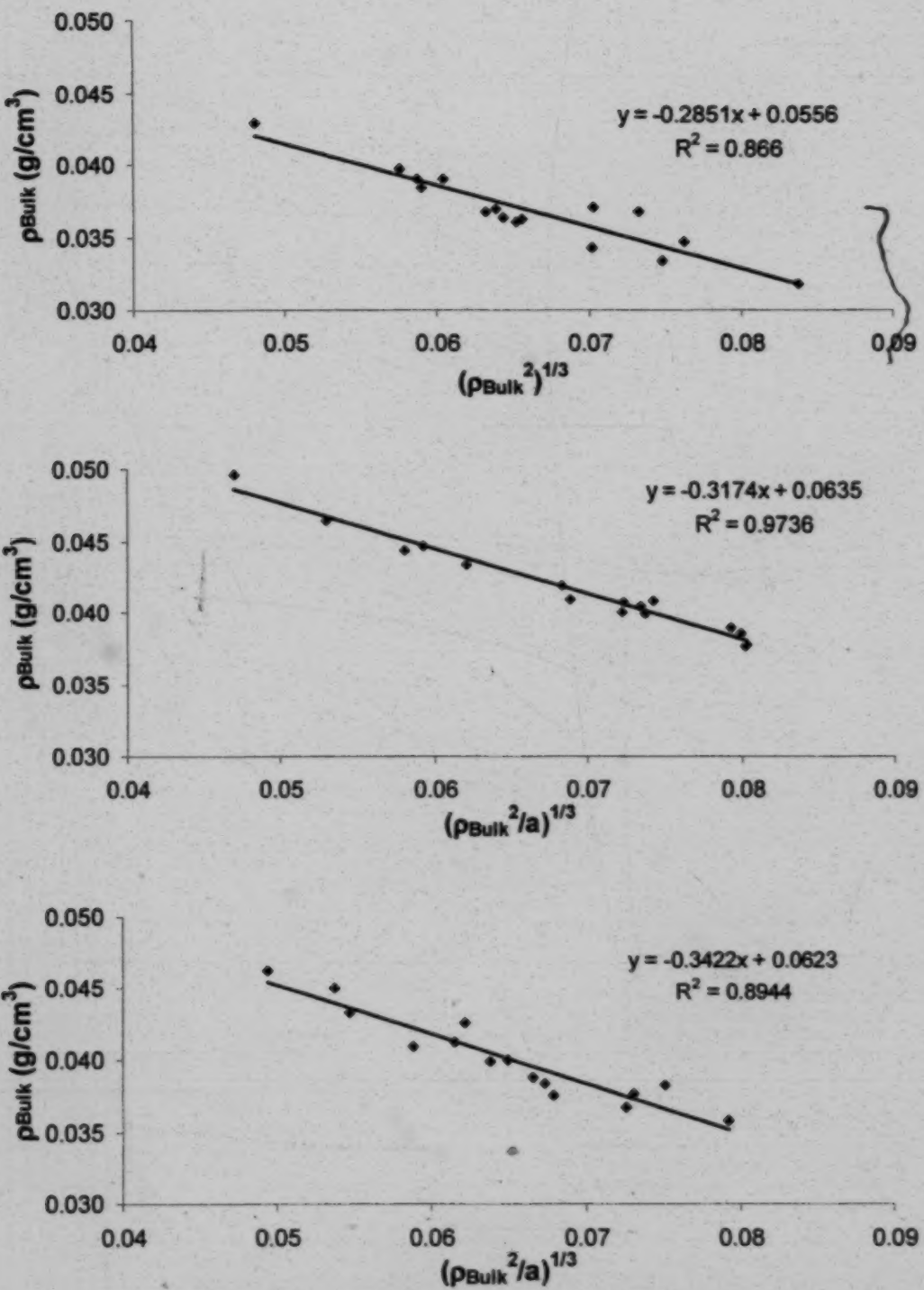

Figure 27. Ergun Equation for Samples A, B, and C for data without visual voids

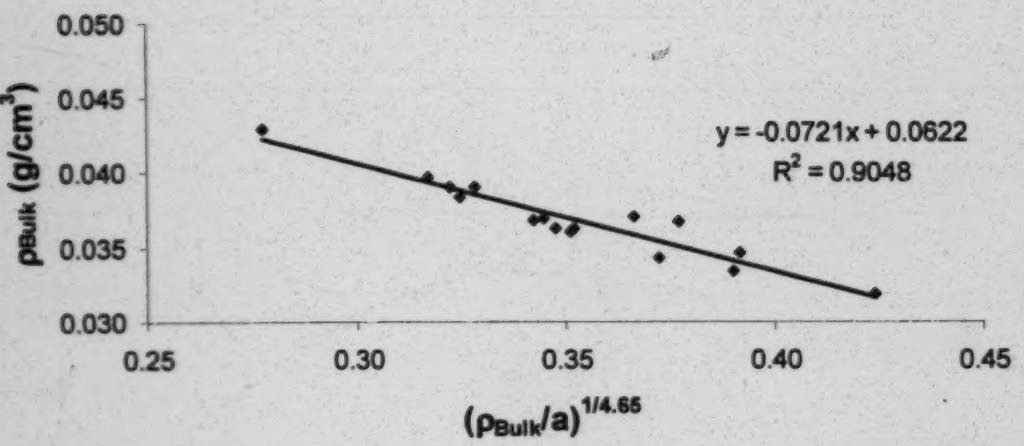

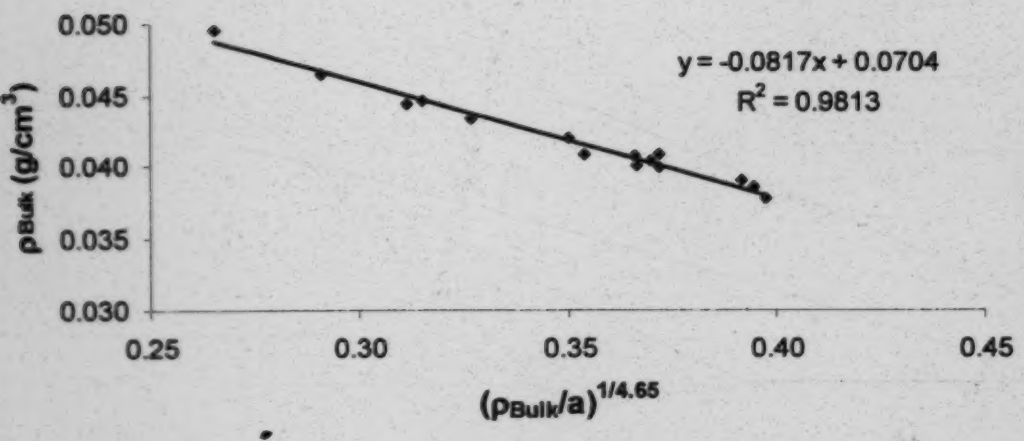

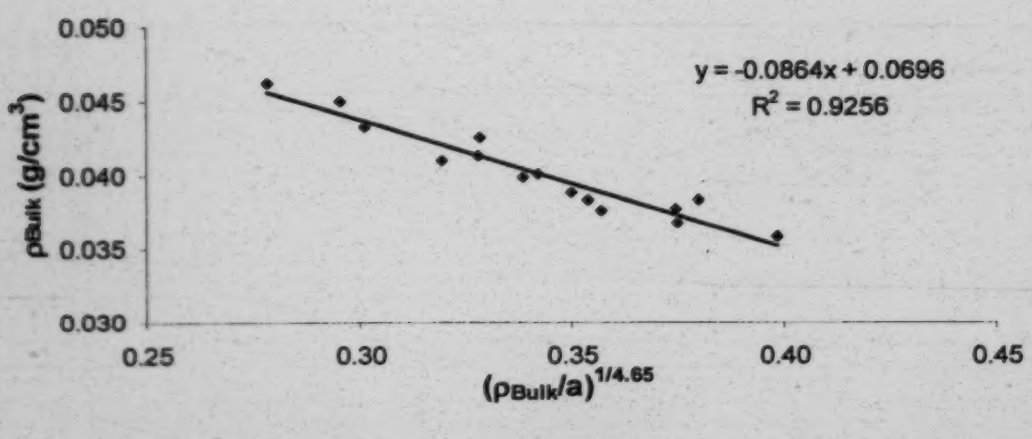

Figure 28. Richardson-Zaki Equation and Packed Bed method for Samples A, B, and C for data without visual voids.

The results from both the Ergun equation and Richardson-Zaki equation are presented in Table 4.

Table 4. Comparison of the Effective Density Results from the Ergun and Richardson-Zaki Equations

Representative Porous Pharmaceutical Powder Sample	Ergun Equation (g/cm^3)		Richardson-Zaki Equation (g/cm^3)
	All Data	Data without macro-voids	Data without macro-voids
A	0.047	0.057	0.062
B	0.050	0.062	0.070
C	0.051	0.063	0.070

From the data presented in Figures 27 and 28, it can now be seen that the effective density relationships for both the Ergun and Richardson-Zaki equations are, as expected linear. Based on the improved agreement between the data and the equations, only data that excludes visual void spaces will be used for analysis from hereon.

The most direct method of verifying the results of the experimental method is to compare the effective density to the available densities and literature. The effective densities of the leucine-mannitol particles as predicted from both the Ergun and Richardson-Zaki equations are, as expected, greater than the supplied bulk and tapped densities of 0.018

g/cm^3 and 0.031 g/cm^3, respectively. This result is logical given the structure of the agglomerates, as can be seen in Figure 21. The effective densities of the leucine-mannitol particles from both the Ergun equation and the Richardson-Zaki equation are far smaller than the density of traditional dry powder aerosols. This result is in agreement with the literature which place the effective density of large, porous particles at approximately 0.1 g/cm^3 (Batycky *et al.*, 1999) or less than 0.4 g/cm^3 (Edwards *et al.*, 1997). The observations are consistent with the expectations and this reinforces the conclusion that the effective density of the particles can be determined with this method. Unfortunately, there is no independent analytical method to verify the effective density value that was calculated from the pressure drop data. A better test of the Ergun and Richardson-Zaki equations in terms of their applicability to dry pharmaceutical powders is the prediction of particle diameter, for which independent data is available.

4.3.3 Diameter of Particles from Pressure Drop Results

To properly model the particles and pressure gradient, the results of the Ergun and Richardson-Zaki equations should be consistent with the observations, previously presented in section 4.3.1. For the Ergun and Richardson-Zaki equations, the calculated diameter should match the observed diameter.

The diameter of the particles was determined by the Ergun equation for samples A, B, and C is 88, 80, and 71 μm, respectively. The diameters determined with the Ergun equation (approximately 80 μm) are more than twice than the equivalent diameter of the agglomerates determined with the method of Davies (1979) (39.4 μm). The difference between the diameters is too large to disregard. The Ergun equation assumes all fluid

flow takes place in channels between the particles, but does not take into account any flow through permeable agglomerates (Polikar, 1977). Thus the lower pressure gradient at a given velocity, as evident in the data, emulates that of much larger particles, which would have correspondingly larger channels from the point of view of the Ergun equation than smaller particles. The Ergun equation does not appear to properly model the flow within a packed bed of porous micron-sized particles based on the determined diameter of the agglomerates (Liu & Masliyah, 1995, Polikar, 1977, Neale *et al.*, 1973).

In contrast, the diameter as determined by the Richardson-Zaki equation using equation (21) for samples A, B, and C is 51, 48, and 41 μm, respectively. The Richardson-Zaki equation gave an average particle diameter of approximately 46 μm which is approximately equal to the equivalent mass-weighted diameter of 39.4 μm from the Davies method (see 4.3.1).

The agreement of the calculated diameter with the mass-weighted diameter implies the Richardson-Zaki equation delivers density of agglomerates seen in the SEMs. This result supports the theoretical underpinning of the Richardson-Zaki equation that flow through a packed bed of permeable particles is analogous to the flow through a swarm of particles. Although the Ergun equation does not appear to be valid for highly porous, micron sized particles, the pressure drop method coupled with the Richardson-Zaki equation may deliver the effective density of the dry pharmaceutical particles.

4.3.4 Aerodynamic Diameter

While determining the geometric diameter is important for testing the method, aerodynamic diameter is important for the actual delivery of dry pharmaceutical powders. The results for effective density and geometric diameter can be used to determine the aerodynamic diameter as per equation (1). Since the results of the Ergun equation do not agree with the observations, no further analysis of the Ergun equation was undertaken. The aerodynamic diameter as determined using the Alkermes supplied geometric particle diameter was compared to the results of the Richardson-Zaki equation.

Table 5 displays the calculated aerodynamic diameters using the determined geometric diameter and effective densities from the Richardson-Zaki equation. The calculated aerodynamic diameters are close to the ideal aerodynamic diameter range for inhaled pharmaceutical powders of 1 to 5 μm, which agrees with the observed ease with which the particles aerosolized. This could further indicate the Richardson-Zaki equation delivered acceptable values of the effective density of the agglomerates, however, no mass median aerodynamic diameter value was immediately available for comparison for the representative porous pharmaceutical particles.

Table 5. Aerodynamic Diameters of the Representative Porous Pharmaceutical Particles

Sample	Geometric Diameter (μm)	Calculated Aerodynamic Diameter* (μm)
A	51	12.7
B	48	12.7
C	41	10.8

*Calculated using Equation (1)

4.3.5 Aerodynamic Diameter of Deagglomerated Particles

Alkermes supplied geometric particle size distributions for the representative porous pharmaceutical particles for a dispersed powder. By combining the effective density from the Richardson-Zaki equation and the geometric particle size distributions from Alkermes (Table 3), an estimate of the aerodynamic diameter distributions of the deagglomerated particles may be calculated and compared to the aerodynamic diameter from the Richardson-Zaki equation (equation (13)). Table 6 summarizes the results of these calculations.

Table 6. Aerodynamic Size Distributions of the AIR® Representative Porous Pharmaceutical Powder

Primary Pressure (bar)	Depression Pressure (mbar)	Aerodynamic Diameter * (μm)		
		$D_{Aero\ 10}$	$D_{Aero\ 50}$	$D_{Aero\ 90}$
0.5	4	1.32	5.49	12.24
1.0	7	.98	3.68	8.31
2.0	16	.70	2.84	5.77
4.0	35	.60	1.89	4.06

* Calculated using the determined effective density, the supplied geometric sizes (Figure 24), and equation (1).

The results in Table 6 appear to be logical. 3 of the 4 median diameters are within the ideal size range for inhaled pharmaceuticals of 1 to 5 μm. All of the size ranges contain at least a portion of the ideal size range. This agreement further reinforces the suitability of using pressure drop measurements through packed beds and the Richardson-Zaki equation to determine the effective density of highly porous micron-sized particles.

It should be acknowledged that a limitation of applying the Richardson-Zaki equation to the prediction of aerodynamic diameter is that the effective density was assumed to be constant. In practice, the effective density may vary depending on the particle size. It has been reported that as the particles become smaller, the effective density increases (Ergun, 1951). This is due to a reduction in porosity of the particles. As the particles break apart,

a portion of the pores of the larger particles are now exposed to flow and no longer contribute to the porosity of the smaller particle. It is not clear if this previous finding would apply to the highly porous agglomerated particles used in this study.

The magnitude of the increase in effective density with deagglomeration is not known and was not estimated herein. However, note that a 20% change in the effective density would have less than a 10% impact on the value of the aerodynamic diameter determined by equation (1), because the effective density is to the power of ½ in equation (1). This would minimize the impact of assuming a relatively constant effective density in equation (1). If the increase in effective density due to deagglomeration is assumed to be negligible, a direct application of the determined effective densities to the size distributions provided by Alkermes using equation (1) may be undertaken. The agreement of the aerodynamic diameter with the expected ideal aerodynamic diameter of inhaled pharmaceuticals would justify this assumption.

The aerodynamic diameter calculated from the Richardson-Zaki equation (Table 5) should be larger than the median aerodynamic diameter calculated for the deagglomerated particles (Table 6). This is because the pressure drop experiments were performed on whole particles that had not experienced deagglomeration. A plot of the median geometric diameters versus the primary pressure applied to deagglomerate is shown in Figure 29. The trend in Figure 29 is based on the diameter data supplied by Alkermes. The aerodynamic diameter from the experimental data and the Richardson-Zaki equation is also shown in Figure 29 as a green square at a pressure of 0 bar. All of

the data appears to follow an exponential decline in the particle diameter with increasing pressure. The agreement of the experimental aerodynamic diameter with the data supplied by Alkermes appears to validate the potential use of packed bed pressure drop experimental methods coupled with the Richardson-Zaki equation for use with highly porous, micron-sized pharmaceutical powders.

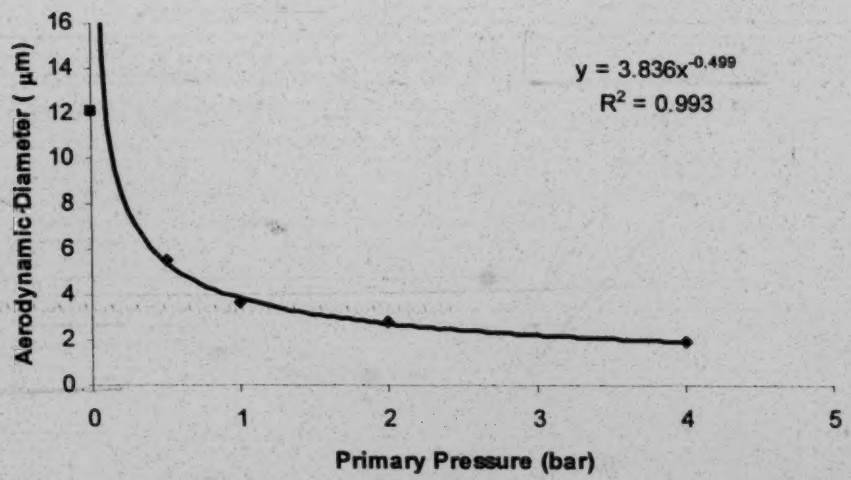

Figure 29. Aerodynamic Diameter of Representative Porous Pharmaceutical Particles versus Primary Pressure. The diamond data points represent the median aerodynamic diameters calculated from the data provided by Alkermes. The square data point represents the aerodynamic diameter determined using Davies method.

Using the trend between primary pressure and aerodynamic diameter seen in Figure 29, a mathematical solution relating the velocity to the aerodynamic diameter of the deagglomerated particles is feasible. The exponent in the relationship that appears in Figure 29 is very close to ½. From the above relationship, it would appear that the

aerodynamic diameter is empirically proportional to the inverse of the root of the primary pressure, which is proportional to the pressure drop experienced by the particle, as follows:

$$d_{aero} \propto \sqrt{\frac{1}{\Delta P}} \tag{23}$$

If some simple assumptions are made, the system may be treated analytically. Since the shear stress may be expressed as follows (Young *et al.*, 1997):

$$\frac{\Delta P}{l} = \frac{4\tau}{D_{Pipe}} \tag{24}$$

Where D_{Pipe} is the diameter of the pipe and τ is the shear stress. Assuming that the relationship expressed in equation (23) is valid, equation (23) may be substituted into equation (24) to yield:

$$\tau \propto \frac{1}{d_{Aero}^2} \tag{25}$$

where τ is the shear stress. It is possible for particles to experience eddies while undergoing deaggregation within the flow (Dunbar *et al.*, 1998). The process of deaggregation refers to small particles separating from larger particles while deagglomeration refers to particles of the same size separating. Although deaggregation differs from deagglomeration, it will be assumed herein that particles experience eddies while undergoing deagglomeration. The following assumption may be made for relating the velocity to the shear stress while in the presence of eddies within a pipe (Young *et al.*, 1997):

$$\tau \propto v^2 \tag{26}$$

Equating shear stress in equations 25 and 26 yields:

$$d_{Aero} \propto \frac{1}{v} \tag{27}$$

Such an equation could be used to better understand the forces behind deagglomeration. The literature does not address the deagglomeration of particles in the direct manner seen in equation (27). It is known that the larger porous pharmaceutical particles deaggregate more easily under shear forces (Vanbever *et al.*, 1999) and that the adhesive forces between particles are proportional to their diameter (Dunbar *et al.*, 1998). It may stand to reason that the large, micron-sized porous particles produced by Alkermes could deagglomerate within certain velocities according to equation (27).

Equation (27) presented above requires further scientific and experimental exploration and the relationship is presented here for supplementary information only. It is not a rigorous analytical solution, as equation (23) is assumed from curve fit in Figure 29. Nor is it a proven empirical relationship, as there is only one set of data to support the relationship from Figure 29. The work presented herein will not extend to include an examination of the validity of equation (27). If the equation is valid, however, this finding will be important to the design of inhalers to be used with a given powder to yield the desired diameter for optimum drug delivery.

5.0 Conclusions

The primary focus of this work has been to develop a pressure drop method of determining the effective density of highly porous micron-sized particles. The driving force behind this thesis has been the desire to characterize the effective density of inhaled pharmaceutical powders where other experimental methods may not be applicable. A system of collecting pressure drop and velocity data for packed beds of particles analogous to that utilized by Ergun (1951) was created and employed.

The method developed required testing and verification. The experimental apparatus and method were adapted for studying particles at low flow rates. To validate and determine the limits of the method, a variety of materials with known properties were employed, some comparable to those used by Ergun. The data was analyzed using the Ergun equation and the Richardson-Zaki equation to obtain both the effective density and the diameter of the particles under study.

It was found that data obtained from the experimental method, when analyzed with the Ergun equation, could be used with nearly all particles save non-spherical particles with very large size distributions. The experimental method combined with the Ergun equation, developed for solid particles in multiple flow regimes, properly determines the effective density and diameter of solid, spherical and non-spherical particles in the size range of 80 to 175 μm with varying size distributions. The agreement between the experimental results and the known densities and diameters of the particles supports the validity of the method. The Richardson-Zaki equation, developed specifically for porous,

permeable particles at low flow rates, did not properly determine the effective density or diameter of the solid particles.

For the highly porous, micron-sized particles supplied by Alkermes, the Ergun equation and the Richardson-Zaki equation were employed to predict the effective density and geometric diameter of the particles. The effective densities from both equations appear valid. Both values are larger than the tapped density, as expected. Both are smaller than the density of traditional dry powder aerosols as prescribed by literature descriptions, and both agree with the literature values of the effective density of highly porous, micron-sized particles.

Further analysis reveals that the geometric diameter from the Ergun equation does not agree with the observed geometric diameter. The Ergun equation over-estimates the geometric diameter and does not appear to properly model flow through highly-porous, micron-sized particles. This was not the case for the Richardson-Zaki equation. The geometric diameter calculated from the Richardson-Zaki agrees with the observed geometric diameter and the Richardson-Zaki equation appears to properly model the flow through packed beds of highly-porous, micron-sized particles.

The effective density and geometric diameter may be used to calculate the aerodynamic diameter of a particle. Alkermes supplied geometric size distributions of deagglomerated particles. The effective density determined with the Richardson-Zaki equation and the supplied geometric diameters were used to calculate the aerodynamic diameters. The

calculated aerodynamic diameters are near to or within the ideal size range for dry powder aerosols. The aerodynamic diameter determined using the effective density and geometric diameter from the Richardson-Zaki equation is in good agreement with the supplied data. This is further evidence that the determination of the effective density of highly porous, micron-sized particles using a packed bed pressure drop method coupled with the Richardson-Zaki equation is credible.

The agreement between the results of the experimental data and literature, the supplied diameters, and the observed diameter provide a persuasive argument for the method, though independent confirmation and a study of the method's accuracy are required. The pressure drop through packed beds experiments coupled with the Richardson-Zaki equation could provide appropriate results for the effective density, geometric diameter, and the aerodynamic diameter for highly porous, micron-sized particles.

From the above agreements, it appears that the experimental method and the Richardson-Zaki equation could be used by dry powder manufacturers to determine the effective density of highly porous, micron-sized particles. This process would provide dry pharmaceutical manufacturers with a valid new method of determining the effective density. The Ergun equation should not be employed with highly porous, micron-sized particles. Further work is required to verify this work, refine the pressure drop method, and qualify the accuracy of the results.

6.0 Future Work

There are several areas identified below that could yield improvements in the accuracy and reliability of the experimental method.

The improvements in the height measurement with the addition of a laser level reduced the error from 2 to 1 mm in the height reading. A further improvement would provide a reduction in error. Using a glass column with volumetrically marked sides should prove sufficient to reduce the error in height to 0.5 mm. This would have the added benefit of reducing the error associated with the diameter of the column, which contributed up to 1% to the overall error in the representative porous pharmaceutical data.

The colum hould be constructed with material or treated in such a manner as to reduce the amount of powder clinging to internal sides of the column whenever possible. Although the mass of powder clinging to the negligible, a reduction in error may be possible.

There are equations other than the Ergun and Richardson-Zaki equations that may be used to describe packed bed systems. These equations may give better estimates of the particle porosity and effective density. However, these equations may require data that are the indirect goals of this project (particle diameter and particle porosity). If such information were to become available, these equations may provide better estimates of the effective density than either the Ergun or Richardson-Zaki equations.

If a SEM or other image of the AIR® particle's cross-section (D'Aquino, 2003), then such information could be used to extrapolate the internal porosity of the particles. The void area of the cross-section should be representative of the porosity of the particle as a whole.

The determined effective densities do not agree within error. A study of the sensitivity of the method could resolve this issue and determine the suitability of the method for use in a diagnostic role. A comparison of the results of regular and off-spec powders would provide the necessary data to determine if the method is sensitive enough to be used as a process troubleshooting tool.

The comparison of the data to values of aerodynamic size distributions without deagglomeration would be of great value. This data would allow for further verification of the effective density determination method. It could validate the application of the determined density to the geometric size distributions provided by Alkermes or quantify the magnitude of the increase in effective density due to deagglomeration.

There are limits to the measurement devices. As particles become smaller, smaller flow controllers are required to ensure accurate results. Two separate sets of small, solid particles were studied (approximately 2 to 20 μm in size), however, smaller flow controllers were not available. In both cases the errors in ρ_{Bulk} and $(\rho_{Bulk}{}^{2}/a)^{1/3}$ were larger than 1/2 the range of the data collected. This resulted in weak fits and poor

predictions of the effective density. This weak fit to the data highlights the need for properly chosen equipment.

7.0 References

Abdullah, E.C. and Geldart, D., The Use of Bulk Density Measurements as Flowability Indicators, Powder Technology, Volume 102, pg. 151-165, 1999

Atkins, Peter, Physical Chemistry, 6th Edition, W.H. Freeman and Company, New York, NY, 1998

Batycky, R., Nice, J., Chen, D., Sung, J., Lipp, M., Mintzes, J., Dunbar, C., Niven, R., and Edwards, D., Production and Characterization of Large Porous Particles for Pulmonary Drug Delivery, Mat. Res. Soc. Symp. Proc., Volume 550, pg. 95-100, 1999

Bird, R.B., Stewart, W.E., and Lightfoot, E.N., Transport Phenomena, 2nd Edition, John Wiley & Sons, Inc, Toronto, 2002

Blake, F.C., The Resistance of Packing to Fluid Flow, Trans. Amer. Inst. Chem. Engrs. V14, pg. 415-421, 1922

Bosquillon, C., Lombry, C., Préat, V., and Vanbever, R., Influence of formulation excipients and physical characteristics of inhalation dry powders on their aerosolization performance, Journal of Controlled Release, Volume 70, pg. 329-339, 2001

Brinkman, H.C., A Calculation of the Viscous Force Exerted by a flowing Fluid on a Dense Swarm of particles, Appl. Sci. Res., A1, pg. 27-34, 1947

Burke, S.P. andPlummer, W.B., Gas Flow Through Packed Columns, Industrial and Engineering Chemistry, Volume 20, #11, pg. 1196-1200, 1928

Carman, P.C., Fluid Flow Through Granular Beds, Transactions of the Institution of Chemical Engineers, Volume 15, pg. 150-166, 1937

Casal, J., Lucas, A., and Arnaldos, J., A New method for the Determination of Shape Factor and Particle Density, The Chemical Engineering Journal, Volume 30, pg. 155 – 158, 1985

Class, Selena, Pharma Overview, Chemical & Engineering News, December 2, pg. 39-49, 2002

D'Aquino, R., Good Drug Therapy: It's Not Just the Molecule – It's the Delivery, Chemical Engineering Progress, Volume 100, #2, pg. 15S, 2004

More-Revealing Ways to Study Materials, Chemical Engineering Progress, D'Aquino, R., Senior Editor, Volume 99, #1, pg. 12-13, 2003

Darcy, H. P. G. (1856) Les Fontaines publique de la ville de Dijon, Victor Dalmount, Paris. English Translation by Muskat, M., Flow of Homogeneous fluids through porous media, McGraw-Hill, New York, 1937

Darby, R. Chemical Engineering Fluid Mechanics, Marcel Dekker, Inc, New York, 2001

Davies, C.N., Particle-Fluid Interaction, Journal of Aerosol Science, Volume 10, pg. 477-513, 1979

Davis, R.H. and Stone, H.A., Flow Through Beds of Porous Particles, Chemical Engineering Science, Volume 48, Number 23, pg. 3993-4005, 1993

Dellamary, L.A, Tarara, T.E., Smith, D.J., Woelk, C.H., Adractas, A., Costello, M.L., Gill, H., and Weers, J.G., Hollow Porous Particles in Metered Dose Inhalers, Pharmaceutical Research, Volume 17, Number 2, pg. 168-174, 2000

Dunbar, C.A., Hickey, A.J., and Holzner, P. Dispersion and Characterization of Pharmaceutical Dry Powder Aerosols. KONA Powder and Particle, Volume 16, pg. 7-44, 1998

Du Plessis, J.P., Analytical Quantification of Coefficients in the Ergun Equation for the Fluid Friction in a Packed Bed, Transport in Porous Media, Volume 16, pg. 189-207, 1994

Edwards, D., Hanes, J., Caponetti, G., Hrkach, J., Ben-Jebria, A., Eskew, M.L., Mintzes, J., Deaver, D., Lotan, N., and Langer, N., Large Porous Particles for Pulmonary Drug Delivery. Science, Volume 276, pg. 1868-1871, 20 June 1997

Edwards, D.A., Delivery of Biological Agents by Aerosols, AIChE Journal, Volume 48, Number 1, pg 2-6, 2002

Ergun, S., Determination of Particle Density of Crushed Porous Solids: Gas Flow Method. Analytical Chemistry, Volume 23, pg. 151-156, 1951

Ergun, S., Fluid Flow Through Packed Columns, Chemical Engineering Progress, Volume 48, Number 2, pg. 89, 1952

Ergun, S. and Orning, A.A., Fluid Flow through Randomly Packed Columns and Fluidized Beds, Industrial and Engineering Chemistry, Volume 4, Number 6, pg. 1179, 1949

Finlay, W.H., The Mechanics of Inhaled Pharmaceutical Aerosol: An Introduction, Academic Press, 2001

Finlay, W.H., Zuberbuhler, P., and Mandl, M., Particle Size Measurements for the Space-Chamber Metered Dose Inhaler holding Chamber with Aerochamber and Metered Dose Inhaler Alone, Journal of Aerosol Medicine, Volume 10, Number 3, pg. 213-219, 1997

Finlay, W.H. and Gehmlich, M.G. Inertial sizing of aerosol inhaled from two dry powder inhalers with realistic breath patterns versus constant flow rates, International Journal of Pharmaceutics, Volume 210, pg. 83-95, 2000

Forchheimer, P., Wasserbewegung Durch Boden, Zeitschrift Des Vereines Deutscher Ingenieure, Volume 45, pg. 1781, 1901

Geldart, D., Gas Fluidization, I. Chem. E. Short Course, Bradford, 1986

Goodman, D., Israel, E., Rosenburg, M., Johnston, R., Weiss, S., and Drazen, J., The Influence of Age, Diagnosis and Gender on Proper Use of Metered-Dose Inhalers, American Journal Respir. Care Med., Volume 150, pg. 1250, 1994

Handbook of Pharmaceutical Additives, 2nd Edition, Compiled by Ash, M. and Ash, I., Synapse Information Resources, Endicott, New York, 2002

Rowe, R.C., Sheskey, P.J., and Weller, P.J.,Handbook of Pharmaceutical Excipients, 4th Edition, Pharmaceutical Press, Grayslake, Illinois, 2003

Hausner, H.H., International Journal of Powder Metallurgy, Volume 3, 7-13, 1986

Heyder, J., Gebhart, J., Rudolf, G., Schiller, C., and Stahlhofen, W., Deposition of Particles in the Human Respiratory Tract in the Size Range 0.005-15 μm, Journal of Aerosol Science, Volume 17, pg. 811, 1986

Holman, J.P., Experimental Methods for Engineers, McGraw-Hill, 3rd Edition, pg. 44, 1978

Incropera, F.P. & Dewitt, D.P., Introduction to Heat Transfer, 3rd Edition, John Wiley & Sons, Toronto, 1996

Kirk-Othmer Encyclopedia of Chemical Technology, Editors J.I. Kroschwitz and M. Howe-Grant, Wiley-Interscience, New York, 1991

Kline, S.J. and McClintock, F.A., Describing Uncertainties in Single-Sample Experiments, Mech. Eng. P.3, Jan. 1953

Koplik, J. and Banavar, J.R., Physics of Fluids at Low Reynolds Numbers – A Molecular Approach, Computers in Physics, Volume 12, Number 5, pg. 424-431, 1998

Kozeny, J., Concerning capillary Conduction of water in the soil Rise, Seepage and Use in Irrigation, Proceedings of the Royal Academy of Science, translated and edited by W.F. Striedieck and C.M. Davis, AIME, 1952, Vienna, Class I, Volume 136, pg. 271-306, 1927

Lee, J. and Koplik, J., Microscopic Motion of Particles Flowing Through a Porous Medium, Physics of Fluids, Volume 11, Number 1, pg. 76-87, 1999

Liu, S., Afacan, A., and Masliyah, J.H., Laminar flow through porous media, Chemical Engineering Science, Volume 49, pg. 3565-3586, 1994

Liu, S. and Masliyah, J.H., Single Fluid Flow in Porous Media, Chem. Eng. Comm. Volumes 148-150, pg. 653-732, 1996

Loudon, G.M., Organic Chemistry 3rd Edition, The Benjamin/Cummings Publishing Company, Inc., Don Mills, Ontario, 1995

Macdonald, I.F., El-Sayed, M.S., Mow, K., and Dullien, F.A.L., Flow through Porous Media – the Ergun Equation revisited, Ind. Eng. Chem. Fundam., Volume 18, Number 3, pg. 199-208, 1979

Margiatoo, C.A. and Siegel, J.H., Determination of Porous Particle Density, Powder Technology, Volume 34, pg. 105-106, 1983

Martys, N., Bentz, D.P., and Garboczi, E.J., Computer Simulation Study of the Effective Viscosity in Brinkman's Equation, Phys. Fluids, Volume 6, pg. 1434-1439, 1994

Martys, N.S., Torquato, S., and Betz, D.P., Universal Scaling of Fluid Permeability for Sphere Packings, Physical Review E, Volume 50, Number 1, pg. 403-408, 1994

Martys, N. and Bentz, D.P., Hydraulic Radius and Transport in reconstructed Model Three-Dimensional Porous Media, Transport in Porous Media, Volume 17, pg. 221-238, 1994

Masliyah, J.H. and Polikar, M., Terminal Velocity of Porous Spheres, The Canadian Journal of Chemical Engineering, Volume 58, pg. 299-302, 1980

Matsumoto, K. and Suganuma, A., Settling Velocity of a Permeable Model Floc, Chemical Engineering Science, Volume 32, pg. 445-447, 1977

Molina, M.J. and Rowland, F.S., Stratospheric sink for chlorofluoromethanes: chlorine catalyzed destruction of ozone, Nature, Volume 249, pg. 810-812, 1974

Montgomery, D.C. and Runger, G.C., Applied Statistics and Probability for Engineers, John Wiley & Sons, Inc, Toronto, 1994

Narayan, R., Coury, J.R., Masliyah, J.H., and Gray, M.R., Particle Capture and Plugging in Packed-Bed Reactors, Ind. Eng. Chem. Res., Volume 36, pg. 4620-4627, 1997

Neale, G., Epstein, N., and Nader, W., Creeping flow relative to permeable spheres, Chemical Engineering Science, Volume 28, pg. 1865-1874, 1973

Nield, D.A. and Bejan, A., Convection in Porous Media, Springer-Verlag, New York, NY, 1992

Niven, R.K., Physical Insight into the Ergun and Wen & Yu Equations for Fluid Flow in Packed and Fluidised Beds, Chemical Engineering Science, Volume 57, pg. 527-534, 2002

Pagano, A.M., Crozza, D.E., and Nolasco, S.M., Pressure Drop Through In-Bulk Flax Seeds, JAOCS, Volume 75, No. 12, pg. 1741-1747, 1998

Patton, J.S. and Platz, R.M., Adv. Drug Delivery Rev., Volume 8, pg. 179, 1992

Pavia, D., Aerosols and the Lung: Clinical and Experimental Aspects, Clarke, S.W., Pavia, D., Editors, Butterworths, London, pg. 200-229, 1984

Perry, R.H. and Green, D., Perry's Chemical Engineering Handbook, 6th Edition, McGraw-Hill Inc., Toronto, 1984

Philipse, A.P. and Pathmamanoharan, C., Liquid Permeation (and Sedimentation) of dense Colloidal Hard-Sphere Packings, J. Colloid and Interface Sci., Volume 159, pg. 96-107, 1993

Polikar, M., Settling Velocity of a Permeable Model Floc, Chemical Engineering Science, Volume 32, pg. 445-447, 1977

Richardson, J.F. and Zaki, W.N., The sedimentation of a suspension of Uniform Spheres, Chemical Engineering Science, Volume 3, pg. 65-73, 1954

Sahimi, Muhammad, Flow and Transport in Porous Media and Fractured Rock, VCH, New York, NY, 1995

Sciarra, J.J. and Cutie, A.J., Modern Pharmaceutics, 2nd Edition, G.S. Banker and C.T. Rhodes, Marcel Dekker, Inc., New York, NY, pg. 605, 1990

Smith, S.J. and Bernstein, J.A., Inhalation Aerosols, Editor Hickey, A.J., Dekker, New York, NY, pg. 233-269, 1996

Stapleton, K.W. and Finlay, W.H., Errors in Characterizing Nebulized Particle Size Distributions with Cascade Impactors. Journal of Aerosol Medicine, Volume 11, Supplement 1, S-80-S-83, 1998

Starov, V.M. and Zhdanov, V.G., Effective Viscosity and Permeability of Porous Media, Colloids and Surfaces A: Physiochemical and Engineering Aspects, Volume 192, pg. 363-375, 2001

Svarovsky, L., Powder Testing Guide: Methods of Measuring the Physical Properties of Bulk Powders, Elsevier Science Publishing Co. Inc., New York, NY, USA, 1987

Voss, A. and Finlay, W.H. Deagglomeration of dry powder pharmaceutical aerosols, International Journal of Pharmaceutics, Volume 248, pg. 39-50, 2002

Warheit, M.B. and Hartsky, M.A., Microscopy Res. Tech. V26, pg. 412, 1993

Williams III, R.O., Repka, M., and Liu, J., Influence of Propellant Composition on Drug Delivery from a Pressurized Metered-Dose Inhaler, Drug Development and Industrial Pharmacy, 24(8), pg. 763-770, 1998

Wu, Y., Pruess, K., and Persoff, P., Gas flow in Porous Media with Klinkenburg Effects, Transport in Porous Media, Volume 32, pg. 117-137, 1998

Wyllie, M.R.J. and Gardner, G.H.F., The Generalized Kozeny-Carman Equation: Part I, World Oil, 146(4), pg. 121-126, 1958

Wyllie, M.R.J. and Gardner, G.H.F., The generalized Kozeny-Carman equation. A novel approach to problems of fluid flow, World Oil Production, Sect.ion 146, pg. 210-228, 1958

Young, D.F, Munson, B.R., and Okiishi, T.H., A Brief Introduction to Fluid Mechanics, John Wiley & Sons, Toronto, 1997

Appendix A: Raw Data

Part 1: Sigma-Aldrich Lactose

Total Height (mm)	height to tap (mm)	Rotameter Reading	ΔP (in H_2O)	Mass (g)
132	123	10	0.3	19.54
132	123	11.9	0.34	19.54
132	123	14	0.39	19.54
132	123	16.1	0.44	19.54
132	123	18	0.48	19.54
132	123	20	0.53	19.54
130	123	9.9	0.26	19.54
130	123	11.9	0.27	19.54
130	123	14	0.3	19.54
130	123	16	0.33	19.54
123	98	10	1.3	19.54
123	98	12	1.6	19.54
123	98	14.1	1.7	19.54
123	98	15.8	2	19.54
123	98	18	2.25	19.54
92	72	9.9	0.64	14.23
92	72	12.1	0.75	14.23
92	72	14	0.84	14.23
92	72	16	0.94	14.23
92	72	18	1	14.23
94	72	10	0.39	14.23
94	72	12	0.46	14.23
94	72	14	0.52	14.23
94	72	16.1	0.59	14.23
94	72	18	0.65	14.23
96	47	8	0.51	14.23
96	47	14	0.81	14.23
96	47	10	0.62	14.23
96	47	12	0.71	14.23
96	47	8	0.51	14.23
96	47	12	0.72	14.23
96	47	10	0.61	14.23
96	47	14	0.81	14.23
98	47	8	0.58	14.23
98	47	11	0.78	14.23
98	47	10	0.71	14.23
98	47	9	0.66	14.23
98	47	8	0.61	14.23
90	72	10	0.44	14.23
90	72	20	0.78	14.23
90	72	16	0.65	14.23
90	72	12	0.5	14.23
90	72	14	0.57	14.23
90	72	18	0.71	14.23
135	99	8	2.8	19.10
135	99	12	4.1	19.10
135	99	10.1	3.6	19.10
135	99	16	5.1	19.10
135	99	14	4.55	19.10

140	99	8	1.65	19.10
140	99	14	2.7	19.10
140	99	12	2.35	19.10
140	99	10	2.05	19.10
142	122	10	0.18	19.10
142	122	8	0.15	19.10
142	122	12	0.21	19.10
130	99	12	3.3	19.10
130	99	14	3.8	19.10
130	99	18	4.8	19.10
130	99	10	2.9	19.10
130	99	15.9	4.3	19.10
127	122	10.1	0.5	19.10
127	122	12	0.58	19.10
127	122	14	0.66	19.10
127	122	20	0.91	19.10
127	122	16	0.75	19.10
127	122	18	0.83	19.10

Part 2: 135 μm Glass Spheres

Total Height (mm)	Flow Controller Reading (%)	ΔP (in H_2O)	Mass (g)
49	15.7	0.7	22.08
49	23.2	1	22.08
49	32.2	1.35	22.08
49	38.4	1.58	22.08
49	27.5	1.17	22.08
49	72.9	2.94	22.08
49	58.6	2.38	22.08
49	45.8	1.88	22.08
49	63.4	2.56	22.08
49	67.2	2.72	22.08
47	34.6	1.76	22.08
47	48.9	2.44	22.08
47	60.4	2.99	22.08
47	52.4	2.61	22.08
47	25.4	1.32	22.08
47	19.7	1.05	22.08
47	36.2	1.83	22.08
47	30	1.54	22.08
47	42.9	2.15	22.08
47	55.6	2.76	22.08
39	37.3	1.6	18.40
39	52.9	2.23	18.40
39	73	3.05	18.40
39	62.4	2.61	18.40
39	55.1	2.32	18.40
39	46.5	1.97	18.40
39	21.8	0.98	18.40
39	27.3	1.2	18.40
39	16.1	0.75	18.40
39	31.2	1.35	18.40
39	13.5	0.64	18.40
41	69.2	2.44	18.40
41	85.9	3.03	18.40

41	47.7	1.7	18.40
41	54.9	1.95	18.40
41	24.9	0.93	18.40
41	31	1.14	18.40
41	62.6	2.22	18.40
41	74.3	2.62	18.40
41	29.9	1.1	18.40
41	42.1	1.51	18.40
41	14.8	0.59	18.40
43	49.8	1.8	19.09
43	73.5	2.64	19.09
43	60.3	2.18	19.09
43	82.1	2.95	19.09
43	67.3	2.42	19.09
43	35.1	1.3	19.09
43	27.5	1.04	19.09
43	41.7	1.53	19.09
43	18.5	0.73	19.09
43	53.3	1.93	19.09
41	47.4	2.1	19.09
41	34	1.54	19.09
41	18	0.87	19.09
41	26.8	1.24	19.09
41	38.2	1.71	19.09
41	70.8	3.1	19.09
41	66.9	2.93	19.09
41	53.9	2.37	19.09
41	60.4	2.65	19.09
54	33.8	1.75	24.75
54	25.4	1.35	24.75
54	48.2	2.45	24.75
54	43	2.2	24.75
54	60.2	3.03	24.75
54	53.2	2.69	24.75
54	48.6	2.46	24.75
54	16.7	0.92	24.75
54	21.3	1.16	24.75
54	42.2	2.17	24.75
53	40.6	2.21	24.75
53	51.7	2.79	24.75
53	48.7	2.64	24.75
53	22.4	1.28	24.75
53	38.2	2.1	24.75
53	56.8	3.07	24.75
53	60.2	3.24	24.75
53	40.3	2.2	24.75
53	17.7	1.04	24.75
53	37.9	2.1	24.75
53	47.9	2.61	24.75
33	56	1.58	15.34
33	72.8	2.05	15.34
33	82	2.31	15.34
33	62.9	1.77	15.34
33	74.7	2.1	15.34
33	27.6	0.81	15.34

33	18.7	0.57	15.34
33	31.1	0.91	15.34
33	49.7	1.41	15.34
33	40.8	1.17	15.34
32	58.4	1.84	15.34
32	30.2	0.98	15.34
32	20.4	0.69	15.34
32	47.3	1.51	15.34
32	38.9	1.25	15.34
32	27.3	0.9	15.34
32	76.3	2.4	15.34
32	68.7	2.16	15.34
32	72.5	2.28	15.34
32	55.4	1.76	15.34
32	81.2	2.56	15.34
44	40.4	1.63	20.07
44	68.3	2.7	20.07
44	78.3	3.08	20.07
44	70.7	2.79	20.07
44	53.2	2.11	20.07
44	61.6	2.44	20.07
44	25.2	1.04	20.07
44	17.3	0.75	20.07
44	43	1.73	20.07
44	35	1.42	20.07
44	52.7	2.1	20.07
42	50.9	2.26	20.07
42	63.6	2.81	20.07
42	73	3.23	20.07
42	26.6	1.25	20.07
42	31.7	1.46	20.07
42	17.9	0.87	20.07
42	25.7	1.2	20.07
42	39.3	1.78	20.07
42	55.3	2.47	20.07
42	47.4	2.12	20.07
42	41.6	1.88	20.07
49	63.9	2.78	22.39
49	70.9	3.07	22.39
49	46.1	2.02	22.39
49	58	2.53	22.39
49	50.9	2.23	22.39
49	21.1	0.98	22.39
49	15.6	0.75	22.39
49	24.2	1.11	22.39
49	39.7	1.76	22.39
49	29.3	1.32	22.39
47	56.9	2.99	22.39
47	45.8	2.42	22.39
47	22.2	1.24	22.39
47	13.8	0.81	22.39
47	32	1.73	22.39
47	42.4	2.25	22.39
47	49.5	2.61	22.39
47	31.7	1.71	22.39

47	25.6	1.41	22.39
33	76.5	2.23	15.53
33	67	1.96	15.53
33	41.4	1.23	15.53
33	20.4	0.64	15.53
33	48	1.42	15.53
33	35.5	1.07	15.53
33	29.3	0.89	15.53
33	39.7	1.19	15.53
33	64.3	1.88	15.53
33	83.5	2.44	15.53
32	53.4	1.82	15.53
32	48	1.64	15.53
32	27.7	0.98	15.53
32	35.6	1.23	15.53
32	16	0.6	15.53
32	31.3	1.09	15.53
32	51.6	1.76	15.53
32	64.7	2.19	15.53
32	72.4	2.44	15.53
32	57	1.93	15.53
40	63.5	1.82	17.47
40	75.8	2.18	17.47
40	36.8	1.08	17.47
40	42.1	1.23	17.47
40	15.8	0.5	17.47
40	23.4	0.72	17.47
40	30.1	0.9	17.47
40	32.1	0.95	17.47
40	47.6	1.38	17.47
40	64.1	1.84	17.47
37	36.9	1.47	17.47
37	18.3	0.77	17.47
37	46.8	1.83	17.47
37	55.4	2.16	17.47
37	63.7	2.47	17.47
37	47.2	1.85	17.47
37	29	1.17	17.47
37	50.7	1.99	17.47
37	59.3	2.31	17.47
37	21.4	0.89	17.47
36	23.1	0.69	16.36
36	33.7	0.98	16.36
36	63	1.79	16.36
36	47	1.35	16.36
36	39.4	1.14	16.36
36	66.6	1.89	16.36
36	74.3	2.1	16.36
36	82.1	2.33	16.36
36	63.3	1.8	16.36
36	51.3	1.47	16.36
34	59.8	2.16	16.36
34	65.2	2.35	16.36
34	75	2.7	16.36
34	31.2	1.16	16.36

34	36.3	1.34	16.36
34	43.1	1.58	16.36
34	17	0.67	16.36
34	27.3	1.03	16.36
34	38.4	1.41	16.36
34	71.5	2.58	16.36
37	50.5	1.5	17.12
37	33.9	1.03	17.12
37	20.6	0.65	17.12
37	45	1.34	17.12
37	76.2	2.24	17.12
37	83.4	2.45	17.12
37	56.4	1.67	17.12
37	64.6	1.9	17.12
37	37.2	1.12	17.12
37	29	0.89	17.12
35	27.3	1.1	17.12
35	35.8	1.41	17.12
35	17.5	0.74	17.12
35	30.8	1.23	17.12
35	52.2	2.02	17.12
35	42.8	1.67	17.12
35	46.9	1.82	17.12
35	61.6	2.37	17.12
35	72.5	2.78	17.12
35	58	2.24	17.12
44	50	1.75	19.80
44	70.6	2.44	19.80
44	37.4	1.32	19.80
44	18.7	0.7	19.80
44	26.4	0.96	19.80
44	44	1.55	19.80
44	52.5	1.83	19.80
44	58.4	2.02	19.80
44	78	2.69	19.80
44	67.4	2.33	19.80
42	67.5	2.79	19.80
42	36.4	1.55	19.80
42	46.7	1.96	19.80
42	40.1	1.7	19.80
42	21.4	0.95	19.80
42	58.2	2.42	19.80
42	52.2	2.18	19.80
42	73.7	3.05	19.80
42	60.6	2.52	19.80
42	48.1	2.01	19.80
40	48.1	1.33	17.45
40	24.2	0.71	17.45
40	14.6	0.45	17.45
40	37.7	1.06	17.45
40	30	0.85	17.45
40	55.5	1.52	17.45
40	64.7	1.76	17.45
40	78.7	2.15	17.45
40	61.2	1.67	17.45

40	42.9	1.19	17.45
36	45.4	1.81	17.45
36	60.6	2.4	17.45
36	70.8	2.78	17.45
36	62.5	2.47	17.45
36	53.3	2.1	17.45
36	35.5	1.43	17.45
36	17.1	0.74	17.45
36	20.6	0.87	17.45
36	23.2	0.96	17.45
36	40.4	1.62	17.45
56	40.4	1.76	25.05
56	33.2	1.46	25.05
56	45.2	1.95	25.05
56	66.4	2.83	25.05
56	62	2.65	25.05
56	26.6	1.19	25.05
56	19.1	0.88	25.05
56	28.7	1.27	25.05
56	44.4	1.92	25.05
56	51.8	2.23	25.05
52	53.3	3.32	25.05
52	35.8	2.28	25.05
52	42.5	2.68	25.05
52	29.8	1.91	25.05
52	33.7	2.15	25.05
52	25.1	1.64	25.05
52	18.3	1.23	25.05
52	14.6	1.01	25.05
52	30.5	1.96	25.05
52	43.5	2.74	25.05
34	43.5	1.49	15.95
34	55	1.89	15.95
34	62.9	2.12	15.95
34	30.2	1.05	15.95
34	37.7	1.3	15.95
34	17.5	0.64	15.95
34	25.3	0.9	15.95
34	30.9	1.08	15.95
34	48.7	1.65	15.95
34	73.3	2.47	15.95
36	55.5	1.53	15.95
36	34.1	0.95	15.95
36	23.6	0.68	15.95
36	14.5	0.44	15.95
36	28.5	0.81	15.95
36	34.9	0.98	15.95
36	43.2	1.2	15.95
36	46.6	1.29	15.95
36	64.5	1.76	15.95
36	75.6	2.06	15.95
36	37.5	1.54	17.03
36	45	1.83	17.03
36	52.8	2.13	17.03
36	57.9	2.33	17.03

36	48.7	1.97	17.03
36	18.4	0.8	17.03
36	23.5	1	17.03
36	14.3	0.64	17.03
36	26.4	1.11	17.03
36	33.2	1.37	17.03
38	48	1.4	17.03
38	64.5	1.87	17.03
38	69.5	2.01	17.03
38	72.8	2.1	17.03
38	58.5	1.7	17.03
38	25.5	0.78	17.03
38	33.6	1	17.03
38	17.7	0.56	17.03
38	40.9	1.2	17.03
38	35.6	1.05	17.03
47	57.4	2.13	20.57
47	37.3	1.42	20.57
47	19.4	0.77	20.57
47	31.2	1.2	20.57
47	48.5	1.82	20.57
47	74.8	2.77	20.57
47	82.2	3.04	20.57
47	76.9	2.85	20.57
47	66.4	2.46	20.57
47	38.5	1.45	20.57
44	28.6	1.37	20.57
44	41.4	1.94	20.57
44	33.7	1.6	20.57
44	13	0.68	20.57
44	17.1	0.86	20.57
44	21.7	1.06	20.57
44	41.2	1.94	20.57
44	47.7	2.23	20.57
44	56	2.6	20.57
44	63.3	2.93	20.57
44	59.7	2.05	19.45
44	30.1	1.07	19.45
44	20.5	0.75	19.45
44	15	0.57	19.45
44	25.6	0.92	19.45
44	42.8	1.49	19.45
44	33.5	1.18	19.45
44	64.9	2.22	19.45
44	71.7	2.45	19.45
44	81.4	2.78	19.45
41	42.9	2.03	19.45
41	65.9	3.08	19.45
41	36.5	1.74	19.45
41	17.1	0.87	19.45
41	22.2	1.1	19.45
41	32.2	1.55	19.45
41	28.7	1.39	19.45
41	49.4	2.33	19.45
41	55.5	2.6	19.45

41	61.4	2.87	19.45
46	54.4	1.97	20.39
46	14.3	0.58	20.39
46	26.4	1	20.39
46	41.2	1.51	20.39
46	34.5	1.28	20.39
46	72.8	2.62	20.39
46	83.1	2.99	20.39
46	78.5	2.82	20.39
46	65.1	2.35	20.39
46	59.1	2.14	20.39
43	50.2	2.51	20.39
43	57.7	2.88	20.39
43	62.5	3.11	20.39
43	32.4	1.66	20.39
43	17.4	0.94	20.39
43	23.9	1.25	20.39
43	30.2	1.55	20.39
43	37.9	1.93	20.39
43	46.7	2.35	20.39
43	52.6	2.63	20.39

Part 3: 175 μm Glass Spheres

Total Height (mm)	Flow Controller Reading (%)	ΔP (in H_2O)	Mass (g)
57	35.2	1.7	29.30
57	42.4	2.02	29.30
57	52.5	2.48	29.30
57	25.6	1.26	29.30
57	16.6	0.86	29.30
57	21.7	1.08	29.30
57	25.8	1.27	29.30
57	39.9	1.91	29.30
57	47.8	2.26	29.30
57	31.1	1.51	29.30
55	20.6	1.35	29.30
55	14.7	1	29.30
55	17.1	1.14	29.30
55	32.3	2.04	29.30
55	26.3	1.68	29.30
55	43.4	2.68	29.30
55	39.9	2.48	29.30
55	50.8	3.12	29.30
55	45.8	2.83	29.30
55	28.3	1.8	29.30
40	36.4	1.35	20.29
40	45.1	1.66	20.29
40	56.7	2.07	20.29
40	66.8	2.42	20.29
40	76.2	2.76	20.29
40	70.4	2.55	20.29
40	52.7	1.92	20.29
40	27.5	1.04	20.29
40	14.4	0.59	20.29
40	20.1	0.79	20.29

39	14.7	0.69	20.29
39	37.3	1.6	20.29
39	24.7	1.09	20.29
39	29.3	1.28	20.29
39	19.4	0.88	20.29
39	42.2	1.8	20.29
39	51	2.17	20.29
39	47.6	2.03	20.29
39	58.5	2.48	20.29
39	69	2.91	20.29
40	35.9	1.24	20.18
40	27.5	0.98	20.18
40	61.1	2.08	20.18
40	44.6	1.53	20.18
40	49.8	1.71	20.18
40	53.8	1.84	20.18
40	81.2	2.75	20.18
40	74.7	2.53	20.18
40	42	1.45	20.18
40	28.6	1.01	20.18
38	48.1	2.35	20.18
38	38.9	1.92	20.18
38	18.2	0.95	20.18
38	23.2	1.19	20.18
38	27.9	1.41	20.18
38	63.4	3.07	20.18
38	47.3	2.31	20.18
38	58.1	2.82	20.18
38	54.1	2.63	20.18
38	41.6	2.05	20.18
54	44.6	2.19	26.89
54	50.9	2.48	26.89
54	62.2	3.02	26.89
54	58	2.82	26.89
54	27	1.37	26.89
54	33	1.65	26.89
54	17	0.9	26.89
54	37.6	1.86	26.89
54	43.8	2.15	26.89
54	54.1	2.63	26.89
50	27.1	1.9	26.89
50	46.1	3.13	26.89
50	48.5	3.29	26.89
50	13.4	1.02	26.89
50	25	1.77	26.89
50	17.7	1.29	26.89
50	20.9	1.5	26.89
50	33.7	2.33	26.89
50	36.8	2.52	26.89
50	27.6	1.93	26.89
52	50.8	2.35	25.76
52	34.2	1.61	25.76
52	26.1	1.26	25.76
52	15.8	0.8	25.76
52	17.2	0.86	25.76

52	23	1.12	25.76
52	32.4	1.53	25.76
52	59.6	2.73	25.76
48	47.3	3.07	25.76
48	18.6	1.3	25.76
48	26.5	1.78	25.76
48	20.9	1.43	25.76
48	37.7	2.47	25.76
48	41.3	2.7	25.76
48	31.4	2.08	25.76
48	23.8	1.62	25.76
48	24.7	1.44	25.33
48	34.8	1.98	25.33
48	46	2.58	25.33
48	52.9	2.95	25.33
48	50.8	2.84	25.33
48	38.6	2.19	25.33
48	27.3	1.58	25.33
48	15.8	0.97	25.33
48	19.4	1.16	25.33
48	23.2	1.36	25.33
51	45.3	1.9	25.33
51	69.8	2.88	25.33
51	62.9	2.6	25.33
51	74.5	3.08	25.33
51	57.1	2.38	25.33
51	38.6	1.63	25.33
51	49.8	2.08	25.33
51	18.2	0.82	25.33
51	21.5	0.95	25.33
51	27.6	1.19	25.33
58	18.9	1.13	29.79
58	27.5	1.59	29.79
58	24.1	1.41	29.79
58	37.7	2.13	29.79
58	45.6	2.55	29.79
58	42.2	2.37	29.79
58	54.1	3	29.79
58	40.7	2.27	29.79
58	25.5	1.47	29.79
58	30.9	1.76	29.79
56	40.2	2.91	29.79
56	43.5	3.14	29.79
56	24.5	1.84	29.79
56	29.2	2.16	29.79
56	32.4	2.38	29.79
56	13.9	1.11	29.79
56	17.8	1.38	29.79
56	16.3	1.28	29.79
56	19.9	1.52	29.79
56	23.9	1.8	29.79
51	58.7	2.82	25.81
51	38.8	1.9	25.81
51	43.2	2.11	25.81
51	49.4	2.4	25.81

51	18.8	0.98	25.81
51	14.9	0.8	25.81
51	23.1	1.18	25.81
51	28.8	1.44	25.81
48	27.8	1.85	25.81
48	36.4	2.38	25.81
48	33.3	2.19	25.81
48	46.5	3.01	25.81
48	49.3	3.18	25.81
48	15.8	1.11	25.81
48	21.1	1.44	25.81
48	17.8	1.24	25.81
46	64.6	2.66	23.62
46	74.3	3.04	23.62
46	67.9	2.78	23.62
46	47.9	1.99	23.62
46	30.1	1.29	23.62
46	24.1	1.05	23.62
46	17.9	0.81	23.62
46	34.8	1.47	23.62
46	42.7	1.78	23.62
46	28	1.2	23.62
43	41.3	2.33	23.62
43	28	1.63	23.62
43	14.8	0.92	23.62
43	18.9	1.14	23.62
43	22.7	1.35	23.62
43	29.8	1.72	23.62
43	37.5	2.13	23.62
43	54.4	3.04	23.62
43	45.9	2.58	23.62
43	50.1	2.81	23.62
54	39.2	2	27.80
54	55	2.76	27.80
54	60.2	3.01	27.80
54	51.5	2.59	27.80
54	46.3	2.34	27.80
54	31.3	1.62	27.80
54	41.5	2.11	27.80
54	18.2	0.99	27.80
54	14.2	0.8	27.80
54	24.1	1.27	27.80
51	19.4	1.44	27.80
51	29.5	2.09	27.80
51	35.6	2.4	27.80
51	40.1	2.79	27.80
51	44.5	3.09	27.80
51	32.3	2.28	27.80
51	41.4	2.89	27.80
51	27.7	1.98	27.80
51	14.7	1.13	27.80
51	24	1.74	27.80
47	51.5	2.83	24.54
47	55.7	3.04	24.54
47	53.3	2.92	24.54

47	43	2.37	24.54
47	46.4	2.55	24.54
47	27.3	1.55	24.54
47	32	1.8	24.54
47	18.8	1.11	24.54
47	13.4	0.83	24.54
47	21.4	1.24	24.54
45	17.7	1.19	24.54
45	12.7	0.89	24.54
45	26.1	1.69	24.54
45	36.6	2.31	24.54
45	44.3	2.76	24.54
45	49.8	3.09	24.54
45	39.5	2.48	24.54
45	32.8	2.08	24.54
45	26.6	1.72	24.54
45	21	1.39	24.54
39	32.7	1.71	20.88
39	40.6	2.1	20.88
39	37.3	1.94	20.88
39	53.7	2.75	20.88
39	49	2.52	20.88
39	60.1	3.07	20.88
39	57.4	2.93	20.88
39	42.3	2.19	20.88
39	24.8	1.33	20.88
39	13.9	0.79	20.88
41	52.3	2.01	20.88
41	60	2.3	20.88
41	68.5	2.62	20.88
41	76.4	2.92	20.88
41	80.1	3.06	20.88
41	49.4	1.9	20.88
41	30	1.19	20.88
41	14.8	0.63	20.88
41	18.5	0.76	20.88
41	23.6	0.95	20.88
52	44.6	2.14	26.13
52	50.5	2.42	26.13
52	55.1	2.64	26.13
52	63	3	26.13
52	41.7	2.02	26.13
52	17.3	0.9	26.13
52	14.1	0.75	26.13
52	25	1.25	26.13
52	31	1.52	26.13
52	37.6	1.83	26.13
49	35.1	2.36	26.13
49	46.4	3.08	26.13
49	29.4	2	26.13
49	22.4	1.56	26.13
49	15.3	1.11	26.13
49	28.2	1.93	26.13
49	32.1	2.17	26.13
49	38	2.55	26.13

49	40.9	2.73	26.13
49	31.7	2.15	26.13
46	45.3	2.7	24.73
46	52	3.09	24.73
46	23.7	1.48	24.73
46	32.3	1.96	24.73
46	29	1.77	24.73
46	38.7	2.32	24.73
46	41.8	2.5	24.73
46	21.7	1.36	24.73
46	17.3	1.11	24.73
46	14.2	0.93	24.73
45	29.1	1.92	24.73
45	32.5	2.14	24.73
45	24.7	1.66	24.73
45	17.6	1.23	24.73
45	40.4	2.63	24.73
45	46.5	3	24.73
45	50.9	3.28	24.73
45	37.3	2.44	24.73
45	29.1	1.93	24.73
45	18.8	1.3	24.73

Part 4: 135 μm and 175 μm Glass Sphere Mixture

Total Height (mm)	Flow Controller Reading (%)	ΔP (in H_2O)	Mass (g)
49	47.4	2.21	23.57
49	50.4	2.34	23.57
49	42.3	1.98	23.57
49	32.7	1.55	23.57
49	21.1	1.04	23.57
49	14.7	0.76	23.57
49	61.2	2.83	23.57
49	70.3	3.23	23.57
48	35.7	1.8	23.57
48	45.5	2.28	23.57
48	55.7	2.77	23.57
48	62.4	3.09	23.57
48	50.6	2.52	23.57
48	26.7	1.37	23.57
48	19.8	1.06	23.57
48	14.4	0.8	23.57
51	52.2	1.93	23.57
51	60.4	2.23	23.57
51	68.2	2.51	23.57
51	38.7	1.45	23.57
51	46	1.71	23.57
51	28	1.08	23.57
51	19.1	0.76	23.57
51	80.5	2.99	23.57
47	59.3	1.98	21.40
47	66	2.2	21.40
47	75.1	2.5	21.40
47	52.9	1.77	21.40
47	33.7	1.15	21.40

47	41.8	1.42	21.40
47	47.7	1.61	21.40
47	18.7	0.67	21.40
44	50.6	2.47	21.40
44	43.5	2.14	21.40
44	36.6	1.82	21.40
44	19.4	1.01	21.40
44	12.2	0.68	21.40
44	42.6	2.11	21.40
44	64	3.11	21.40
44	57.6	2.8	21.40
41	60	1.97	19.08
41	48.8	1.61	19.08
41	42.2	1.41	19.08
41	34.3	1.16	19.08
41	18.6	0.66	19.08
41	22.9	0.8	19.08
41	42	1.39	19.08
40	57.2	2.16	19.08
40	66.4	2.5	19.08
40	79.6	2.99	19.08
40	47	1.79	19.08
40	29.8	1.17	19.08
40	20.4	0.83	19.08
40	13.5	0.58	19.08
42	67.9	2.08	19.08
42	74	2.26	19.08
42	84.5	2.58	19.08
42	57.9	1.78	19.08
42	61.8	1.89	19.08
42	31.3	0.99	19.08
42	40.2	1.25	19.08
42	21	0.69	19.08
63	59.3	2.93	29.35
63	64.1	3.17	29.35
63	49.7	2.48	29.35
63	34.5	1.75	29.35
63	41.2	2.07	29.35
63	30.4	1.55	29.35
63	17.4	0.94	29.35
63	22.4	1.18	29.35
60	37	2.51	29.35
60	40.5	2.74	29.35
60	46	3.09	29.35
60	31.2	2.14	29.35
60	12.9	0.98	29.35
60	17.9	1.29	29.35
60	23	1.62	29.35
62	49.3	2.72	29.35
62	53.1	2.92	29.35
62	59.2	3.25	29.35
62	31.1	1.76	29.35
62	26.1	1.49	29.35
62	17.6	1.05	29.35
62	37.9	2.12	29.35

64	47.4	2.42	29.61
64	61.5	3.11	29.61
64	44.4	2.27	29.61
64	53.9	2.74	29.61
64	35.3	1.83	29.61
64	18.9	1.03	29.61
64	29.3	1.54	29.61
64	22	1.18	29.61
61	38.6	2.38	29.61
61	46.2	2.83	29.61
61	51.7	3.15	29.61
61	41.9	2.58	29.61
61	30.8	1.93	29.61
61	15.6	1.05	29.61
61	29.7	1.87	29.61
61	24.9	1.59	29.61
43	66.1	2.3	20.00
43	76.5	2.65	20.00
43	82.2	2.85	20.00
43	70.3	2.44	20.00
43	29.9	1.07	20.00
43	15.6	0.6	20.00
43	43.9	1.55	20.00
43	48.1	1.69	20.00
41	52.6	2.31	20.00
41	61.4	2.68	20.00
41	39.1	1.73	20.00
41	71.5	3.12	20.00
41	35.3	1.57	20.00
41	20.2	0.94	20.00
41	39.5	1.76	20.00
41	43.9	1.94	20.00
54	65.4	2.68	25.08
54	74.7	3.05	25.08
54	71.7	2.93	25.08
54	44.4	1.84	25.08
54	50.6	2.09	25.08
54	29.9	1.27	25.08
54	20.8	0.91	25.08
54	15.7	0.71	25.08
51	34.7	1.98	25.08
51	39.1	2.23	25.08
51	53.2	2.99	25.08
51	57.7	3.24	25.08
51	47.7	2.68	25.08
51	17.9	1.08	25.08
51	21.5	1.28	25.08
51	26	1.52	25.08

Part 5: Pharmatose

Part 6: Respitose

Total Height (mm)	Flow Controller Reading (%)	ΔP (in H_2O)	Mass (g)
31	20	3.2	7.69

31	15.1	2.51	7.69
31	12.1	2.08	7.69
31	10.3	1.83	7.69
31	13.3	2.26	7.69
31	16.6	2.73	7.69
31	18	2.94	7.69
31	17.2	2.84	7.69
31	19	3.1	7.69
31	20	3.24	7.69
29	15.5	3.16	7.69
29	9.2	2.06	7.69
29	11	2.38	7.69
29	12.3	2.6	7.69
29	9.9	2.18	7.69
29	12.8	2.7	7.69
29	13.8	2.89	7.69
29	14.4	2.97	7.69
29	11.8	2.52	7.69
22	14.7	1.96	5.12
22	10.7	1.5	5.12
22	12.5	1.71	5.12
22	17.4	2.27	5.12
22	15.5	2.05	5.12
22	19.5	2.52	5.12
22	18.2	2.38	5.12
22	13.7	1.87	5.12
22	11.8	1.64	5.12
20	8.6	1.81	5.12
20	11.9	2.36	5.12
20	10.9	2.19	5.12
20	15.7	2.98	5.12
20	13.8	2.67	5.12
20	14.7	2.82	5.12
20	12.3	2.42	5.12
20	9.5	1.97	5.12
20	12.4	2.44	5.12
20	15.5	2.94	5.12
23	13.2	1.98	5.54
23	18.1	2.61	5.54
23	10.3	1.63	5.54
23	12	1.84	5.54
23	15.5	2.29	5.54
23	17	2.48	5.54
23	14.7	2.16	5.54
23	11.4	1.74	5.54
23	20.9	2.95	5.54
23	19.2	2.73	5.54
21	17.5	3.22	5.54
21	9.6	1.95	5.54
21	13.5	2.58	5.54
21	11.2	2.21	5.54
21	10.3	2.07	5.54
21	14.5	2.75	5.54
21	15.8	2.95	5.54
21	16.3	3.04	5.54

21	12.8	2.47	5.54
21	11.5	2.26	5.54
20	13.7	1.85	4.79
20	9.1	1.31	4.79
20	12.5	1.71	4.79
20	17.9	2.36	4.79
20	16.3	2.17	4.79
20	15.1	2.04	4.79
20	10.8	1.53	4.79
20	11.9	1.66	4.79
20	14.7	1.99	4.79
19	13.4	2.42	4.79
19	17.1	2.99	4.79
19	9.2	1.79	4.79
19	10.5	1.97	4.79
19	12.8	2.33	4.79
19	14.8	2.64	4.79
19	15.9	2.81	4.79
19	13.5	2.44	4.79
19	16	2.82	4.79
19	19	3.29	4.79
19	18.4	3.2	4.79
19	14.9	2.65	4.79
30	14.9	2.21	6.48
30	16.7	2.44	6.48
30	18.6	2.7	6.48
30	13.8	2.09	6.48
30	11.5	1.79	6.48
30	9.3	1.5	6.48
30	13.6	2.06	6.48
30	19.1	2.76	6.48
30	15.6	2.31	6.48
27	8.6	1.84	6.48
27	10.5	2.17	6.48
27	13.2	2.62	6.48
27	16.2	3.12	6.48
27	14.7	2.87	6.48
27	15.7	3.04	6.48
27	12.2	2.45	6.48
27	10.4	2.15	6.48
27	9.3	1.97	6.48
27	14.3	2.81	6.48
21	14	1.89	4.93
21	20.4	2.63	4.93
21	16.9	2.23	4.93
21	13.5	1.84	4.93
21	9.9	1.42	4.93
21	12.5	1.74	4.93
21	17.3	2.29	4.93
21	11.3	1.58	4.93
21	18.4	2.41	4.93
21	19.4	2.52	4.93
20	9.8	1.68	4.93
20	19.4	3	4.93
20	15.9	2.53	4.93

20	18.9	2.94	4.93
20	13.1	2.13	4.93
20	11.4	1.9	4.93
20	14.4	2.32	4.93
20	16.9	2.66	4.93
20	18.5	2.88	4.93
20	9.5	1.64	4.93
20	11.3	1.89	4.93
35	12.2	2.19	7.76
35	16.8	2.91	7.76
35	19.1	3.27	7.76
35	13.8	2.47	7.76
35	14.8	2.62	7.76
35	11	2.05	7.76
35	9.5	1.82	7.76
35	13.3	2.4	7.76
35	18	3.11	7.76
32	9	2.22	7.76
32	13.1	3.01	7.76
32	14.7	3.33	7.76
32	11.8	2.78	7.76
32	10.4	2.51	7.76
32	12	2.81	7.76
32	14.1	3.2	7.76
32	11	2.63	7.76
32	10	2.42	7.76
32	13.2	3.04	7.76
27	13.1	2.07	6.31
27	9.8	1.64	6.31
27	12.1	1.95	6.31
27	17	2.6	6.31
27	19.5	2.95	6.31
27	21.9	3.27	6.31
27	16.1	2.49	6.31
27	18.1	2.76	6.31
27	20.9	3.13	6.31
27	13.6	2.16	6.31
27	15.2	2.38	6.31
25	9.9	2.36	6.31
25	12.4	2.84	6.31
25	14.8	3.3	6.31
25	12.9	2.93	6.31
25	10.4	2.46	6.31
25	13.5	3.05	6.31
25	11.6	2.69	6.31
25	11	2.57	6.31
23	13	1.31	5.03
23	15.2	1.5	5.03
23	19	1.89	5.03
23	22.7	2.23	5.03
23	20.8	2.06	5.03
23	10.4	1.14	5.03
23	9.5	1.07	5.03
23	15.2	1.57	5.03
23	12.4	1.31	5.03

23	17.4	1.76	5.03
20	9.5	1.98	5.03
20	17.4	3.28	5.03
20	15.1	2.91	5.03
20	12.2	2.42	5.03
20	11	2.23	5.03
20	14	2.72	5.03
20	15.1	2.91	5.03
20	16.5	3.14	5.03
20	13.4	2.63	5.03
21	9.2	1.54	5.04
21	11	1.78	5.04
21	15.2	2.35	5.04
21	14.3	2.26	5.04
21	12.8	2.06	5.04
21	17.6	2.7	5.04
21	19.6	2.97	5.04
21	13.3	2.13	5.04
21	10.5	1.75	5.04
21	11	1.79	5.04
20	9.2	1.89	5.04
20	15.1	2.85	5.04
20	13.4	2.58	5.04
20	17	3.18	5.04
20	14.5	2.76	5.04
20	11.5	2.28	5.04
20	12.2	2.39	5.04
20	15.1	2.86	5.04
20	17.7	3.29	5.04
20	13.2	2.56	5.04
20	10.8	2.16	5.04

Part 10: Leucine/Mannitol Jar #1

Packing with large visible macro-voids
Packing with small visible macro-voids

Total Height (mm)	Flow Controller Reading (%)	ΔP (in H_2O)	Mass (g)
118	21.6	0.18	1.0611
118	31.5	0.27	1.0611
118	65.1	0.56	1.0611
118	54.3	0.47	1.0611
118	72.5	0.62	1.0611
118	80.9	0.7	1.0611
118	47.6	0.42	1.0611
114	47.6	0.64	1.0611
114	56.6	0.76	1.0611
114	67.1	0.9	1.0611
114	78.2	1.05	1.0611
114	15.3	0.23	1.0611
114	23.3	0.34	1.0611
114	38.8	0.54	1.0611
108	38.8	0.74	1.0611
108	62.7	1.17	1.0611

108	75	1.39	1.0611
108	83.7	1.55	1.0611
108	48.4	0.92	1.0611
108	53.4	1.01	1.0611
108	20.4	0.42	1.0611
108	26.5	0.53	1.0611
102	49.1	1.11	1.0611
102	62.3	1.44	1.0611
102	58.1	1.34	1.0611
102	76.7	1.8	1.0611
102	18.9	0.39	1.0611
102	26.4	0.57	1.0611
102	44.8	1.02	1.0611
101	44.8	1.1	1.0611
101	64.2	1.61	1.0611
101	74.3	1.89	1.0611
101	59.3	1.52	1.0611
101	32.8	0.84	1.0611
101	24.9	0.65	1.0611
101	16.7	0.56	1.0611
100	32.9	0.27	0.8748
100	27	0.23	0.8748
100	18.3	0.17	0.8748
100	52.2	0.42	0.8748
100	59	0.47	0.8748
100	43.8	0.36	0.8748
93	80.6	1.03	0.8748
93	74.1	0.95	0.8748
93	50	0.66	0.8748
93	63.4	0.83	0.8748
93	27.5	0.39	0.8748
93	19.5	0.3	0.8748
93	33.4	0.46	0.8748
79	23	0.72	0.8748
79	16.1	0.48	0.8748
79	40.1	1.36	0.8748
79	54.2	1.88	0.8748
79	64.9	2.29	0.8748
79	74.1	2.64	0.8748
79	44.4	1.57	0.8748
79	20.9	0.75	0.8748
79	59.9	2.16	0.8748
174	38.1	0.12	1.2719
174	33.1	0.11	1.2719
174	18.6	0.07	1.2719
174	23.2	0.08	1.2719
174	33.1	0.11	1.2719
174	27.8	0.09	1.2719
169	71.1	0.26	1.2719
169	59.9	0.22	1.2719
169	46.4	0.18	1.2719
169	35.4	0.14	1.2719
169	25.4	0.1	1.2719
153	25.4	0.21	1.2719
153	17.3	0.16	1.2719

153	59	0.5	1.2719
153	50	0.42	1.2719
153	80.4	0.71	1.2719
153	40.2	0.37	1.2719
141	40.2	0.6	1.2719
141	81.7	1.26	1.2719
141	67.7	1.05	1.2719
141	60.3	0.95	1.2719
141	20	0.35	1.2719
141	29.3	0.49	1.2719
131	29.3	0.85	1.2719
131	21.5	0.64	1.2719
131	15.9	0.51	1.2719
131	45.8	1.28	1.2719
131	64.6	1.82	1.2719
131	78.2	2.24	1.2719
131	50.2	1.49	1.2719
122	50.2	2.12	1.2719
122	64.2	2.66	1.2719
122	76.5	3.17	1.2719
122	29.1	1.3	1.2719
122	19.7	0.94	1.2719
122	35	1.53	1.2719
113	35	2.21	1.2719
113	42.2	2.61	1.2719
113	51.9	3.14	1.2719
113	45.8	2.8	1.2719
113	24	1.61	1.2719
113	13.4	1.05	1.2719
113	19.1	1.36	1.2719
151	52.1	0.62	1.3063
151	43.8	0.54	1.3063
151	39.2	0.49	1.3063
151	22	0.31	1.3063
151	15.5	0.24	1.3063
151	29.8	0.4	1.3063
148	80.5	1.03	1.3063
148	72	0.92	1.3063
148	61.7	0.8	1.3063
148	45	0.6	1.3063
148	26.8	0.38	1.3063
148	30.1	0.43	1.3063
148	15.1	0.25	1.3063
141	15.1	0.39	1.3063
141	28.4	0.65	1.3063
141	22.3	0.53	1.3063
141	51.3	1.13	1.3063
141	57.4	1.25	1.3063
138	69.9	1.57	1.3063
138	84.9	1.97	1.3063
138	62.6	1.48	1.3063
138	39	0.97	1.3063
138	30.9	0.79	1.3063
138	20.1	0.56	1.3063
128	75.4	2.83	1.3063

128	67.9	2.57	1.3063
128	61.4	2.34	1.3063
128	42.5	1.68	1.3063
128	28.3	1.19	1.3063
128	36	1.46	1.3063
128	17.4	0.81	1.3063
128	40.3	1.61	1.3063
120	43	2.44	1.3063
120	58.9	3.25	1.3063
120	52.1	2.91	1.3063
120	38.1	2.19	1.3063
120	21.7	1.38	1.3063
120	14.6	1.04	1.3063
120	26.3	1.62	1.3063
118	26.3	1.66	1.3063
118	17.5	1.21	1.3063
118	13.3	1	1.3063
118	29.5	1.84	1.3063
118	40.8	2.4	1.3063
118	32.4	1.97	1.3063
118	48.8	2.82	1.3063
133	49.6	0.42	1.1214
133	44.5	0.38	1.1214
133	38.8	0.33	1.1214
133	31.9	0.28	1.1214
133	23.9	0.23	1.1214
133	28.8	0.26	1.1214
133	17.7	0.18	1.1214
122	55.5	0.95	1.1214
122	44.5	0.78	1.1214
122	49.3	0.85	1.1214
122	28.7	0.53	1.1214
122	35.7	0.65	1.1214
122	18.6	0.38	1.1214
113	76.7	2.12	1.1214
113	68.4	1.89	1.1214
113	59.4	1.67	1.1214
113	44.5	1.29	1.1214
113	28.7	0.88	1.1214
113	33.9	1.02	1.1214
113	16	0.56	1.1214
109	16	0.65	1.1214
109	36.2	1.25	1.1214
109	41.7	1.41	1.1214
109	30	1.06	1.1214
109	21	0.8	1.1214
107	41.7	1.55	1.1214
107	54.8	1.98	1.1214
107	63.2	2.26	1.1214
107	39.1	1.46	1.1214
107	29.6	1.16	1.1214
107	18.4	0.79	1.1214
107	33.6	1.29	1.1214
156	75.8	0.1	1.0808
156	51.9	0.08	1.0808

156	41.1	0.06	1.0808
156	31.7	0.05	1.0808
156	17	0.03	1.0808
112	16.9	0.47	1.0808
112	71	1.61	1.0808
112	76.1	1.72	1.0808
112	42.4	1	1.0808
112	63.2	1.45	1.0808
112	53.9	1.25	1.0808
112	23.6	0.61	1.0808
112	33.1	0.82	1.0808
105	33.1	1.17	1.0808
105	81.9	2.67	1.0808
105	58.7	1.94	1.0808
105	68	2.23	1.0808
105	76.4	2.49	1.0808
105	43.4	1.48	1.0808
105	19.4	0.77	1.0808
105	12.2	0.55	1.0808
105	23.7	0.9	1.0808
89	23.7	2.5	1.0808
89	19.5	2.15	1.0808
89	17.5	1.99	1.0808
89	11.1	1.45	1.0808
89	14.1	1.7	1.0808
89	16.3	1.9	1.0808
89	9.6	1.33	1.0808
89	7.9	1.19	1.0808
89	6.4	1.06	1.0808

Part 11: Leucine/Mannitol Jar #3

Packing with large visible macro-voids
Packing with small visible macro-voids

Total Height (mm)	Flow Controller Reading (%)	ΔP (in H_2O)	Mass (g)
114	52.3	0.41	1.1268
114	43.3	0.35	1.1268
114	34.6	0.28	1.1268
114	28.1	0.24	1.1268
114	22.6	0.2	1.1268
106	68.6	0.93	1.1268
106	60.3	0.82	1.1268
106	47.6	0.66	1.1268
106	41.1	0.58	1.1268
106	25.6	0.39	1.1268
102	25.6	0.6	1.1268
102	62.7	1.31	1.1268
102	73.7	1.53	1.1268
102	52.1	1.1	1.1268
102	39.2	0.85	1.1268
102	30.2	0.69	1.1268
89	18.4	1.17	1.1268
89	14.4	0.99	1.1268
89	8.4	0.76	1.1268

89	28.6	1.77	1.1268
89	37.9	2.12	1.1268
89	45.1	2.48	1.1268
104	51.1	0.37	1.0300
104	42.9	0.31	1.0300
104	26.3	0.2	1.0300
104	31.1	0.24	1.0300
104	16	0.14	1.0300
96	62	0.86	1.0300
96	52.3	0.73	1.0300
96	42.6	0.6	1.0300
96	23.8	0.37	1.0300
96	15	0.26	1.0300
89	55.6	1.25	1.0300
89	64.2	1.46	1.0300
89	71	1.62	1.0300
89	47.7	1.14	1.0300
89	33	0.84	1.0300
89	38.8	0.96	1.0300
89	22.5	0.62	1.0300
131	60	0.54	1.3033
131	47.1	0.43	1.3033
131	38.4	0.36	1.3033
131	23.1	0.24	1.3033
131	30.3	0.3	1.3033
122	30.3	0.61	1.3033
122	74.2	1.39	1.3033
122	67.2	1.27	1.3033
122	48	0.93	1.3033
122	53.6	1.03	1.3033
122	20.8	0.46	1.3033
118	74	1.68	1.3033
118	66.3	1.52	1.3033
118	47.2	1.11	1.3033
118	51.6	1.2	1.3033
118	26.8	0.68	1.3033
118	30.7	0.76	1.3033
118	14.7	0.42	1.3033
106	37.6	2.1	1.3033
106	43.6	2.39	1.3033
106	29.1	1.69	1.3033
106	18.8	1.21	1.3033
106	23	1.39	1.3033
106	13.4	0.93	1.3033
163	20.8	0.02	1.2451
163	10	0.01	1.2451
163	6.5	0.01	1.2451
163	16.9	0.02	1.2451
123	16.9	0.24	1.2451
123	25.5	0.32	1.2451
123	21.4	0.28	1.2451
123	19	0.26	1.2451
117	68	1.19	1.2451
117	60.9	1.07	1.2451
117	46	0.82	1.2451

117	28.9	0.55	1.2451
117	36.6	0.68	1.2451
117	15.7	0.34	1.2451
114	62.3	1.32	1.2451
114	72.8	1.53	1.2451
114	43.7	0.95	1.2451
114	31.2	0.71	1.2451
114	14.9	0.4	1.2451
114	23.7	0.57	1.2451
108	23.7	0.81	1.2451
108	38	1.2	1.2451
108	54.6	1.66	1.2451
108	72.3	2.15	1.2451
108	65.3	1.96	1.2451
108	31.5	1.03	1.2451
108	14.2	0.56	1.2451
119	50.3	0.55	1.2371
119	33.3	0.38	1.2371
119	40.5	0.46	1.2371
119	28.2	0.34	1.2371
119	16.4	0.22	1.2371
111	16.4	0.47	1.2371
111	63	1.52	1.2371
111	45	1.12	1.2371
111	38.9	0.98	1.2371
111	52.9	1.3	1.2371
111	27.9	0.76	1.2371
111	31.4	0.82	1.2371
111	14.5	0.43	1.2371
111	20.5	0.57	1.2371
108	20.5	0.67	1.2371
108	33.6	1.01	1.2371
108	73.6	2.08	1.2371
108	68	1.92	1.2371
108	52.3	1.51	1.2371
108	58.5	1.68	1.2371
108	46.8	1.36	1.2371
108	17.1	0.59	1.2371
94	25.9	2.52	1.2371
94	34.3	3.17	1.2371
94	29.2	2.78	1.2371
94	12.7	1.47	1.2371
94	8.6	1.15	1.2371
94	15.8	1.72	1.2371
94	20.3	2.08	1.2371
94	23.4	2.32	1.2371
88	5	1.29	1.2371
88	6.4	1.47	1.2371
88	9.7	1.88	1.2371
88	13.2	2.29	1.2371
88	8.5	1.73	1.2371
88	10.4	1.96	1.2371
96	50.5	0.78	1.0194
96	34.9	0.56	1.0194
96	40.4	0.64	1.0194

96	29	0.48	1.0194
96	17.8	0.33	1.0194
96	23.2	0.4	1.0194
91	70	1.63	1.0194
91	61.3	1.43	1.0194
91	53.2	1.26	1.0194
91	41.5	1.01	1.0194
91	18.6	0.52	1.0194
91	25.8	0.68	1.0194
91	32.6	0.83	1.0194
88	32.6	1	1.0194
88	38.5	1.16	1.0194
88	60.8	1.75	1.0194
88	48.6	1.42	1.0194
88	23.3	0.75	1.0194
88	17.5	0.61	1.0194
88	27.4	0.87	1.0194
81	6.8	0.57	1.0194
81	13.6	0.88	1.0194
81	17.7	1.2	1.0194
81	15	1.07	1.0194
81	24	1.35	1.0194
81	29.6	1.61	1.0194
81	21.8	1.26	1.0194
133	41.6	0.14	1.1529
133	36.8	0.12	1.1529
133	25	0.09	1.1529
133	30.3	0.11	1.1529
133	16.7	0.07	1.1529
113	16.7	0.23	1.1529
113	54.2	0.61	1.1529
113	45.5	0.52	1.1529
113	33.5	0.4	1.1529
113	19.9	0.26	1.1529
113	29.5	0.36	1.1529
108	29.5	0.6	1.1529
108	64.8	1.22	1.1529
108	74	1.39	1.1529
108	47.5	0.92	1.1529
108	34.3	0.69	1.1529
108	16	0.38	1.1529
108	50	0.97	1.1529
102	50	1.32	1.1529
102	62.3	1.61	1.1529
102	57.2	1.49	1.1529
102	37.7	1.03	1.1529
102	44.1	1.18	1.1529
102	26.4	0.76	1.1529
102	18.2	0.56	1.1529
97	6.1	0.37	1.1529
97	28	1.05	1.1529
97	37	1.34	1.1529
97	45.5	1.6	1.1529
97	72.4	2.45	1.1529
97	63.9	2.17	1.1529

97	54.2	1.87	1.1529
97	17.7	0.73	1.1529
108	63.1	0.05	0.9308
108	31.7	0.03	0.9308
108	46	0.04	0.9308
108	7.2	0.01	0.9308
108	35.3	0.03	0.9308
90	35.3	0.42	0.9308
90	75.4	0.84	0.9308
90	65.2	0.73	0.9308
90	50.6	0.58	0.9308
90	23.6	0.3	0.9308
90	14.1	0.2	0.9308
90	43	0.5	0.9308
87	43	0.67	0.9308
87	83.4	1.25	0.9308
87	75	1.13	0.9308
87	41.3	0.65	0.9308
87	11.1	0.23	0.9308
87	18.4	0.34	0.9308
87	27.7	0.47	0.9308
87	32.7	0.54	0.9308
87	62.5	0.95	0.9308
87	51.2	0.79	0.9308
82	31.2	0.75	0.9308
82	50.1	1.13	0.9308
82	65	1.44	0.9308
82	82.8	1.81	0.9308
82	73.5	1.61	0.9308
82	53.7	1.2	0.9308
82	36.5	0.86	0.9308
82	19.1	0.5	0.9308
82	27.6	0.69	0.9308

Part 12: Leucine/Mannitol Jar #4

Packing with large visible macro-voids
Packing with small visible macro-voids

Total Height (mm)	Flow Controller Reading (%)	ΔP (in H_2O)	Mass (g)
170	30.2	0.04	1.1525
170	21.5	0.03	1.1525
170	16.4	0.02	1.1525
170	8.1	0.02	1.1525
170	27.6	0.04	1.1525
143	52.9	0.22	1.1525
143	42.6	0.18	1.1525
143	29.9	0.13	1.1525
143	16.1	0.08	1.1525
143	24	0.11	1.1525
118	24	0.42	1.1525
118	15.3	0.3	1.1525
118	30.6	0.52	1.1525
118	44.4	0.71	1.1525
118	50.7	0.8	1.1525

118	38.3	0.62	1.1525
106	38.3	1.3	1.1525
106	56.8	1.85	1.1525
106	76.5	2.47	1.1525
106	66.4	2.16	1.1525
106	62.1	2.03	1.1525
106	19.1	0.73	1.1525
106	23.8	0.88	1.1525
102	8.1	0.5	1.1525
102	15.3	0.77	1.1525
102	32.4	1.39	1.1525
102	28.8	1.25	1.1525
102	57.3	2.31	1.1525
102	65.7	2.61	1.1525
102	43.5	1.79	1.1525
102	48.5	1.98	1.1525
137	48.5	0.09	1.0421
137	40.3	0.08	1.0421
137	26.6	0.05	1.0421
137	31.5	0.06	1.0421
137	11.2	0.03	1.0421
109	11.2	0.19	1.0421
109	64.4	0.79	1.0421
109	49.5	0.62	1.0421
109	52.9	0.66	1.0421
109	32.8	0.43	1.0421
109	37.4	0.49	1.0421
109	26.2	0.36	1.0421
100	26.2	0.65	1.0421
100	15.8	0.44	1.0421
100	20.3	0.53	1.0421
100	44.4	1.02	1.0421
100	40.1	0.93	1.0421
100	55.8	1.25	1.0421
100	68.8	1.53	1.0421
100	79.3	1.77	1.0421
85	15.7	1.22	1.0421
85	25.9	1.78	1.0421
85	33.8	2.22	1.0421
85	30.6	2.06	1.0421
85	17.5	1.32	1.0421
85	44.7	2.85	1.0421
85	39.5	2.55	1.0421
85	20.2	1.47	1.0421
85	8	0.79	1.0421
147	8	0.12	1.3001
147	18.6	0.21	1.3001
147	35.2	0.35	1.3001
147	26.8	0.27	1.3001
147	13.7	0.16	1.3001
132	13.7	0.42	1.3001
132	27.1	0.67	1.3001
132	46.5	1.05	1.3001
132	37.8	0.88	1.3001
132	19.6	0.53	1.3001

129	73.1	1.62	1.3001
129	55	1.24	1.3001
129	68.9	1.54	1.3001
129	31.3	0.75	1.3001
129	37.7	0.89	1.3001
129	44.3	1.03	1.3001
129	22.4	0.58	1.3001
122	22.4	0.87	1.3001
122	71.9	2.5	1.3001
122	54.6	1.93	1.3001
122	59.2	2.08	1.3001
122	19.6	0.81	1.3001
122	41.7	1.53	1.3001
122	35.3	1.32	1.3001
122	27.8	1.08	1.3001
122	73.5	2.57	1.3001
122	25.3	1.01	1.3001
112	25.3	1.66	1.3001
112	18.4	1.3	1.3001
112	13.4	1.04	1.3001
112	40	2.45	1.3001
112	53.8	3.2	1.3001
112	49.3	2.96	1.3001
112	30.3	1.94	1.3001
112	36.1	2.25	1.3001
112	25.3	1.67	1.3001
112	22.3	1.51	1.3001
111	28.3	0.21	1.0048
111	23.3	0.18	1.0048
111	17.3	0.15	1.0048
111	34.2	0.26	1.0048
111	12	0.11	1.0048
105	12.1	0.18	1.0048
105	32.7	0.38	1.0048
105	27.7	0.34	1.0048
105	21	0.27	1.0048
105	14.6	0.2	1.0048
103	63.9	0.75	1.0048
103	58.9	0.7	1.0048
103	77.8	0.91	1.0048
103	29.4	0.38	1.0048
103	35.6	0.45	1.0048
103	18	0.25	1.0048
103	23.9	0.32	1.0048
99	70.8	1.14	1.0048
99	78.7	1.26	1.0048
99	42.5	0.71	1.0048
99	51.7	0.85	1.0048
99	19.5	0.37	1.0048
99	28.1	0.5	1.0048
99	57.7	0.95	1.0048
94	19.9	0.51	1.0048
94	76.2	1.63	1.0048
94	70.7	1.52	1.0048
94	56	1.28	1.0048

129	73.1	1.62	1.3001
129	55	1.24	1.3001
129	68.9	1.54	1.3001
129	31.3	0.75	1.3001
129	37.7	0.89	1.3001
129	44.3	1.03	1.3001
129	22.4	0.58	1.3001
122	22.4	0.87	1.3001
122	71.9	2.5	1.3001
122	54.6	1.93	1.3001
122	59.2	2.08	1.3001
122	19.6	0.81	1.3001
122	41.7	1.53	1.3001
122	35.3	1.32	1.3001
122	27.8	1.08	1.3001
122	73.5	2.57	1.3001
122	25.3	1.01	1.3001
112	25.3	1.66	1.3001
112	18.4	1.3	1.3001
112	13.4	1.04	1.3001
112	40	2.45	1.3001
112	53.8	3.2	1.3001
112	49.3	2.96	1.3001
112	30.3	1.94	1.3001
112	36.1	2.25	1.3001
112	25.3	1.67	1.3001
112	22.3	1.51	1.3001
111	28.3	0.21	1.0048
111	23.3	0.18	1.0048
111	17.3	0.15	1.0048
111	34.2	0.26	1.0048
111	12	0.11	1.0048
105	12.1	0.18	1.0048
105	32.7	0.38	1.0048
105	27.7	0.34	1.0048
105	21	0.27	1.0048
105	14.6	0.2	1.0048
103	63.9	0.75	1.0048
103	58.9	0.7	1.0048
103	77.8	0.91	1.0048
103	29.4	0.38	1.0048
103	35.6	0.45	1.0048
103	18	0.25	1.0048
103	23.9	0.32	1.0048
99	70.8	1.14	1.0048
99	78.7	1.26	1.0048
99	42.5	0.71	1.0048
99	51.7	0.85	1.0048
99	19.5	0.37	1.0048
99	28.1	0.5	1.0048
99	57.7	0.95	1.0048
94	19.9	0.51	1.0048
94	76.2	1.63	1.0048
94	70.7	1.52	1.0048
94	56	1.28	1.0048

91	71.6	3.11	1.0971
86	10.6	1	1.0971
86	14.3	1.26	1.0971
86	18.1	1.49	1.0971
86	25.3	1.94	1.0971
86	34.4	2.68	1.0971
86	30.8	2.46	1.0971
86	27.1	2.22	1.0971
86	7.4	0.82	1.0971
152	7.4	0.02	1.1000
152	22.9	0.04	1.1000
152	42.1	0.06	1.1000
152	34.1	0.05	1.1000
152	15.8	0.03	1.1000
109	15.8	0.31	1.1000
109	72.6	1.2	1.1000
109	62.1	1.03	1.1000
109	40.2	0.69	1.1000
109	52.3	0.88	1.1000
109	23.3	0.44	1.1000
109	37.4	0.66	1.1000
100	37.4	1.24	1.1000
100	76.5	2.44	1.1000
100	51.7	1.69	1.1000
100	60.1	1.95	1.1000
100	23.6	0.86	1.1000
100	14.8	0.61	1.1000
100	35	1.21	1.1000
100	67.8	2.27	1.1000
94	26.9	1.3	1.1000
94	57.2	2.54	1.1000
94	69	3.02	1.1000
94	47.9	2.17	1.1000
94	33.7	1.61	1.1000
94	17.2	0.92	1.1000
94	44	1.99	1.1000
94	63	2.75	1.1000

Part 13: Leucine/Mannitol Jar #1, Second Collection

Total Height (mm)	Flow Controller Reading (%)	ΔP (in H_2O)	Mass (g)	
107	56.7	3.23	1.28	
107	40.5	2.41	1.28	
107	27.3	1.74	1.28	
107	31.9	1.98	1.28	
107	37.9	2.28	1.28	
107	21.6	1.44	1.28	
107	17	1.2	1.28	
99	15.2	1.88	1.28	
99	21.4	2.44	1.28	
99	25.5	2.81	1.28	
99	27.7	3.01	1.28	
99	17.3	2.1	1.28	
99	13	1.71	1.28	
85	70.5	0.61	0.90	

85	66.1	0.58	0.90
85	47.8	0.43	0.90
85	27.8	0.27	0.90
85	17.5	0.19	0.90
85	39.2	0.36	0.90
79	73.5	1.47	0.90
79	41.1	0.87	0.90
79	55.1	1.13	0.90
79	61.1	1.24	0.90
79	22.7	0.53	0.90
79	32.7	0.72	0.90
79	38.1	0.82	0.90
75	19.3	0.65	0.90
75	62.1	1.71	0.90
75	52.1	1.45	0.90
75	34.9	1.03	0.90
75	41.5	1.19	0.90
75	25.1	0.78	0.90
69	33.4	1.93	0.90
69	49.8	2.72	0.90
69	41.1	2.3	0.90
69	22	1.37	0.90
69	17.6	1.16	0.90
69	26.8	1.61	0.90
69	12.2	0.9	0.90
86	67.5	1.51	1.02
86	52.5	1.2	1.02
86	34.9	0.83	1.02
86	42.3	0.99	1.02
86	19.4	0.52	1.02
86	28.3	0.7	1.02
88	28.3	0.67	1.02
88	72.2	1.54	1.02
88	61.3	1.32	1.02
88	43.6	0.97	1.02
88	38.7	0.88	1.02
88	17	0.45	1.02
88	21.9	0.55	1.02
83	16.8	0.68	1.02
83	29.9	1.06	1.02
83	36.1	1.24	1.02
83	50.1	1.66	1.02
83	21.6	0.82	1.02
83	43.3	1.45	1.02
83	64.5	2.08	1.02

Part 14: Leucine/Mannitol Jar #4, Second Collection

Total Height (mm)	Flow Controller Reading (%)	ΔP (in H_2O)	Mass (g)
110	65.8	0.88	1.02
110	42.9	0.59	1.02
110	47.4	0.65	1.02
110	55.9	0.76	1.02
110	21.9	0.33	1.02
110	32.6	0.47	1.02

110	28.1	0.42	1.02
102	28.1	0.69	1.02
102	74.3	1.66	1.02
102	21.4	0.55	1.02
102	51.5	1.18	1.02
102	57.2	1.3	1.02
102	45.4	1.05	1.02
102	38.4	0.9	1.02
102	31.6	0.76	1.02
97	81.2	2.66	1.02
97	65.3	2.17	1.02
97	47.5	1.61	1.02
97	22.4	0.86	1.02
97	32.4	1.17	1.02
97	50.6	1.73	1.02
97	69.1	2.3	1.02
80	69.3	1.63	0.86
80	55.3	1.33	0.86
80	40.6	1	0.86
80	18.6	0.52	0.86
80	26.9	0.71	0.86
80	32.1	0.82	0.86
80	35.8	0.91	0.86
77	35.8	1.01	0.86
77	71.7	1.92	0.86
77	59.3	1.59	0.86
77	35.1	1	0.86
77	24.3	0.74	0.86
77	14.8	0.5	0.86
77	42.6	1.19	0.86
77	62.3	1.68	0.86
74	50.5	1.69	0.86
74	35.1	1.23	0.86
74	43.2	1.47	0.86
74	27.6	1	0.86
74	20.1	0.78	0.86
74	30.8	1.11	0.86
74	41.4	1.42	0.86
111	62.8	2.07	1.19
111	48	1.62	1.19
111	40.2	1.39	1.19
111	23.8	0.89	1.19
111	18.5	0.74	1.19
111	32.1	1.15	1.19
111	28.3	1.03	1.19
109	28.3	1.11	1.19
109	72.4	2.56	1.19
109	57.3	2.05	1.19
109	62.9	2.24	1.19
109	39.9	1.48	1.19
109	47	1.72	1.19
109	22.4	0.92	1.19
101	16.9	1.18	1.19
101	24.4	1.56	1.19
101	27.5	1.72	1.19

101	19.4	1.3	1.19
101	32.2	1.96	1.19
101	37.7	2.24	1.19
101	43.1	2.52	1.19

Part 15: 175 um glass spheres at high flow rates

		Pressure (psi)	
Total Height (mm)	Rotameter Reading	Upstream	Downstream
25	10	24.000	1.000
25	47.8	30.000	1.500
25	31.1	34.000	2.000
20	20.6	30.000	1.000
20	28.3	34.000	1.500
20	36.4	20.000	0.500
20	14.4	26.000	1.500
20	20.1	33.000	2.250
17	14.7	28.000	1.000
17	69	32.500	1.500
21	35.9	20.000	0.500
21	42	26.000	1.500
21	28.6	32.000	2.000
17	48.1	26.000	1.000
17	41.6	32.000	1.500
18	44.6	18.000	
18	37.6	24.000	1.000
18	43.8	29.000	2.000
18	54.1	32.000	2.500
15	27.1	22.000	0.750
15	36.8	29.000	1.500
15	27.6	32.000	2.000
20	50.8	21.000	
20	32.4	26.000	1.500
20	59.6	32.000	2.000
17	47.3	26.000	1.000
17	23.8	33.000	1.500
19	24.7	19.000	
19	19.4	25.000	1.250
19	23.2	31.000	2.000
16	45.3	23.000	0.750
16	69.8	30.000	1.500
16	27.6	33.000	1.750
17	18.9	19.000	0.500
17	25.5	24.000	1.250
17	30.9	30.000	2.000
14	40.2	22.000	0.750
14	19.9	28.000	1.500
14	23.9	34.000	2.000
16	58.7	18.000	
16	38.8	24.000	1.250
16	23.1	30.000	2.000
16	28.8	32.000	2.500
14	27.8	22.000	0.750
14	21.1	27.000	1.500

14	17.8	34.000	2.000
18	64.6	20.000	
18	42.7	25.000	1.500
18	28	31.000	2.000
16	41.3	24.000	1.000
16	45.9	30.000	1.500
16	50.1	34.000	2.000
15	39.2	16.000	
15	55	22.000	1.000
15	14.2	27.000	2.000
15	24.1	32.000	2.750
13	19.4	20.000	0.000
13	14.7	26.000	1.250
13	24	32.000	2.000

Appendix B: Sample Calculations

Based on Ergun's 1951 paper, the following details the deduction of the calculations required to predict the effective density of particles (ρ_{eff}) from flow data of a packed bed at particle Reynold's numbers (Re_p) less than 1.

The pressure gradient was calculated with the following equation:

$$\frac{\Delta P}{l} = \frac{\Delta P}{h_{Packing} - h_{ToTap}} \tag{1}$$

Where ΔP is the measured pressure drop, $h_{Packing}$ is the height of the packing, h_{ToTap} is the distance from the bottom of the column to the low pressure tap of the manometer or differential pressure cell. This equation was employed only for the Sigma-Aldrich lactose as follows:

$$\frac{\Delta P}{l} = \frac{0.3 inH_20 \times 249.1 Pa/inH_20}{132mm - 123mm} = 8.3 Pa/mm$$

In the case of the column without taps, $h_{Packing}$ is the height of the packing and h_{ToTap} was zero. The equation reduces to:

$$\frac{\Delta P}{l} = \frac{\Delta P}{h_{Packing}} \tag{2}$$

This equation was employed for the 135 μm glass spheres as follows:

$$\frac{\Delta P}{l} = \frac{0.7 inH_20 \times 249.1 Pa/inH_20}{49mm} = 3.56 Pa/mm$$

The volumetric flow rate for the Matheson 8272-0421 Mass Flow Transducer was calculated using the following calibration equation:

$$V = 0.0591 \frac{ml/s}{\%} \times \%ofRange \tag{3}$$

where %ofRange is the % of range for the flow transducer. This equation was employed for the 135 μm glass spheres as follows:

$$V = 0.0591 \frac{ml/s}{\%} \times 15.7\% = 0.298 ml/s$$

The volumetric flow rate for the Matheson 8272-0432 Mass Flow Transducer was calculated using the following calibration equation:

$$V = 0.00414222\frac{ml/s}{\%} \times \%ofRange \oplus 0.02297952 \quad (4)$$

This equation was employed for Jar#1 of the leucine/mannitol powder as follows:

$$V = 0.00414222\frac{ml/s}{\%} \times 21.6\% \oplus 0.02297952 = 0.112\text{ml/s}$$

The superficial velocity was calculated with the following equation:

$$U = \frac{V}{\left(\frac{\pi d_{Column}^2}{4}\right)} \quad (5)$$

where U is the superficial velocity, V is the volumetric flow rate, and d_{Column} is the column diameter. This equation was employed for the 135 μm glass spheres as follows:

$$U = \frac{0.298ml/s}{\left(\frac{\pi(1.9cm)^2}{4}\right)} \times 10\frac{mm/s}{cm/s} = 0.40mm/s$$

The pressure drop was adjusted to account for the pressure losses through the sintered plates for some powders. The following was used to estimate the pressure loss through the sintered plates based on experimental data:

$$\Delta P = \Delta P_{Measured} - \quad (6)$$

where $\Delta P_{Measured}$ is the measured pressure drop. This equation was employed for the 135 μm glass spheres as follows:

$$\Delta P = \Delta P_{Measured} -$$

The bulk density was calculated using the equation:

$$\rho_{Bulk} = \frac{m}{h_{Packing}\left(\frac{\pi d_{Column}^2}{4}\right)} \quad (7)$$

This equation was employed for the 135 μm glass spheres as follows:

$$\rho_{Bulk} = \frac{m_{Full} - m_{Empty}}{h_{Packing}\left(\frac{\pi d_{Column}^2}{4}\right)}$$

where m of powder.

Error Calculations

The error calculations were done in accordance with Holman (1978).

The error in the velocity was calculated as follows:

$$\partial U = \left[\left(\frac{\partial V}{\left(\frac{\pi d_{Column}^2}{4} \right)} \right)^2 + \left(\frac{2U}{d_{Column}} \partial d_{Column} \right)^2 \right]^{1/2} \tag{8}$$

The error in the velocity was calculated for Jar#1 of the leucine/mannitol powder as follows:

$$\partial U = \left[\left(\frac{0.0095 ml/s}{(2.835 cm^3)} \right)^2 + \left(\frac{2 \times 0.0397 cm/s}{1.9 cm} 0.01 cm \right)^2 \right]^{1/2} \times \frac{10 mm/s}{1 cm/s} = 0.038 mm/s$$

The error in the pressure gradient was calculated as follows:

$$\partial \frac{\Delta P}{l} = \left[\left(\frac{\partial P}{h} \right)^2 + \left(\frac{\Delta P / l}{h} \partial h \right)^2 \right]^{1/2} \tag{9}$$

The error in the pressure gradient was calculated for Jar#1 of the leucine/mannitol powder as follows:

$$\partial \frac{\Delta P}{l} = \left[\left(\frac{2.18 Pa}{118 mm} \right)^2 + \left(\frac{0.38 Pa/mm}{118 mm} 0.5 mm \right)^2 \right]^{1/2} = 0.0185 Pa/mm$$

The error in the value of a was calculated as follows:

$$\partial a = \left[\left(\frac{\partial \frac{\Delta P}{l}}{U} \right)^2 + \left(\frac{\Delta P / l}{U^2} \partial U \right)^2 \right]^{1/2} \tag{10}$$

The error in a was calculated for Jar#1 of the leucine/mannitol powder as follows:

$$\partial a = \left[\left(\frac{0.0185 Pa/mm}{0.397 mm/s} \right)^2 + \left(\frac{0.38 Pa/mm}{(0.397 mm/s)^2} 0.038 mm/s \right)^2 \right]^{1/2} = 0.094 Pa \cdot s/mm^2$$

The error in the bulk density was calculated as follows:

$$\partial\rho_{Bulk} = \left[\left(\frac{\rho_{Bulk}}{h}\partial h\right)^2 + \left(\frac{\rho_{Bulk}}{d}\partial d\right)^2\right]^{1/2} \quad (11)$$

The error in the bulk density was calculated for Jar#1 of the leucine/mannitol powder as follows:

$$\partial\rho_{Bulk} = \left[\left(\frac{0.0317g/cm^3}{118mm}0.5mm\right)^2 + \left(\frac{0.0317g/cm^3}{19mm}0.01mm\right)^2\right]^{1/2} = 0.000334g/cm^3$$

The error in $(\rho_{Bulk}^2/a)^{1/3}$ was calculated as follows:

$$\partial\left(\frac{\rho_{Bulk}^2}{a}\right)^{1/3} = \left[\left(\frac{2}{3\rho_{Bulk}^{1/3}a^{1/3}}\partial\rho_{Bulk}\right)^2 + \left(\frac{\rho_{Bulk}^{2/3}}{3a^{4/3}}\partial a\right)^2\right]^{1/2} \quad (12)$$

The error in the $(\rho_{Bulk}^2/a)^{1/3}$ was calculated for Jar#1 of the leucine/mannitol powder as follows:

$$\partial\left(\frac{\rho_{Bulk}^2}{a}\right)^{1/3} = \left[\left(\frac{2}{3(0.0317)^{1/3}(1.154)^{1/3}}0.000334\right)^2 + \left(\frac{(0.0317)^{2/3}}{3(1.154)^{4/3}}0.094\right)^2\right]^{1/2} = 0.0027$$

An average of the error in $(\rho_{Bulk}^2/a)^{1/3}$ at every point was used.

The error in $(\rho_{Bulk}/a)^{1/4.65}$ was calculated as follows:

$$\partial\left(\frac{\rho_{Bulk}}{a}\right)^{1/4.65} = \left[\left(\frac{1}{4.65\rho_{Bulk}^{3.65/4.65}a^{1/4.65}}\partial\rho_{Bulk}\right)^2 + \left(\frac{\rho_{Bulk}^{1/4.65}}{4.65a^{5.65/4.65}}\partial a\right)^2\right]^{1/2} \quad (13)$$

The error in the $(\rho_{Bulk}/a)^{1/4.65}$ was calculated for Jar#1 of the leucine/mannitol powder as follows:

$$\partial\left(\frac{\rho_{Bulk}}{a}\right)^{1/4.65} = \left[\left(\frac{0.000334}{4.65(0.0317)^{3.65/4.65}1.154^{1/4.65}}\right)^2 + \left(\frac{(0.0317)^{1/4.65}}{4.65(1.154)^{5.65/4.65}}0.094\right)^2\right]^{1/2} = 0.00815$$

An average of the error in $(\rho_{Bulk}/a)^{1/4.65}$ at every point was used.

The error in effective density using the Ergun Method was calculated as follows using the slope from the relationship between ρ_{Bulk} and $(\rho_{Bulk}^2/a)^{1/3}$ (m), and average values of the bulk density and a, as well as average values for the error in the bulk density and a:

$$\partial\rho_{Eff} = \left[\left(\frac{m\rho_{Bulk}^{2/3}}{3a^{4/3}}\partial a\right)^2 + \left(\left(1-\frac{2m}{3}\frac{}{\rho_{Bulk}^{1/3}a^{1/3}}\right)\partial\rho_{Bulk}\right)^2\right]^{1/2} \quad (14)$$

The error in the effective density was calculated for Jar#1 of the leucine/mannitol powder as follows:

$$\partial\rho_{Eff} = \left[\left(\frac{-0.285(0.0317)^{2/3}}{3(4.73)^{4/3}}0.284\right)^2 + \left(\left(1-\frac{2(-0.285)}{3(0.0317)^{1/3}(4.73)^{1/3}}\right)0.000334\right)^2\right]^{1/2} = 0.006 g/cm^3$$

This value for the error in $(\rho_{Bulk}^2/a)^{1/3}$ was used at every point was used.

The error in the effective density predicted with the Richardson-Zaki equation was calculated as follows:

$$\partial\rho_{Eff} = \left[\left(\frac{m\rho_{Bulk}^{1/4.65}}{4.65a^{5.65/4.65}}\partial a\right)^2 + \left(\left(1-\frac{m}{4.65}\frac{1}{\rho_{Bulk}^{3.65/4.65}a^{1.4.65}}\right)\partial\rho_{Bulk}\right)^2\right]^{1/2} \quad (15)$$

The error in the effective density was calculated for Jar#1 of the leucine/mannitol powder as follows:

$$\partial\rho_{Eff} = \left[\left(\frac{(-0.072)(0.0317)^{1/4.65}}{4.65(4.73)^{5.65/4.65}}0.284\right)^2 + \left(\left(1-\frac{(-0.072)}{4.65(0.0317)^{3.65/4.65}(4.73)^{1.4.65}}\right)0.00036\right)^2\right]^{1/2} = 0.0005$$

This value for the error in $(\rho_{Bulk}/a)^{1/4.65}$ was used at every point was used.

Appendix C: Extra SEMs

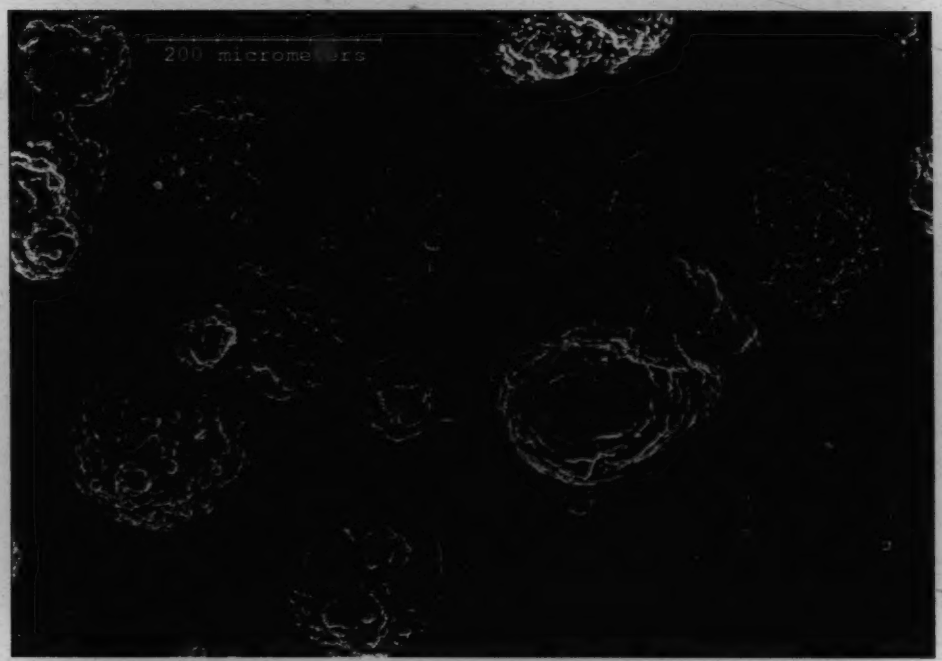

Figure C.1 SEM of Pharmatose. Scale bar is 200μm.

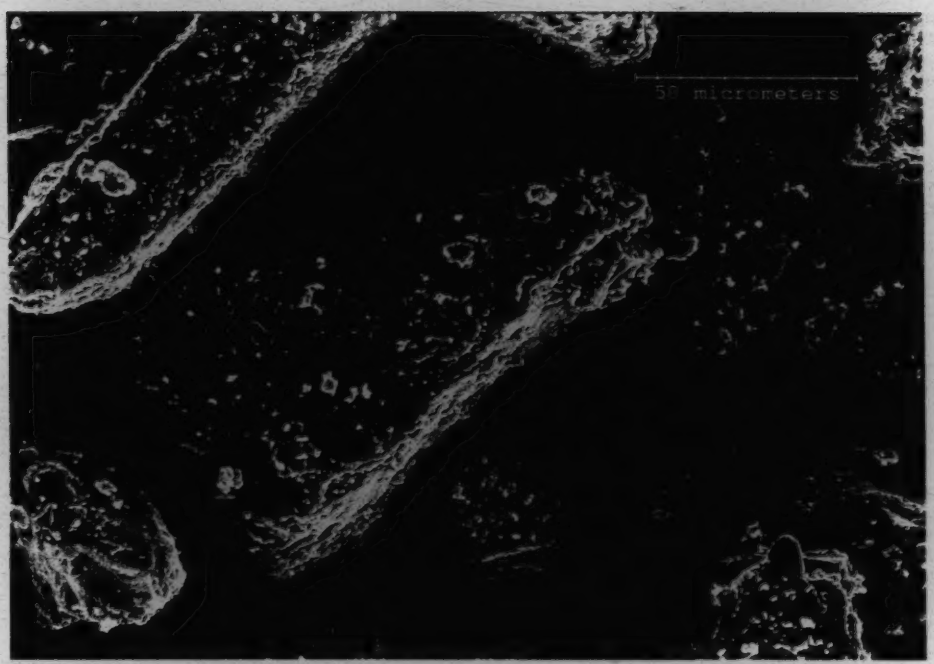

Figure C.2 SEM of Respitose. Scale bar is 50μm.

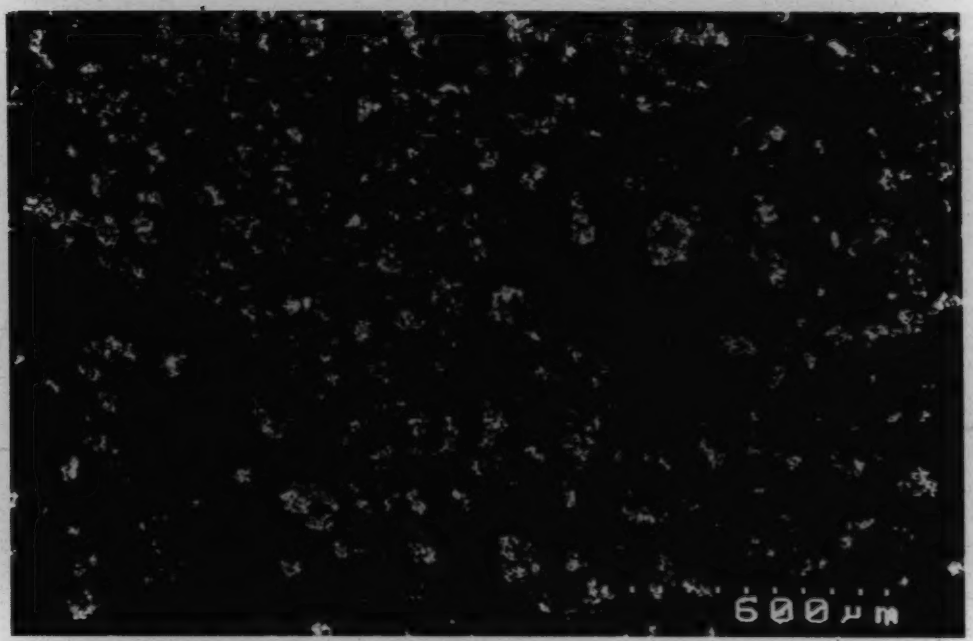

Figure C.3 Scanning Electron Micrograph of Leucine/Mannitol after use. Scale bar is 600µm.

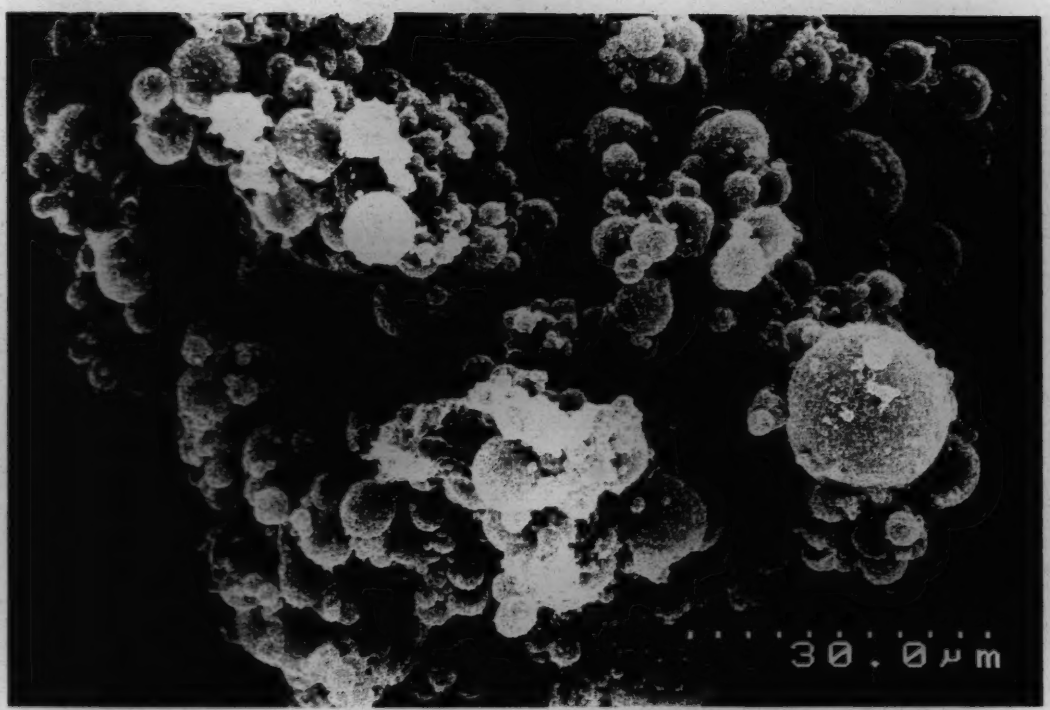

Figure C.4 Scanning Electron Micrograph of Leucine/Mannitol after use. Scale bar is 30µm.

Appendix D: Apex Silica and Hollow Glass Spheres

Apex Silica

A 10g sample of Apex Silica packing (catalog number JCPM300) was obtained from Chromatographic Specialties Inc. The silica particles are stated as having a diameter of 5 μm.

Figure D.1 displays the experimental data for the relationship between ρ_b and $(\rho_b{}^2/a)^{1/3}$ for the Apex silica. The weak relationship reveals a density of 0.77 ± 0.02 g/cm^3. Figure 19 also contains the calculated error associated with the data.

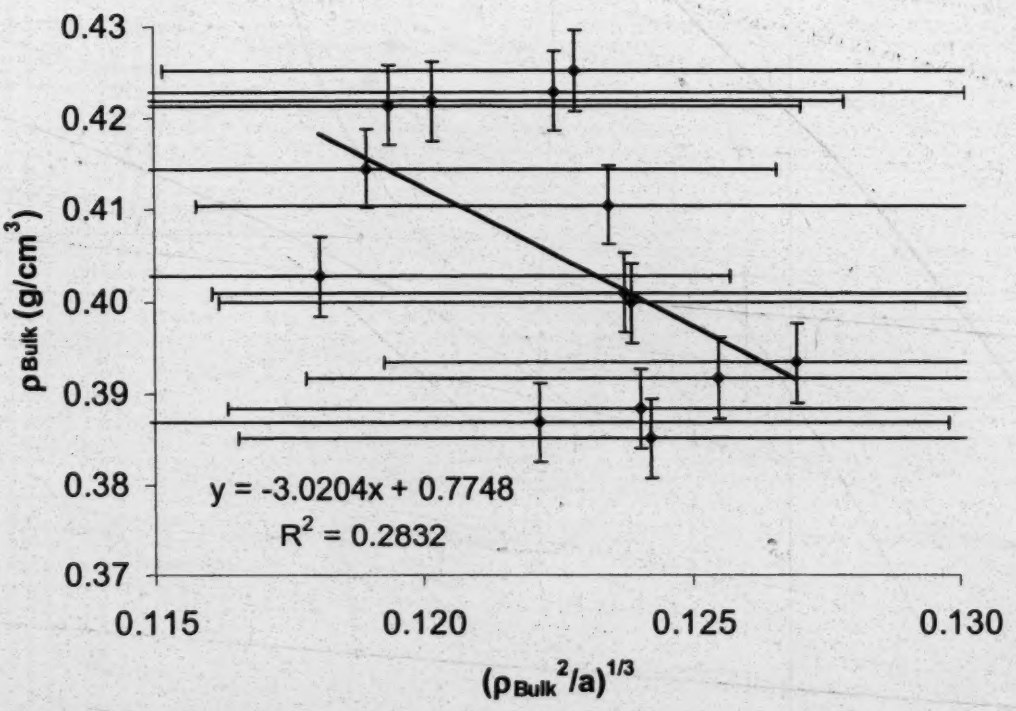

Figure D.1. Ergun Method for Apex Silica

Polysciences Inc. Hollow Glass Spheres

Two 5g vials of Polysciences Inc. Hollow Glass Spheres were acquired (catalog number 19823). The manufacturer states the Hollow Glass Spheres have a nominal density of 1.1 g.cm^3 and diameters ranging from 2 to 20 μm, with a mean size of 8 μm.

Figure 20 displays the experimental data for the relationship between ρ_b and $(\rho_b{}^2/a)^{1/3}$ for the hollow glass spheres particles. The relationship reveals an effective density of 0.74 ± 0.01 g/cm^3. The hollow glass spheres have a nominal density of 1.1 g/cm^3, and the determined effective density does not include this value. Figure D.2 also contains the calculated error associated with the data.

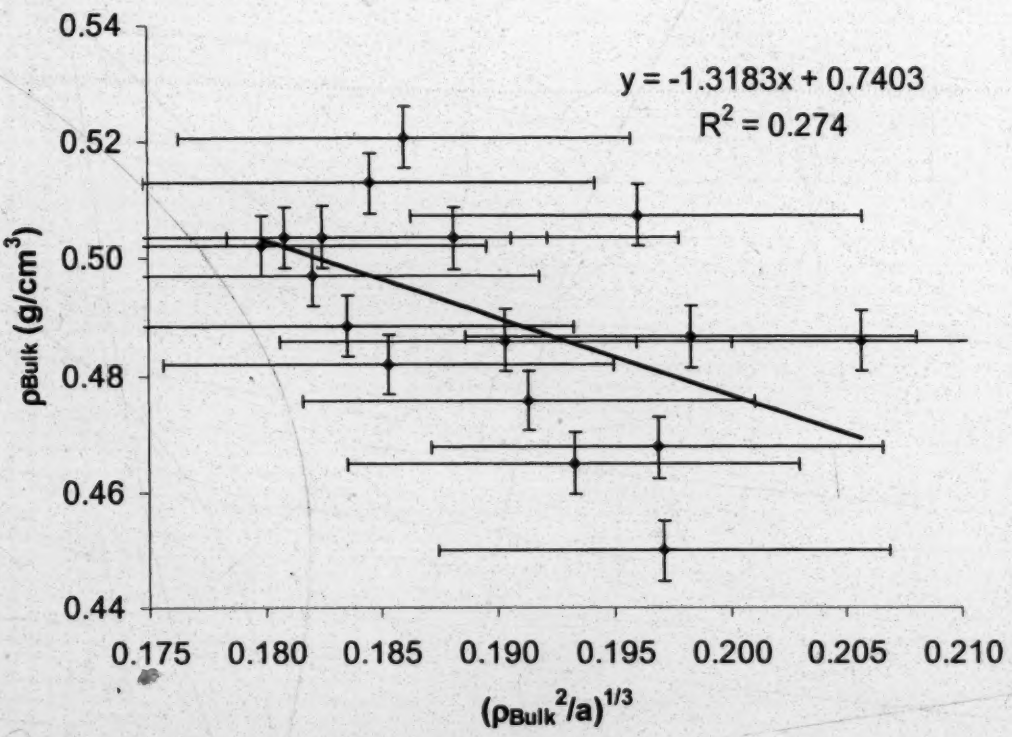

Figure D.2. Ergun Method for Hollow Glass Spheres

Discussion

Both of these materials appear to suffer the same fate with respect to the experimental setup. Neither of the effective density predictions agree with available values. Both display weak relationships for ρ_b versus $(\rho_b{}^2/a)^{1/3}$. The determined diameters are not equivalent to those stated by the manufacturers.

In both cases, the flow-meter could not exceed ~20% of its range without compacting the bed or causing a pressure drop that exceeded the range of the DP-cell of 3.5 inches of H_2O. The data collected for the Apex silica is not worth analyzing as the resulting error bars for $(\rho_b{}^2/a)^{1/3}$ are approximately ¾ of the range of the data collected. The data collected for the hollow glass spheres is not worth analyzing as the resulting error bars for $(\rho_b{}^2/a)^{1/3}$ are larger than the range for the data collected.

Although the Apex Silica and Hollow Glass Spheres do not nullify the experimental setup, the data do establish limits on the experimental setup. Worthwhile data for these particles could be collected if another, smaller flow controller were available. If this were attempted, air leaks throughout the system should be eliminated.

Appendix E: Bulk Density, Tapped Density, and Geometric Particle Size Distribution from AIR™